UNIVERSITY OF CALIFORNIA,
IRVINE

Gene Expression and Chromatin Dynamics During Macrophage Polarization in Health and Disease

DISSERTATION

submitted in partial satisfaction of the requirements
for the degree of

DOCTOR OF PHILOSOPHY

in Pharmaceutical Sciences

by

Klebea Carvalho

Dissertation Committee:
Professor Ali Mortazavi, Chair
Professor Celia Goulding
Professor John Chaput
Professor Robert Spitale

2021

DEDICATION

To

my parents, my sister, my dear husband, and my son

in recognition of their worth and for their unconditional love and support

"People are capable, at any time in their lives, of doing what they dream of."

"The act of discovering who we are will force us to accept that we can go further than we think"

Paulo Coelho

TABLE OF CONTENTS

LIST OF FIGURES

LIST OF TABLES

ACKNOWLEDGEMENTS

I would like to express my gratitude to my advisor Professor Ali Mortazavi for his guidance throughout my graduate studies. With his support I have become an independent scientist and was exposed to opportunities to improve my academic growth.

I would like to thank my committee members, Professor Celia Goulding, Professor John Chaput, and Professor Robert Spitale who have helped guide my academic and dissertation progress and have shown great commitment in this regard.

I would like to thank Dr. Andrea Tenner who has been an inspirating collaborator and great influence in my academic and professional life.

I would like to thank Dr. Eric Pearlman who has been a constant source of positivity, advice, and encouragement.

I would like to thank my mother Zilda Moreira, my father Carlos Mariano, and my sister Karlla Carvalho, who have been the most positive influence and a great support during my graduate studies.

I would like to thank my dear husband Dinsmore Sohn and his parents Young and Richmond Sohn for their continued support, dedication, and encouragement during my graduate and professional journey.

I would like to thank my son who is my daily motivation to improve my academic, professional, and personal growth.

I would like to thank Mochi for his company and love during my studies.

I would like to thank Dr. Harinder Grewal and the GPS-STEM project who have provided several opportunities to further my professional growth.

I would like to thank Dr. Paul dePompo who has been instrumental in some of my most important decisions during my graduate studies.

I would like to thank LASPAU/CNPq for their funding support.

In addition, I would like to thank all my estimated UCI colleagues and former members of the Mortazavi Lab Dr. Marissa M., Dr. Lorrayne S., Katherine W., Christina W., Dr. Camden J., Dr. Nicole S., Elisabeth R., Heidi L., Gabriela B., Fairlie R., Dr. Rabi M., Dr. Angela G. and wish all great success in their future endeavors.

VITA

Klebea Carvalho

EDUCATION

Doctor of Philosophy in Pharmaceutical Sciences **2021**
University of California, Irvine, CA

Master of Science in Biosciences **2014**
Federal University of Rio de Janeiro, RJ, Brazil

***Latu sensu* Specialization in Pharmacology** **2012**
Federal University of Lavras, MG, Brazil

Doctor of Pharmacy in Hospital Pharmacy **2007**
Federal University of Juiz de Fora, MG, Brazil

AWARDS AND FELLOWSHIPS

Ph.D Research Fellowship **2015-2019**
LASPAU – affiliated with Harvard University
National Council for Scientific and Technological Development – CNPq, Brazil

Scholarship Award for the Gene Regulatory Networks Course **2018**
Marine Biological Laboratory - MBL

Master of Science Research Fellowship **2012-2014**
FAPERJ / Ministry of Education – Brazil

PUBLICATIONS & MANUSCRIPTS

Carvalho K. et al., **"**A soluble pyrophosphatase is essential to oogenesis and is required for polyphosphate metabolism in the red flour beetle (*Tribolium castaneum*)". Int. J. Mol. Sci., doi: 10.3390/ijms16046631, **2015.**

Bianca M., **Carvalho K.,** Curitiba B., et al., **"**Inorganic pyrophosphatase from the red flour beetle (Tribolium castaneum) modulates mitochondrial polyphosphate metabolism**"**. Arch. Insect Biochem. Physiol., doi: 10.1002/arch.21606, **2019**.

Carvalho K. et al., "Uncovering the Gene Regulatory Networks Underlying Macrophage Polarization Through Comparative Analysis of Bulk and Single-Cell Data", doi: 10.1101/2021.01.20.427499 (under review, Cell Reports).

Carvalho K. & Schartz N., et al., "Complement C5aR1 signaling promotes inflammatory cascades and modulates the expression of select glial activation genes in a mouse model of Alzheimer's disease" (in preparation).

Carvalho K. & Rebooah E. et al., "Investigating macrophage differentiation and polarization using long reads and microRNA sequencing" (in preparation).

PROFESSIONAL EXPERIENCE

Graduate Researcher **2015-2021**
School of Pharmacy and Pharmaceutical Sciences – UC Irvine, CA

Graduate Professional Success for Scientists in STEM (GPS-STEM) Council **2019-2021**
GPS-STEM – UC Irvine, CA

Science Policy and Advocacy Course Coordinator **2020**
GPS-STEM – UC Irvine, CA

Hospital Pharmacist Director **2010-2015**
UPA – Rio de Janeiro, RJ, Brazil

SKILLS

Computational: Programming in R, Bash, UNIX/Linux, and python. Working with Github, HPC, and Docker.
Experimental: Single-cell and bulk RNA-seq and ATAC-seq library preparation and sequencing across Illumina and PacBio platforms; cell culture; HPLC; molecular biology techniques such as PCR, qPCR, cell sorting, molecular cloning, gel electrophoresis, and IHC.

LICENSES AND CERTIFICATIONS

Science Policy and Advocacy for STEM Scientists (Course coordinator) **2020**
GPS-STEM – UC Irvine, CA

Basics of Medical Writing **2020**
GPS-STEM – UC Irvine, CA

Mentoring Excellence Program **2020**
Division of Continuing Education – UC Irvine, CA

Regulatory Requirements for Pharmaceutical Products **2020**
UCI Division of Continuing Education – UC Irvine, CA

Business Concepts for STEM Scientists **2019**
Beall of Applied Innovation – UC Irvine, CA

IDIOMS

Brazilian Portuguese (Native), English (Fluent), Spanish (Fluent)

ABSTRACT OF THE DISSERTATION

Gene Expression and Chromatin Dynamics During Macrophage Polarization in Health and Disease

by
Klebea Carvalho
Doctor of Philosophy in Pharmaceutical Sciences
University of California, Irvine, 2021
Professor Ali Mortazavi, Chair

The complex task of maintaining homeostasis and fighting diseases involves an intricate network of immune cells with many relevant players. This thesis is focused on the plasticity and versatility of a critical class of innate immune cells called macrophages. Most naïve macrophages, named M0s, have the ability to polarize into two main subtypes, M1s and M2s, which help maintain a balance of inflammatory and anti-inflammatory responses, respectively. An imbalance in the ratio of M1s to M2s is associated with poor prognoses for a variety of diseases. Thus, understanding the markers and the gene regulatory networks (GRNs) that underlie the M0 to M1 or M2 polarization is crucial to help modulate these cells ratios for therapeutic purposes. Here, we applied bulk and single-cell RNA-seq and ATAC-seq to a high-resolution time series of HL-60-derived M0s polarizing towards M1 or M2 over 24 hours. We identified transient M1 and M2 markers and the main transcription factors (TFs) that drive polarization. In addition, we identified a novel M2 marker, ID2. We built bulk and single-cell polarization GRNs and identified at least 30 novel TF-TF interactions during M1/M2 polarization. We further compared the strengths of using bulk and single-cell technologies to build our GRNs providing experimental and computational guidelines for building GRNs of cellular maturation in response to microenvironmental cues. We concluded that despite the great advances of single-cell analysis, a combination of bulk and single-cell techniques provided a more complete GRN.

The brain resident macrophages, named microglia, do not fit into the dichotomic M1/M2 dogma of polarization. However, microglial activation and inflammation are directly linked to progression of Alzheimer's disease (AD). Neuroinflammation, hyperphosphorylated tau, and accumulation of amyloid beta plaques in the brain are hallmarks of AD, which presents progressive dementia as its main clinical feature. Amyloid plaques can activate the complement system. Complement activation, specifically activation of complement factor C5a and its receptor C5aR1 enhances microglial inflammation, which can worsen disease pathology through local injury and neuronal death. Thus, the C5a-C5aR1 signaling pathway is a potential target for modulation of AD. In order to investigate the effects of C5a in AD progression, we observed changes in hippocampal gene expression, hippocampal-dependent memory decline, and neuronal loss in two variants of the Artic mouse model of AD: one which lacks C5aR1 (cohort ArcticC5ar1KO) and one that overexpresses C5a under the GFAP promoter (cohort ArcticC5a+). The ArcticC5aR1KO group showed decreased inflammation, reduced activity of phagocytic and lysosomal pathways, and reduced cholesterol biosynthesis compared to Arctic mice. Furthermore, C5a overexpression led to poor cognitive performance, neuronal loss, and advanced disease progression compared to control. Our results suggest that pharmacological inhibition of C5a-C5aR1 signaling is a promising therapeutic strategy to treat AD.

CHAPTER 1

Introduction: Macrophage Plasticity in either Fighting or Promoting Diseases

1.1 Dynamics of cellular specialization and cellular maturation in response to microenvironmental stimuli

Cell fate decisions define a cell's morphology, migratory status, proliferation, and behavior. The decision-making process is often binary, allowing cells to assume one of two major states (Olsson et al., 2016). The chosen fate will determine a cell's competence to carry out an array of particular functions. Distinct cell identities exhibit non-identical and stable profiles of gene expression, despite the fact that they share an identical genotype. Important regulatory events can be determined by identifying temporal changes in gene expression and chromatin accessibility during cell differentiation and maturation in response to microenvironmental stimuli (Klemm et al., 2019; Scharer et al., 2018; Ramirez et al., 2017). Typically, only a subset of genes change expression during differentiation in a time-specific fashion, which are termed differentiation markers. Identifying the markers that define cellular identity and specificity is critical in order to determine how cells play roles in either fighting or promoting disease and to help modulate their ratios. Of particular interest are macrophages which are innate myeloid immune cells that are able to coordinate immune responses to inflammatory conditions, tumors, and neurodegenerative disorders (Li et al., 2021; Parisi et al., 2018; Sevenich, 2018). Macrophages are present in all stages of development, from embryo to adulthood, and reside in almost all tissues in the body, including skin Langerhans cells, liver Kupffer cells, and importantly brain microglia (Davies & Taylor, 2015). Tissue-resident macrophages are one of the first cells to react to disturbances in homeostasis assuming functions consistent with their niches. Macrophages are essential for health and disease and are therefore the theme of this study.

1.2 Macrophages: more than just phagocytes

Macrophages (from the Greek "*makrós*" meaning big and "*phageín*" meaning eater) are well known for phagocytosis of external pathogens and clearance of apoptotic cells in order to maintain tissue homeostasis (Hirayama et al., 2018). Macrophages are multitaskers playing important roles in innate immunity and cross talking with the adaptive immune system by recruiting other immune cells, such as lymphocytes (Gaudino & Kumar, 2019). An efficient immune system requires a good balance of pro- and anti-inflammatory responses, to which macrophages are key players. The current accepted model of macrophage activation or polarization (both terms can be used interchangeably) states that naïve tissue resident macrophages, termed M0s, polarize into major subtypes, a pro-inflammatory M1 or an anti-inflammatory M2, in response to environmental stimuli (Mills et al., 2000). Macrophage polarization is the theme of Chapter 2.

The M1 phenotype is induced by bacterial lipopolysaccharides (LPS) and/or pro-inflammatory cytokine interferon-gamma (IFN-δ), whereas the M2 phenotype is induced by interleukins 4 (IL-4) and 13 (IL-13) (Huang et al., 2018; Gordon & Martinez, 2010). M2 subtypes can be further subdivided into M2a, M2b, M2c and M2d macrophages, which are activated by distinct stimuli (Rőszer, 2015a). Although the M1/M2 dogma of polarization is a useful framework to investigate the regulatory functions and phenotypic characteristics of both major groups, macrophages *in vivo* might not follow such convention, showing more complexity with a spectrum of cells going towards either or both directions (Sica & Mantovani, 2012).

Polarization stimuli initiate a network of transcriptional mechanisms that take part in the dichotomic macrophage activation/polarization process (Zhou et al., 2017). In response to environmental stimuli, canonical IRF/STAT pathway signaling via STAT1 promotes M1

phenotype, which will express high levels of IRF1, IRF7, GATA2, SOCS3, and IL1β; whereas signaling via STAT6 promotes a distinct M2 phenotype, which will express high levels of STAT3, MEF2A/C, ID2, RARA, RXRA and ICAM3 (Orecchioni et al., 2019a; XIE et al., 2016; Rőszer, 2015b). A balance between M1s and M2s is crucial to maintain homeostasis. For instance, a high M1/M2 ratio can be associated with anti-tumorigenic effects and worsening auto-immune disorders, whereas a high M2/M1 ratio can be associated with pro-tumorigenic effects and improving skin regeneration (Xiao et al., 2020; Atri et al., 2018; Yuan et al., 2015). Characterizing the main transcription factors (TFs) that drive M1 and M2 polarization is crucial to determine how these subtypes interfere with disease pathology and to investigate therapeutics that modulate the M1/M2 ratio to treat cancers and immune disorders. Therefore, one of the goals of Chapter 2 is to determine the main TFs and polarization markers that underlie M1 and M2 activation, which can guide pre-clinical studies targeting polarization.

1.3 Tissue-resident macrophages and brain microglia: same but different

Most tissue resident macrophages are capable of polarizing into the two major groups: M1 or M2. However, brain microglia might not fit into this dichotomic division. As other tissue resident macrophages, microglia are phagocytes mainly originated from yolk-sac derived myeloid progenitors, which are able to proliferate and differentiate *in situ* (Hoeffel & Ginhoux, 2018; Ginhoux & Guilliams, 2016). They are important modulators of the central nervous system (CNS) immune surveillance, repair, and regeneration. Microglia are constantly scavenging and extending or retracting their ramifications in order to monitor brain activity and maintain tissue integrity (Nayak et al., 2014). However, microglial activation and dysfunction can also contribute to CNS

damage and neurodegenerative diseases. Hence, understanding the heterogeneous populations of CNS microglia have the potential to lead to therapies to treat multiple brain disorders.

In homeostatic conditions, the blood brain barrier (BBB) is an essential gatekeeper of the CNS keeping its immune privilege and regulating brain permeability, hemodynamics, and nutrient transport (Pachter et al., 2003). Although the immune privilege is not absolute, the BBB is important to control and limit the brain immune response during homeostasis. The pools of cytokines and chemokines that make up the CNS microenvironment are those from cell-to-cell signaling, as well as those from the unique composition of the CNS given its separation from the circulation (Deczkowska et al., 2018). Hence, the CNS microenvironmental cues are distinct from the pool of signaling molecules present in other tissues. The microglial transcriptome differs from other tissue resident macrophage transcriptomes as it is strongly shaped by the immune isolated CNS milieu (Gosselin et al., 2014).

Increasing evidence suggests that microglia do not fit the conceptual M1/M2 framework of polarization and still lack a nomenclature that will take the population diversity into account (Ransohoff, 2016). Nonetheless, a subset of microglia named disease-associated microglia (DAM) shows a unique transcriptional and functional signature associated with the progression of neurodegenerative diseases, such as Alzheimer's disease (AD) (Keren-Shaul et al., 2017). Some of the signatures genes upregulated in this activated microglia are TREM2, a receptor needed for DAM activation, TYROBP, CTSD, LPL, CST7, and APOE (also expressed by astrocytes) (Deczkowska et al., 2018). DAM are conserved in mice and humans and mainly display an inflammatory phenotype with upregulation of genes involved in lipid metabolism, lysosomal and phagocytic pathways (Keren-Shaul et al., 2017). Targeting DAM's inflammatory response is explored in Chapter 3 and may lead to a potential therapeutic approach to treat AD.

1.4 Macrophage polarization in health and disease: the good and the bad

Primitive macrophages are generated without monocytic progenitors in the yolk sac and seed most of the embryonic tissues. They are typically the only tissue resident immune cells and are maintained by self-renewal throughout life in homeostatic conditions (Hoeffel & Ginhoux, 2018). Macrophages reside in the heart, gut, eyes, cornea, epidermis, ovaries and virtually every tissue in the body, even inside joints that lack blood vessels, and human breast milk (Mosser, Hamidzadeh, & Goncalves, 2021). They perform engulfment and recycling of apoptotic cells and tissue debris preventing their accumulation, which could lead to local tissue injury and organ failure. Macrophages are able to capture a variety of microenvironmental inputs and transduce them into a myriad of responses to maintain tissue homeostasis.

Macrophage polarization can influence the outcome of a variety of diseases. Hence, many studies document the imbalance of M1/M2 or M2/M1 showing beneficial or detrimental effects in disease pathology. However, it is less clear whether this imbalance is the causal force or if it is a consequence of the disease pathology. M1 macrophages usually show an inflammatory and cytotoxic phenotype, being associated with positive effects in tumor elimination and negative effects for wound healing. M1s highly express surface markers CD80, CD86, TL4 and secrete pro-inflammatory cytokines, such as IL-6, IL-1β, and TNF (Chávez-Galán et al., 2015). On the other hand, M2 macrophages usually show an anti-inflammatory phenotype, being associated with positive effects in chronic inflammation and negative effects in many cancers (Funes et al., 2018). M2s highly express surface markers CD206, CD163 and secrete anti-inflammatory cytokines, such as IL-10 (Figure 1.1).

1.4.1 Macrophages in immune disorders

Many immune-related diseases are associated with an increased M1/M2 ratio. M1-polarized macrophages have been linked with the pathophysiology of severe allergic asthma, specifically in patients that didn't respond to treatment with systemic corticoids (Saradna et al., 2018). Another study showed that myeloid cells isolated from patients with active systemic lupus erythematosus (SLE) presented higher number of differentially expressed M1-like genes when compared to patients with inactive SLE who showed higher expression of M2-associated genes (Labonte et al., 2018). Moreover, the comparison of myeloid cells from both active and inactive SLE patients showed bias towards pro-inflammatory M1 cells during flare-ups.

Macrophages are also believed to be the main source of pro-inflammatory signaling molecules around adipocytes. Diet-induced obese mice seem to have higher infiltration of M1-like macrophages in adipose tissue, which was not seen on lean mice that showed higher infiltration of M2s (Lumeng et al., 2007). The inflammatory process caused by M1s is associated with insulin-resistance in obese mice, leading to Type II diabetes (Cucak et al., 2014). In addition, an increased M1/M2 ratio seems to be associated with rheumatoid arthritis (RA) pathology, whereas decreased M1/M2 ratio has been associated with improved RA prognostics (Yang Wang et al., 2017).

1.4.2 Macrophages in solid cancers

Macrophages located within solid tumor microenvironments known as tumor-associated macrophages (TAMs) are major contributors to the prognosis of cancer patients. They secrete cytokines, chemokines, growth factors, and promote chemotaxis of other immune cells (Lin et al., 2019). TAMs may assume either M1 or M2 phenotypes, but researchers tend to consider most of the TAMs as M2-like macrophages. M2 TAMs provide an immunosuppressive environment by

secreting an array of anti-inflammatory molecules besides promoting angiogenesis *in vivo* (Shu et al., 2020; Jetten et al., 2014). Clinical observations show that the accumulation of M2 TAMs in tumorigenic tissues are thought to affect tumor initiation, progression, metastasis, and drug resistance (Jayasingam et al., 2019). Higher densities of TAMs around tumors are usually observed in advanced tumor stages. Thus, targeting TAM is a promising therapeutic strategy to treat cancer (DeNardo & Ruffell, 2019; Lin et al., 2019).

Both human and mice TAMs express programmed cell death protein 1 (PD-1), which is an immune checkpoint receptor that induces immunotolerance. TAM PD-1 expression increases over time during tumor progression and culminates with decreased TAM phagocytic activity against tumorigenic cells in a variety of cancers (S. R. Gordon et al., 2017). M2-like TAMs are associated with poor prognosis in breast cancer, which is the leading cause of cancer related death in women around the world (S.-Q. Qiu et al., 2018). TAM infiltration of breast cancer is linked to accumulation of hyaluronan, increase in tumor aggressiveness, and treatment resistance (Tiainen et al., 2015). In addition, M2 TAM presence in the lung tumor stroma was correlated with worse overall patient survival, whereas M1 presence in tumor islet was linked to more favorable patient survival in lung cancer (Wu et al., 2016). Ovarian cancer patients that showed a high M1/M2 TAM ratio presented higher and progression-free survival when compared to patients that had a lower M1/M2 TAM ratio (Macciò et al., 2020). Other examples of cancers in which TAM invasion showed great clinical relevance and M2 TAM negatively affected prognosis are skin cancer (Fujimura et al., 2018), gastric cancer (Räihä & Puolakkainen, 2018), and kidney cancer (Kovaleva et al., 2016).

1.4.3 Macrophages in muscle repair and muscular dystrophy

Macrophages play important roles in skeletal muscle repair, as well as muscle fibrosis. Resident and infiltrating macrophages are responsible for clearance of necrotic myofibers and release of signaling molecules that promote stromal remodeling and regeneration (Stepien et al., 2020). Fibroadipogenic progenitors (FAP) are stem cells within skeletal muscle tissues that can differentiate into myofibroblasts or adipocytes in response to macrophage signaling, contributing to muscle repair or fibrosis, respectively (Dort et al., 2019; Contreras et al., 2016). Different subtypes of polarized macrophages will exert distinct functions during muscle repair, depending on the stage of the insult. M1 macrophages are usually more abundant during the early stages of muscle injury. M1s promote phagocytosis of necrotic muscle debris, killing of intracellular pathogens, antigen presentation, and FAP apoptosis (Dort et al., 2019; Wynn, 2008). M2 macrophages are usually found at later stages of muscle repair and promote FAP survival. M2s also secrete IL-10, which seems to be key to tissue survival post-transplantation, and wound healing (Bosurgi et al., 2012). Targeting macrophages at different stages of muscle repair can significantly affect the balance between muscle regeneration and fibrosis during injury.

Duchenne muscular dystrophy (DMD) is a severe X-linked disorder in humans. DMD is characterized by chronic inflammation and muscle fibrosis that lead to muscle degeneration and necrosis (Duan et al., 2021; Dreyfus et al., 1958). A study has shown that pro-inflammatory macrophages (M1-like) derived from the circulating monocytes ($Ly6C^{pos}$) secrete high levels of TGF-β1 which sustains collagen production and matrix deposition by fibroblasts culminating with fibrosis in mouse and human DMD muscle (Juban et al., 2018). Another study showed that inflammatory monocyte-derived macrophages recruited by increased CCR2 signaling activation reduced muscle strength and worsened DMD muscle histopathological features in mice

(Mojumdar et al., 2014). Both studies suggest that inflammatory M1-like cells that arise from circulating monocytes but not local resident macrophages are linked to progression of DMD and may be therapeutically targeted to treat the disorder.

1.4.4 DAM microglia in neurodegeneration: focus on AD

Microglia are potent immune sensors of CNS damage. Accumulating evidence suggests that DAM, a subset of brain macrophages with unique transcriptome as aforementioned, are able to play protective as well as detrimental roles in neurodegenerative disorders (Guzman-Martinez et al., 2019). DAM-like phenotype was primarily detected around sites of neurodegeneration and not in other regions. One recent study proposed that when damaged, the CNS sends out danger signals named neurodegeneration-associated molecular patterns (NAMPS), which are recognized by microglia and promote their transition into a DAM phenotype (Deczkowska, et al., 2018). Studies have shown that DAM are usually co-localized with β-amyloid (Aβ) plaques in mouse models of AD and in tauopathy models. DAM density also increase with aging, as well as with progression of other neurodegenerative diseases, such as amyotrophic lateral sclerosis (ALS) and multiple sclerosis (MS) (Keren-Shaul et al., 2017). Importantly, microglia with DAM signature genes were found in AD patients' postmortem brain (Friedman et al., 2018).

CNS neuroinflammation along with accumulation of intraneuronal hyperphosphorylated tau protein forming the neurofibrillary tangles (NFTs) and the presence of neuritic plaques of Aβ are hallmarks of Alzheimer's disease. AD is a neuropsychiatric disorder that affects mainly people over 65 years old that presents progressive dementia as its main clinical feature and has no effective treatment available able to stop or reverse the progression of the disease (Guzman-Martinez et al., 2019). Neuroinflammatory pathways are linked to patients' cognitive decline and the activation of

two types of glial cells (microglia and astrocytes) seem to be directly implicated in the process. Damage signals including complement factors, cytokines, and chemokines will polarize microglia that in turn activate astrocytes and amplify the immune response. Both reactive microglia and astrocyte release signaling molecules that will modulate CNS lesions in AD (Jha et al., 2019).

The AD brain tissue has an increased number of total microglia as well as an increased proportion of DAM to homeostatic microglia. The density of homeostatic microglia declines with the progression of the disease, as they switch to a DAM-like phenotype (Mathys et al., 2017). Once activated, microglia express different surface markers, such as phagocytic receptors CD33 and TREM2 (Griciuc & Tanzi, 2021), major histocompatibility complex II (MHC-II), and molecular pattern recognition receptors (PPRs). DAM secrete pro-inflammatory cytokines and chemokines such as IL-1β, IL-6, TNF, and IFN-δ, as well as cytotoxic factors nitric oxide (NO), and reactive oxygen species (ROS) (Guzman-Martinez et al., 2019). DAM genetic signature includes down-regulation of homeostatic genes TMEM119*,* SELPLG*,* P2RY12*,* and CX3CR1, as well as overexpression of genes CST7*,* APOE*,* LPL*,* LILRB4A*,* TYROBP*,* and SPI1*,* which are dependent on TREM2 activation (Zhou et al., 2020). One recent study showed that a subpopulation of DAM with unique transcriptome including AD risk genes CLU*,* INPP5D*,* PLCG*2,* SPI1, and CD33 is responsive to Aβ but not tau pathology, suggesting that Aβ pathology drive the AD genetic signature, which might be upstream of tau pathology (Sierksma et al., 2020).

The complement system is an important effector mechanism of innate immunity which has been implicated as a contributor to AD pathology. The complement cascade can be activated by three pathways named classical, which is directly involved in the AD pathology, alternative, and lectin pathways (Reis et al., 2019). C1q is the initiating protein that activates the classical pathway. C1q engagement with fibrillar Aβ plaques in both human and mice initiates the cascade

culminating with the formation of the terminal complement membrane attack complex C5b-C9 (MAC) (Zhou et al., 2008). MAC has been found co-localized with fibrillar Aβ and tangles in human AD brain, suggesting that there's complete complement cascade activation in AD (Webster et al., 1997). Complement activation products C5a and C3a in combination Aβ ligate to toll-like-receptors (TLR) on the surface of glial cells inducing an inflammatory response, including microglia activation. C5a is a potent inflammatory mediator of the complement cascade, and binds to C5a receptor 1 (C5aR1). In Chapter 3, we study the effects of C5a overexpression and ablation of C5aR1 in the pathology of AD and suggest that pharmacologic inhibition of C5aR1 is a promising therapeutic strategy to treat AD (Hernandez, Jiang, et al., 2017).

1.5 Therapeutics targeting macrophages

1.5.1 Cancer therapeutics: targeting TAMs

Macrophages are characterized by high plasticity and heterogeneity under both physiological and pathological contexts. Reverting the macrophage polarization subtype can be an important therapeutic strategy to treat diseases in which an M1/M2 imbalance affects the prognosis. For example, in solid cancers macrophages can make up to 50% of the number of cells within the tumor and can stablish a immunosuppressive tumor microenvironment (TME) (Qiu et al., 2018). Different types of molecular compounds against TAMs are currently being tested to prevent tumor progression and metastasis. There are three main cancer strategies targeting TAMs under investigation, which will be further discussed: repolarizing M2 TAMs to M1-like macrophages; disturbing M2 TAM survival or depleting TAMs; and inhibiting the recruitment of TAMs to the tumorigenic site (X. Zheng et al., 2017a).

Repolarization of immunosuppressive/tumor-promoting M2-like TAMs to a tumor-suppressive M1-like phenotype was evaluated in multiple pre-clinical cancer studies. One study used iron chelated melanin-like nanoparticles to repolarize TAM towards M1 *in vitro* and *in vivo*. As a result, the newly repolarized M1-like macrophages were able to increase chemotaxis of T cells and effector T cells to the tumor site, culminating with reduced tumor growth and metastasis (Rong et al., 2019). Another study showed that zoledronic acid at clinically compatible doses reduced the number of peritoneal TAMs and promoted TAMs switch to an M1-like phenotype, leading to reduced tumor vascularization and inhibiting spontaneous mammary carcinogenesis (Coscia et al., 2010). Zoledonic acid is currently evaluated in a randomized clinical trial to treat women with breast cancer that metastasize to bone (Hortobagyi et al., 2017).

In order to provide further insight into the repolarization strategy, in Chapter 2 we identified the transcriptome profile of M2 repolarized towards M1 (M2M1) highlighting M2M1 markers and identified the main differences between M1, M2 and M2M1. Targeting M2 polarization markers has become a useful yet challenging repolarization approach. Immune side effects are the main concern of this approach, because the phenotypic conversion of M2 to M1 can happen in multiple *loci* during treatment causing an unnecessary M1 imbalance in healthy tissues. In light of this, one study applied a "smart" micellar nanodrug with M2 targeting peptides (M2peptide) which only became active inside the acidic TME. The STAT6 inhibitor nanodrug AS1517499 effectively suppressed tumor growth and metastasis *in vitro* and *in vivo* in a mouse model of breast cancer. In addition, it was observed to reduce immune side effects since the healthy organs' neutral pH did not trigger the drug "stealth-to-nonstealth" stages (Xiao et al., 2020). Another study used legumain-targeting liposomal nanoparticles (NPs) to modulate the M2-TAM polarization marker STAT3. Hydrazinocurcumin (HC) encapsuled nanoparticles inhibited STAT3

signaling in TAM, switching its phenotype to an M1-like which reduced 4T1 cells migration and invasion *in vitro* and suppressed breast cancer angiogenesis, growth, and metastasis *in vivo* (X. Zhang et al., 2013).

Different approaches have been used to reduce TAM survival, including the use of cytotoxic agents to induce apoptosis and targeting of TAM cell surface proteins. The chemotherapeutic agent trabectedin (ET-743) is specifically cytotoxic to mononuclear phagocytes due to activation of caspase-8, which is the initiator caspase of extrinsic monocyte apoptosis. The depletion of mononuclear phagocytes, including TAM, was shown to be essential for trabectedin anti-tumor activity (Germano et al., 2013). Targeting cell surface protein CSF1 receptor (CSF1R) is another cancer treatment strategy. CSF1 is a tumor stimulating factor that attracts macrophages and leads to their polarization towards a TAM-like phenotype. AMG820, a monoclonal anti-CSF1R antibody that inhibits the CSF1/CSF1R pathway, showed anti-tumor activity against advanced solid tumors in a Phase I study and is thus a promising cancer therapeutic (Papadopoulos et al., 2017). The high frequency of TAM around the tumor site can predict metastasis and poor prognosis in around 60% of patients with neuroblastoma. The CSF1R inhibitor BLZ945 in combination with chemotherapeutics cyclophosphamide and topotecan inhibited neuroblastoma growth, and increased mouse survival time. Furthermore, blocking CSF1R enhanced therapeutic efficacy in neuroblastoma patients with limited anti-tumor T lymphocytes (Webb et al., 2018).

Many preclinical and clinical studies aim to reduce intratumor accumulation of TAM by inhibiting their recruitment to the tumorigenic site. A subset of pro-tumoral TAMs in the TME express kinase receptor Tie2. One study shows that a kinase switch control inhibitor named rebastinib inhibits Tie2 signaling, reducing TAM-induced tumor progression in pancreatic and breast cancers. Tie2 inhibition reduced TAM incidence in the TME and is a promising cancer

therapeutic (Harney et al., 2017). Many tumors have shown high expression of chemokine CCL2 and its receptor CCR2, which were directly associated with TAM chemoattraction (Peña et al., 2015). Inhibition of CCL2/CCR2 signaling showed great efficacy in many preclinical studies using solid tumor models (Argyle & Kitamura, 2018). However, clinical trials using CCL2/CCR2 inhibitors were not successful or only showed minor tumor improvement with CCL2 levels rapidly increasing after treatment, suggesting that there are other mechanisms that compensate the CCR2 inhibition (Malfitano et al., 2020). Thus, other TAM chemoattractant-targeting agents should be further investigated in order to produce more effective results in reducing TAM recruitment to TME.

1.5.2 AD therapeutics: inflammation as a target?

AD clinical trials have shown over 99% failure rate so far. As of February 2020, there were 136 active clinical trials testing 121 unique AD therapies, of which 29 were in Phase III trials (Cummings et al., 2020). Many of the failed clinical trials in the past 25 years were centered on Aβ pathology and mainly focused on reducing Aβ formation or enhancing its clearance. Though these agents were successful in decreasing Aβ accumulation, they failed in improving cognitive function or slowing cognitive impairment, suggesting that other pathological features of AD should be evaluated and targeted (Oxford et al. 2020). Other factors that limited the success of AD clinical trials were the inability of many compounds to cross the blood brain barrier and the limiting number of patients able to enroll. Those patients should be asymptomatic or in transitional disease state designated mild cognitive impairment (MCI) (Cooper et al., 2014). Over the last 5 years there was a diversification of the trials pipeline including agents that target synaptogenesis, neurogenesis, and importantly neuroinflammation (Cummings et al., 2020). There is an urgent

need for development of treatments that can slow the progression or cure Alzheimer's disease and microglia-induced neuroinflammation is a promising therapeutic strategy under investigation.

Multiple clinical trials have explored the potential effects of on non-steroidal anti-inflammatory drugs (NSAIDs) to treat AD. Some NSAIDs, such as ibuprofen and the fenamate class have shown inhibition of inflammasome activation *in vitro*, but did not show positive effects in decreasing AD cognitive decline in clinical trials (Dong et al., 2019). One ongoing Phase I clinical trial investigates the effects of NSAID salsalate in patients with mild to moderate Alzheimer's disease (NCT03277573). Another recently concluded Phase III clinical trial study evaluated the combination of ibuprofen and the mast cell stabilizer cromolyn to treat AD, but its results are yet to be released (NCT02547818). The main challenges of using systemic anti-inflammatory drugs in treating AD is the promotion of systemic side effects that can be detrimental to healthy tissues, as well as the poor ability to penetrate the BBB. Therefore, a therapy with efficient brain penetration and selectivity to treat microglia-induced inflammation is needed and one possible approach is discussed in Chapter 3.

1.6 HL-60-derived macrophages: a useful model to study macrophage polarization

Promyelocytic HL-60 cells differentiate into macrophages when induced with phorbol-12-myristate-13-acetate (PMA) (Ramirez et al., 2017; Murao et al., 1983). These cells, stemmed from a female patient with acute myeloid leukemia, grow and divide continuously providing a perpetual source of cells (Collins et al., 1977). A large amount of gene expression and chromatin accessibility data has been generated using the HL-60 model system (Wenzel et al., 2020; Cusanovich et al., 2015; Poplutz et al., 2014; Annabi et al., 2007). Upon PMA stimulus, HL-60 cells show increased expression of PU.1, which dictates myeloid cell commitment and maintains macrophage

differentiation and proliferation (DeKoter & Singh, 2000; Nerlov & Graf, 1998). In a recent study, HL-60 cells differentiated into macrophages and neutrophils were used as a model to study differential methylation during myeloid differentiation (Antwi et al., 2020). Another study used the HL-60-derived macrophages to model immune functions of human microglia (Wenzel et al., 2020). Thus, promoting HL-60 differentiation to macrophage and further polarization, which we applied in Chapter 2, is a valuable model to study the key transcriptional events involved in the M1/M2 activation process (Chistiakov et al., 2018).

1.7 Bulk genomics techniques applied to our model of macrophage polarization

Dynamics of mRNA expression are coordinated by an intricate network of regulatory elements. Characterizing cell state transitions and the gene regulatory networks that coordinate cellular differentiation and maturation are key challenges of developmental biology. An important tool for solving the puzzle is to leverage time-series analysis, which facilitates the understanding of transient states between the initial pre-stimulus and the terminally differentiated states. Another important question in developmental biology is how changes in gene expression drive cellular differentiation in a coordinated manner as cells could potentially take more than one path to the same end state. Cells change their chromatin landscape and gene expression as they become more specialized (Briggs et al., 2018; Buenrostro et al., 2018). Thus, combinatorial genomic approaches are needed to identify the regulatory mechanisms at work during myeloid progenitor to terminal macrophage differentiation and polarization (Chistiakov et al., 2018; Ramirez et al., 2017).

ATAC-seq is used to identify open regions of DNA and sites of active transcription factor (TF) binding using a hyperactive Tn5 transposase that fragments and inserts synthetic adapters in double-stranded DNA at accessible regions of chromatin (Buenrostro et al., 2015; Corces et al.,

2017). RNA-seq is a standard transcriptome profiling method to measure gene expression in a cell or a population of cells (Mortazavi et al., 2008). Dynamic gene regulatory networks can be computationally reconstructed by pairing these data sets with perturbation assays (Ramirez et al., 2017). Key transcriptional events during cellular specification can be determined with comprehensive profiles of mRNA expression and chromatin accessibility with fine time resolution (Briggs et al., 2018). The characterization of transient states is particularly relevant to identify early signs of cellular maturation which could determine the specialization outcome (Olsson et al., 2016).

1.8 Single-cell genomics techniques applied to our model of macrophage polarization

Analysis of expression changes using pooled populations of cells, generally known as "bulk" studies, cannot capture the heterogeneity of multifunctional cell types. Transient states that express low levels of TFs are often not detected in bulk studies. Furthermore, identifying cell types in bulk studies relies on known markers and cellular subtypes that have previously been described (Jaitin et al., 2014). Single-cell genomics techniques have greatly improved our understanding of transient genetic changes in complex multicellular populations (Shalek et al., 2013). Uncovering discrete intermediate cell states that delineate cell-type specification has been greatly accelerated (Ziegenhain et al., 2017). Single-cell RNA-seq (scRNA-seq) methods such as Drop-seq can measure the individual mRNA profiles of thousands of single-cells by encapsulating each cell in a nanodroplet with unique DNA-barcoded beads for each cell (Macosko et al., 2015). This technology has been used to demonstrate the binary decisions during cellular specification, such as in myeloid progenitors that undergo an early bifurcation which segregates myeloid cells from the erythroid lineage (Drissen et al., 2016).

scRNA-seq of hematopoietic progenitors revealed mixed lineage states expressing distinct levels of either Irf8, which is a monocytic TF, or Gfi1, which is a granulocytic TF (Olsson et al., 2016). No single-cell study to date has clearly captured the heterogeneity of the macrophage subpopulations that undergo M0 to M1 or M2 polarization. Machine learning tools have contributed to the identification of distinct cell states by constructing an *in-silico* cellular trajectory, termed "pseudo time-course", using a time-course of scRNA-seq data (Qiu et al., 2017). Such tools apply an unsupervised algorithm which is able to uncover branch points throughout the differentiation process. Another useful computational tool contributed to building the GRN of cellular differentiation using scRNA-seq and scATA-seq data (Jansen et al., 2019). Taking advantage of those methods, we propose to investigate the heterogeneous macrophage populations and the bulk and single-cell based gene regulatory networks that underlie macrophage polarization in Chapter 2, as well as the main changes in gene expression in cortex and hippocampus upon ablation of glial receptor C5aR1 and its ligand overexpression in Chapter 3.

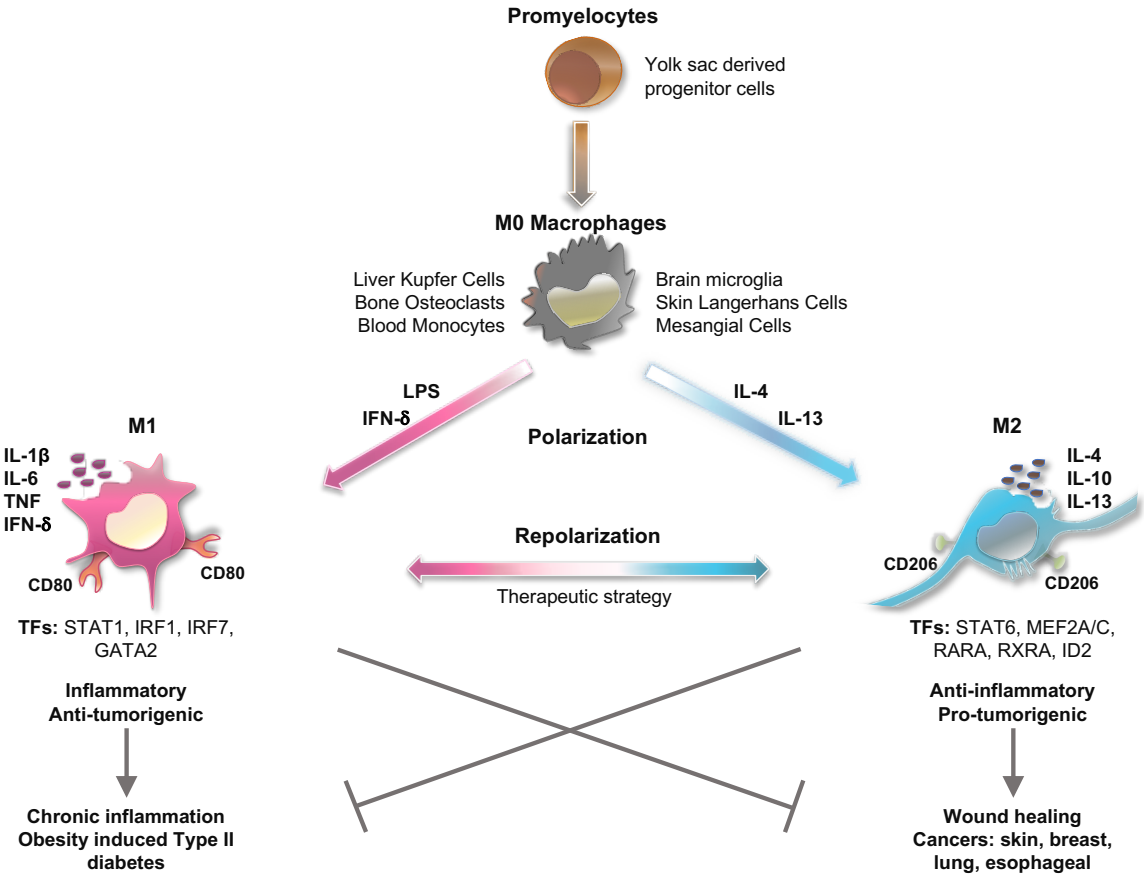

Figure 1.1 Tissue-resident macrophage polarization

CHAPTER 2

Uncovering the Gene Regulatory Networks Underlying Macrophage Polarization Through Comparative Analysis of Bulk and Single-cell Data

Notes:
(1) I performed macrophage differentiation, polarization, and repolarization, RNA-seq and ATAC-seq libraries preparation and sequencing, scRNA-seq libraries preparation, as well as data analysis and interpretation of RNA-seq, ATAC-seq, and scRNA-seq
(2) Elisabeth Rebboah performed scATAC-seq libraries preparation and bulk footprinting analysis
(3) Camden Jansen performed SOM-linking analysis
(4) Katherine Williams performed odds-ratio analysis
(5) Andrew Dowey maintained HL-60 cell culture
(6) Cassie McGill sequenced the scRNA-seq and scATAC-seq libraries
(7) Dr. Ali Mortazavi conceived the study and provided continued support and guidance throughout the project

2.1 Abstract

Gene regulatory networks (GRNs) provide a powerful framework for studying cellular differentiation. However, it is less clear how GRNs encode cellular responses to everyday microenvironmental cues. Macrophages can be polarized and potentially repolarized based on environmental signaling. In order to identify the GRNs that drive macrophage polarization and the heterogeneous single-cell subpopulations that are present in the process, we used a high-resolution time course of bulk and single-cell RNA-seq and ATAC-seq assays of HL-60-derived macrophages polarized towards M1 or M2 over 24 hours. We identified transient M1 and M2 markers, including the main transcription factors that underlie polarization, and subpopulations of naïve, transitional, and terminally polarized macrophages. We built bulk and single-cell polarization GRNs to compare the recovered interactions and found that each technology recovered only a subset of known interactions. Our data provide a resource to study the GRN of cellular maturation in response to microenvironmental stimuli in a variety of contexts in homeostasis and disease.

2.2 Introduction

The developmental programs controlling cellular differentiation are encoded in the genome. The controlled spatiotemporal expression of specific transcription factors (TFs) is at the core of these regulatory events and are hallmarks of cellular differentiation. Each TF interacts transiently with downstream targets that can be described as a dynamic gene regulatory network (GRN) (Peter & Davidson, 2015). The links that make up such networks dictate patterns of gene expression during development and differentiation (Gnanakkumaar et al., 2019; Peter & Davidson, 2011). However, how GRNs apply in the context of cellular maturation in response to

microenvironmental stimuli is less clear than in the context of cellular differentiation. While robust GRNs can be built by identifying temporal changes in gene expression and chromatin accessibility using bulk RNA-seq and ATAC-seq data (Duren et al., 2020; Ramirez et al., 2017), whether current single-cell RNA-seq and single-cell ATAC-seq are able to recapitulate or improve bulk-derived GRN connections is unclear. Thus, a side-by-side analysis of GRNs derived using bulk and single-cell techniques in the same model system allows us to quantify the relative strengths of bulk vs single-cell.

GRNs are of particular interest in macrophages, which are able to coordinate immune response to inflammatory conditions, tumors and degenerative disorders (Sharma et al., 2020; Chan & Viswanathan, 2019; DeNardo & Ruffell, 2019). Macrophages are innate immune cells that reside in almost all tissues in the body and play key roles in maintenance of tissue homeostasis and clearance of apoptotic cells (S. Gordon & Plüddemann, 2018). While heterogeneous, most naïve macrophages, termed M0, have the ability to polarize into two main activated states, M1 and M2, based on microenvironmental stimuli (Mills et al., 2000). The ratio of M1:M2 is highly regulated and synchronized in homeostatic tissues (Fujisaka et al., 2009). M1 polarization is induced by bacterial lipopolysaccharides (LPS) and/or the pro-inflammatory cytokine interferon-gamma (IFN-γ) and is therefore generally associated with a pro-inflammatory phenotype, bacterial phagocytosis and anti-tumorigenic activity (Orecchioni et al., 2019; Huang et al., 2018). M2 polarization is induced by interleukins 4 (IL-4) and 13 (IL-13), and is linked to an anti-inflammatory phenotype, helminth resistance and pro-tumorigenic activity (Shaked, 2019; Gordon & Martinez, 2010; Reece et al., 2006). While the M1/M2 framework has been useful to identify major polarization regulatory elements, macrophages *in vivo* may present more complex transcriptional signatures. Multiple M2-like subtypes with different gene expression profiles have

been described such as M2a, M2b, M2c and M2d, which are determined by distinct inducing stimuli (Rőszer, 2015c). Nonetheless, the M1/M2 dogma of polarization is still a useful conceptual framework to illustrate the main functions as well as the regulatory mechanisms of both major groups (Budhu et al., 2021; Leonard et al., 2020; Bok et al., 2018).

The macrophage phenotype present in a microenvironment can be used as a predictor of disease prognosis. For example, M1 plays an important role in promoting potentially fatal cytokine storms in high risk patients with COVID19 (Lara et al., 2020). Also, prolonged activation of resident macrophages of the brain (microglia) increases both amyloid and tau pathology and may be linked to Alzheimer's disease (AD) pathogenesis (Kinney et al., 2018). The potential role of activated macrophages in disease has motivated the search for drugs to control polarization (Zhang et al., 2019; Guerriero, 2018). One cancer treatment in development attempts to switch the phenotype of M2-like tumor associated macrophages to an anti-tumorigenic M1 phenotype, highlighting M2's ability to repolarize towards M1 (Zheng et al., 2017). However, little is known about the transcriptome profile of M2 repolarized towards M1. Although progress has been made in understanding gene expression in terminally polarized M1 and M2 subtypes (Orecchioni et al., 2019b), temporal transcriptional changes that drive polarization and repolarization remain poorly understood. Thus, reliable transient polarization markers are needed (Walentynowicz et al., 2018). Recent studies demonstrated that the TFs STAT1 and IRF7 are upregulated in M1, whereas STAT6 is upregulated in M2 both *in vivo* and *in vitro* (Orecchioni et al., 2019; Yu et al., 2019). Albeit relevant, most of the current polarization studies focus mainly on changes in the STAT family of TFs, perhaps overlooking other transcriptional regulators (Ding et al., 2019). Furthermore, no single-cell study to date has clearly captured the heterogeneity of the spectrum of cells that undergo

M0 to M1 or M2 activation.

Promoting or inhibiting M0 polarization towards M1 or M2 requires insight into changes to the chromatin landscape and gene expression that precede cell specialization (Briggs et al., 2018; Buenrostro et al., 2018). A useful framework to study macrophage differentiation is the HL-60-derived human macrophage model induced with phorbol-12-myristate-13-acetate (PMA) (Dao et al., 2020; Ramirez et al., 2017; Murao et al., 1983). A considerable amount of gene expression and chromatin accessibility data has been generated using the HL-60 model system (Wenzel et al., 2020; Antwi et al., 2020; Cusanovich et al., 2015; Poplutz et al., 2014). We have previously used bulk RNA-seq and ATAC-seq to build GRNs of HL-60 differentiation into M0s (Ramirez et al., 2017). Thus, profiling mRNA expression and chromatin accessibility during the transition from HL-60-derived-M0 to M1 or M2 with fine time resolution is a valuable approach to identify the genomic mechanisms that drive macrophage polarization (Chistiakov et al., 2018). Last but not least, with the increasing adoption and throughput of single-cell techniques, we can now compare in a well-defined setting the quality of the networks derived using bulk or single-cell techniques.

Here, we characterized the genomic regulatory events promoting macrophage polarization using the macrophage-differentiated HL-60 model to identify cell state transitions, intermediary markers and the gene regulatory networks between the initial M0 pre-stimulus and the terminally polarized M1 and M2 states. Our approach profiled the dynamic changes in the transcriptome and the chromatin landscape at bulk and single-cell levels at 3, 6, 12, and 24 hours of macrophage polarization. Furthermore, we explored the transcriptome profile of M2 repolarized towards M1. We identified key TFs at the core of the regulatory pathways that control polarization into M1 and M2 states and M2 to M1 repolarization. We built GRNs using bulk and single-cell data, and we validated the targets of multiple TFs in M2 polarization. Finally, we compared the GRNs that we

derived separately using bulk and single-cell data to identify what portions of the GRNs are recovered by either or both sets of methods.

2.3 Results

2.3.1 Distinct subsets of genes drive macrophage polarization towards M1 or M2 states

We activated HL-60-derived M0 either to M1 with LPS and IFN-γ or to M2 with IL-13 and IL-4, respectively, in order to identify how subtype-specific polarization affects macrophage gene expression. We collected samples for bulk RNA-seq at 3, 6, 12, and 24 hours post-stimulation (Figures 2.1A and S2.1A). We identified 7,601 genes (alpha < 0.05, FDR < 0.05%) whose expressions vary in a time-specific fashion using maSigPro. These genes grouped into 18 distinct clusters from which we selected 11 clusters (4,760 genes) representing four major patterns of expression for HL-60-, M0-, M1-, and M2-specific responses (Figure 2.1B). Each cluster contains distinct subtype-specific signaling molecules and TFs (Figure 2.1B). We identified 1,269 genes whose expression is higher in M1 (clusters Rc2, Rc5, Rc6 and Rc15) and 1,462 genes whose expression is higher in M2 (clusters Rc1, Rc7 and Rc13). We used an UpSet plot of maSigPro detected genes to identify a subset of 1,194 genes that had a similarly increased expression in both M1 and M2, and another subset of 149 genes that had a higher expression in HL-60 and M2 only (Figure 2.1C). These subtype specific genes showed distinct temporal expression patterns (Figures 2.1D & S2.1B). Canonical M1 polarization markers such as *CXCL10, CXCL11* and *GBP4* (Tang et al., 2017; Mantovani et al., 2006) increased expression rapidly by 3 hours post-stimuli and peaked expression around 6 hours (Figure 2.1D Upper). Canonical M2-associated genes *CCL24* and *CLEC4A* (Makita et al., 2015; Tang et al., 2017) were also induced at 3 hours post-stimuli and reached peak expression around 6 hours (Figure 2.1D Lower). M2 also showed higher expression

of signaling molecule *CSF2* that was recently shown to promote macrophages transition into an M2 phenotype (Li et al., 2020). Therefore, important expression changes leading to terminal polarization of macrophage subtypes were established within the first 6 hours following addition of stimuli. We also identified a subset of pro-inflammatory chemokines present in M1-specific clusters, such as *CCL7*, *CCL8*, *CXCL9*, *CXCL10*, and *CXCL11* (Gurvich et al., 2020; Lu et al., 2018) (Figure S2.1C). M2 clusters showed higher expression of chemokines *CCL24*, which is upregulated in macrophages stimulated with IL-4 (Lee et al., 2020) and *CKLF*, which has been associated with decreasing inflammation in dermal disorders (Zheng et al., 2017). Overall, we found substantial and rapid differences in gene expression as the result of macrophage polarization.

We performed gene ontology analysis on M0-, M1-, and M2-specific clusters to identify biological processes and pathways associated with subtype specific genes (Figure 2.1E). M0-specific genes are enriched for Rap1 and insulin signaling pathways, which are important for macrophage response to pathogens and phagocytosis, respectively (Chung et al., 2008; Liang et al., 2007; Rosa et al., 1996). M1-specific genes are enriched for regulation of inflammatory signaling, such as tumor necrosis factor (TNF) and IFN-γ response, which is a hallmark of M1 macrophages (Figure 2.1E). Activation of mitogen-activated protein kinase (MAPK) pathway, which is important for cellular proliferation and M2 polarization (Neamatallah, 2019), is enriched in M2-specific clusters. Thus, M2-specific genes are enriched for cellular division (Figure 2.1E). Interestingly, M2 cells are able to proliferate in our system, whereas M1 are not.

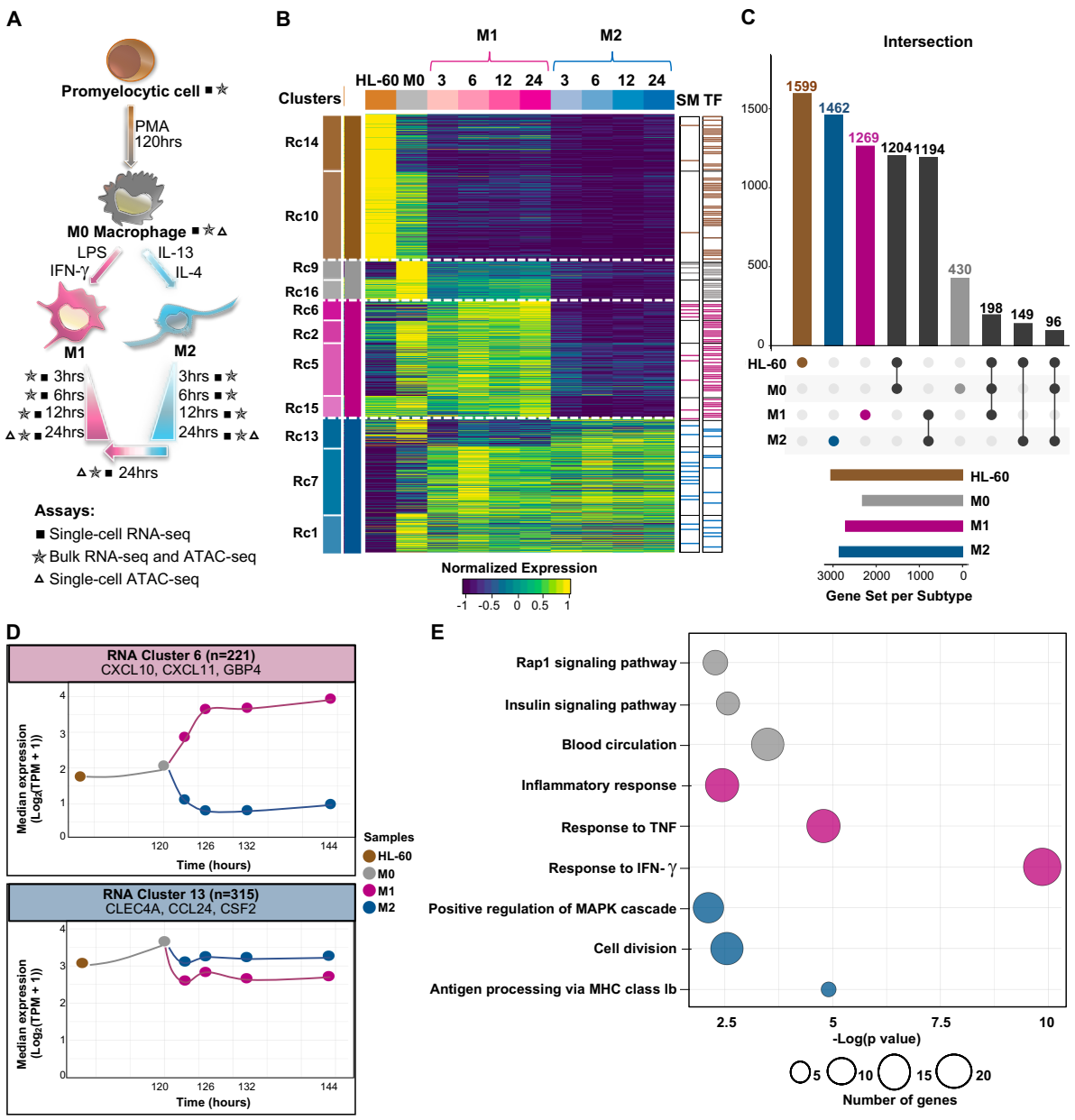

Figure 2.1 HL-60-derived M0 polarization reveals distinct clusters of M1- and M2-specific genes

A) Schematic diagram of experimental design highlighting samples processed and distinct assays performed.

B) Heatmap of 4,760 genes with dynamic temporal profiles identified by MaSigPro clustering (alpha < 0.05, FDR < 0.05%). Each column represents the average expression for a time point and each row represents a gene. Each cluster represents a subset of genes that show a similar pattern of expression along the time course. Brown, grey, pink, and blue represent HL-60-, M0-, M1-, and M2-specific clusters, respectively. RNA-seq data (TPM) is row-mean normalized. Signaling molecules (SM) and transcription factors (TF) present in each cluster are shown.

C) UpSet plot highlights distinct and overlapping genes across main subtypes (HL-60, M0, M1, and M2).

D) Representative cluster of 221 genes (RNA Cluster 6) that exhibit increased expression during the M1 polarization time course. Representative cluster of 315 genes (RNA Cluster 13) that exhibit increased expression during the M2 polarization time course.
E) Gene ontology (GO) enrichment analyses of M0 (430), M1 (1269), and M2 (1462) differentially regulated genes.

We collected a time course of M1 and M2 polarizing macrophages to identify dynamic temporal expression changes and intermediary markers regulated in response to polarization signaling. 500 genes showed increased expression as early as 3 hours post-stimuli; 400 of those were higher in M1 and 100 higher in M2 (Figure S2.1D). *FCGR1A*, whose expression is increased in immuno-inflammatory syndromes (Minar et al., 2014), reacted to M1 but not M2 stimuli and was activated as early as 3 hours of polarization. The signaling molecule *CSF2* displayed increased expression at 3 hours during M2 polarization but not during that of M1 (Figure S2.1D). *CSF2* over-expression leads to increased autophagy that promotes M0 polarization towards an M2 subtype (Chen et al., 2014; Liu et al., 2015). Other known M1-specific genes such as chemokine *CXCL9* and TF GATA2 (Yin et al., 2020) displayed differential expression in intermediary polarization states at 6 and 12 hours post-stimuli, respectively. Intermediary M2 polarization states showed differential expression of *COX6A1* (Codoni et al., 2016), which participates in macrophage oxidative phosphorylation, and M2 TF RXRA (Czimmerer et al., 2018) at 6 and 12 hours of polarization, respectively. Some genes displayed delayed response to stimuli, highlighting the dynamic nature of polarization. For instance, cytokine *CCL7* only showed higher expression in M1 compared to M2 at 24 hours after stimuli, whereas *CLECL1* gene that has been shown to stimulate IL-4 production in T helper cells and is overexpressed in nonclassical monocytes (M2) (Talker et al., 2020) comes up later in M2 polarization at 24 hours. Therefore, distinct subsets of M1- and M2-specific genes were regulated at early, intermediary and late polarization stages.

2.3.2 Dynamic shifts in chromatin accessibility occur in response to polarization stimuli and are sustained across differentiation

We clustered regions with similar accessibility profiles over time to identify chromatin regions that change during macrophage polarization (Figure 2.1A). We associated each chromatin region with its nearest gene and identified 25,331 differentially accessible regions (alpha < 0.05, FDR < 0.05%) using MaSigPro. These regions grouped into 21 distinct clusters from which we selected 12 clusters (14,174 regions) representing four major patterns of chromatin accessibility for HL-60-, M0-, M1-, and M2-specifific responses. Eight of these clusters contained regions overall more open in M1 (clusters Ac19, Ac13, Ac11 and Ac5) or M2 (clusters Ac18, Ac6, Ac7 and Ac17) (Figure 2.2A). The M1-specific cluster Ac13 highlighted regions around genes known to be upregulated in M1, such as apolipoproteins *APOL1, APOL4 and APOL6* (Gurvich et al., 2020; Lee et al., 2020; Mantovani et al., 2006) that became more accessible as M1 polarized and slightly less accessible as M2 polarized (Figure 2.2B Upper). Cluster Ac18 highlighted regions near known M2-specific genes, such as *STAT6, ADK* and *CCL1* (Mantovani et al., 2006, 2004) that in turn became more accessible during M2 polarization compared to M1 (Figure 2.2B Lower). Principal component analysis (PCA) revealed that PC2, which accounted for 18.1% of the variance, separated M1 from M2, with M0 sitting at 0 (Figure S2.2A). Pearson correlation analysis also showed great differences between macrophage subtypes (Figure S2.2B). Therefore, chromatin landscape reorganization was subtype-specific.

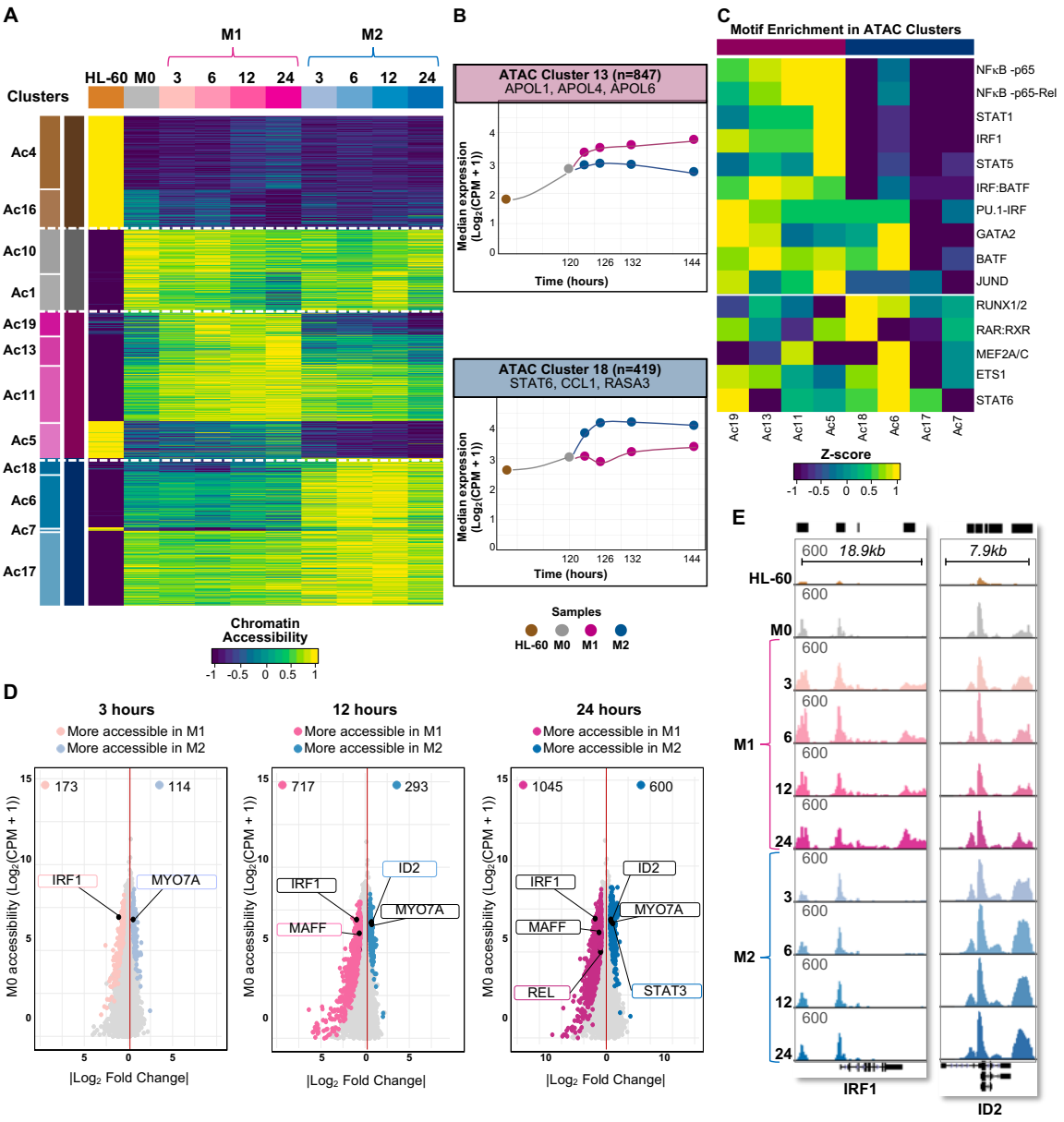

Figure 2.2 Differential chromatin accessibility occurs early in response to polarization stimuli

A) Heatmap of 14,174 differentially accessible chromatin regions identified by MaSigPro clustering (alpha < 0.05, FDR < 0.05%). Each column represents the average chromatin accessibility for a time point and each row represents a genomic region. Brown, grey, pink, and blue represent HL-60-, M0-, M1-, and M2-specific clusters, respectively. Read counts were TMM normalized, scaled by library size, and row-mean normalized.

B) Representative cluster of 847 genomic regions (ATAC Cluster 13) that exhibit increased accessibility during the M1 polarization time course. Representative cluster of 419 genomic regions (ATAC Cluster 18) that exhibit increased accessibility during the M2 polarization time course.

C) Hierarchical clustering of known motif enrichment in regions included in the 8 M1- or M2-accessible clusters.
D) Genomic regions with differential chromatin accessibility between M1 and M2 ($log_2FC>1$, FDR<0.05) compared to normalized M0 accessibility. Genomic regions associated with IRF1, MYO7A, MAFF, ID2, REL, and STAT3 are indicated.
E) UCSC genome browser screenshots depicting accessibility around IRF1 and ID2 genes in M1 and M2 samples (y axis scaled from 0 to 600).

We looked for enrichment of TF binding motifs in the M1- or M2-accessible regions of each cluster in order to determine whether a subset of transcription factors drive M1- or M2-specific chromatin changes (Figure 2.2C). Pro-inflammatory TFs NFκB, STAT1, STAT5, and IRF1, which are known to control M1 polarization (Chauhan et al., 2018; Platanitis & Decker, 2018), showed binding motifs enriched in M1 clusters (Figure 2.2C). JUND, an early target of LPS activation (Srivastava et al., 2013), also showed binding motifs enriched in M1 clusters. In M2 clusters, RAR, STAT6, RUNX and MEF2 motifs were enriched (Figure 2.2C). While RAR and STAT6 are known to be essential TFs in M2 macrophage activation (Lee et al., 2016), the RUNX and the MEF2 families of TFs are less well-described. RUNX2 has been implicated in the promotion of osteogenic events in both M1 and M2 (Dube et al., 2017; Li et al., 2019) and MEF2 was shown to be repressed by IFN-γ signaling (Kang et al., 2017). Notably, the binding motifs for the RUNX family of TFs are nearly identical, as well as the MEF2 family of TFs have very similar binding motifs. Based on expression, RUNX1 or RUNX2 as well as MEF2A and MEF2C were predicted to bind their family motif match in our data. After scanning for motifs in all open regions, we increased the specificity of our analyses by only scanning for footprints of 8-31nt in regions likely bound by TFs using HINT-ATAC (Li et al., 2019) by pooling the ATAC-seq data for all time points (3 to 24 hours) for M1 (~350 million reads) or M2 (~260 million reads). We recovered 362,198 footprints for M1 and 362,809 footprints for M2. The output mostly recapitulated the results from scanning for motifs in clusters of regions identified as M1- or M2-specific seen in

Figure 2.2C. Again, the NFκB, JUND, STAT1, and STAT5 TFs had more footprints in M1 than M2; RUNX and MEF2 families of TFs had more footprints in M2 than M1 (Figure S2.2C). The PU.1-IRF (CGGAAGTGAAAC) and the IRF1 (GAAAGTGAAAGT) motifs were enriched in the M1 subtype (Figure S2.2C). PU.1-IRF play important roles in macrophage transcriptional response to IFN-γ (Langlais et al., 2016). In summary, we found that distinct subsets of TF are associated with M1 and M2 polarization in our model.

We compared chromatin accessibility between M1 and M2 cells at 3, 12, and 24 hours to investigate temporal changes in the chromatin landscape leading to altered gene regulation upon polarization to M1 or M2 macrophages (Figure 2.2D). At the 3-hour time point, we detected 173 genes more open in M1 than M2, and 114 genes more open in M2 than M1 ($log_2FC > 1$, FDR < 0.05), indicating some early changes in gene accessibility in response to polarization stimuli (Figure 2.2D). While gene expression changes leading to polarization were established rapidly within the first 6 hours, important chromatin changes occurred later in the time course, after 12 hours (Figures S2.1D & 2.2D). M1 stimuli led to increased *IRF1* accessibility (as early as 3 hours of polarization) that was sustained along the time course. IRF1 is known to induce interferon transcription to drive M1 polarization (Platanitis & Decker, 2018). The core macrophage signature gene *MYO7A* (Puranik et al., 2018) became more accessible in M2 at 3 hours and maintained higher accessibility throughout M2 polarization (Figure 2.2D). TFs MAFF and REL, both induced by LPS signaling (Baillie et al., 2017), became more accessible in M1 than M2 later in the polarization process, at 12 and 24 hours, respectively (Figure 2.2D). TFs ID2 and STAT3 became more accessible in M2 than M1 at 12 and 24 hours post-stimuli, respectively. *ID2* expression increased greatly and its genomic region became more accessible during M2 polarization (Figures 2.2D & 2.2E). Thus, *ID2* is a possible new M2 marker identified in our model.

2.3.3 Integration of transcriptome and chromatin accessibility dynamics during polarization

Since the bulk ATAC-seq and bulk RNA-seq libraries were prepared from the same pool of cells, their transcriptome profiles and chromatin accessibility landscapes are directly comparable. We hypothesized that tightly regulated genes, such as targets of crucial TFs that share similar expression dynamics, would also share similar accessibility dynamics. In order to compare our previously identified open chromatin and gene expression clusters, we used a Pearson's $\chi 2$ test to determine enrichment between each RNA-seq and ATAC-seq cluster (Figure 2.3A). Several linked RNA-seq and ATAC-seq clusters show similar dynamics in expression and accessibility. For instance, Rc2 and Ac13 as well as Rc5 and Ac19 had genes with higher expression and associated regions with chromatin more accessible in M1 (Figure 2.3A). These clusters contained *PU.1* and *IRF9,* respectively, which are consistently higher in M1 over M2. M1-enriched clusters also contained *IRF1, CCL8* and *STAT1*. M2-enriched clusters contained *CSF2, MEF2A* and *IL10RA*, which regulate anti-inflammatory function in macrophages (Shouval et al., 2014). Rc1 and Ac6 as well as Rc1 and Ac7 have higher expression and chromatin accessibility in M2 (Figure 2.3A). These clusters were enriched in *ID2* and M2-specific gene *TIMP1* that is known to respond to M2 cytokine IL-4 (Wang & Joyce, 2010). We therefore detected coordinated changes in chromatin and gene expression for key regulatory factors and polarization markers.

2.3.4 Construction of gene regulatory networks from bulk expression and chromatin footprinting data reveals subtype-specific transcription factor interactions

Based on the results above, we narrowed our GRN construction to a set of 17 transcription factors and 6 signaling molecules that stood out in our analyses. *PU.1/SPI1, NFκB2, STAT1, STAT2, IRF1, IRF7,* and *IRF9* were highly expressed and more accessible in M1, while *IL10RA,*

MEF2A, *ID2*, *CSF2,* and *TIMP1* were highly expressed and more accessible in M2 (Figures 2.3A & 3B). The specific role of PU.1 during macrophage polarization is unclear. However, one study has shown that a microRNA suppressing *PU.1* promotes M2 polarization (Li et al., 2018). Another study has demonstrated that knockout of *PU.1* leads to a decrease in NFκB activation and subsequent inflammation, a M1-specific process (Karpurapu et al., 2011) suggesting that PU.1 plays an important role during M1 polarization.

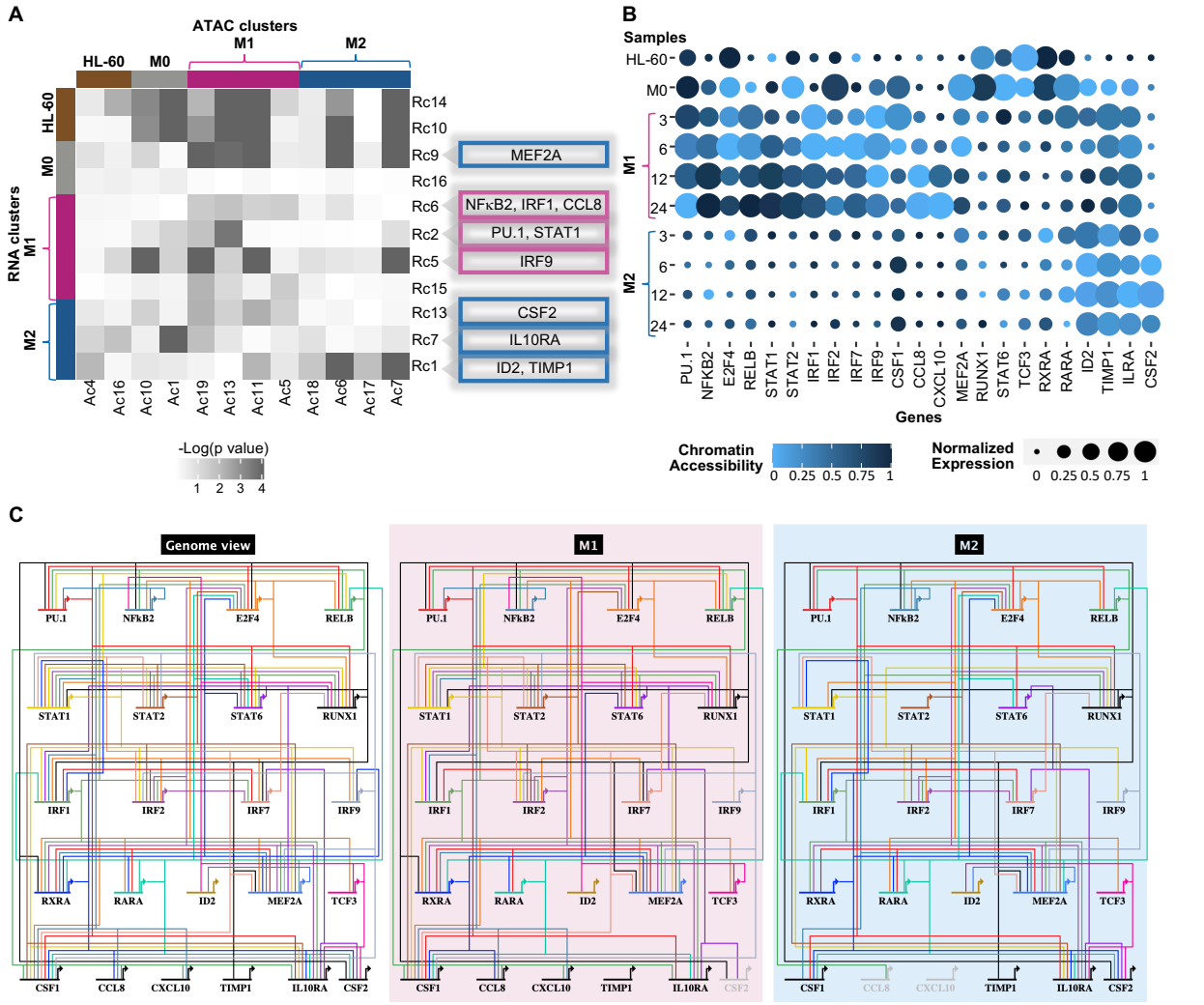

Figure 2.3 Bulk RNA-seq and ATAC-seq derived gene regulatory networks reveal subtype-specific transcription factor interactions
A) Heatmap of enrichment between each RNA-seq and ATAC-seq cluster calculated using Pearson's $\chi 2$ test. Examples of matching M1-enriched and M2-enriched clusters are indicated in grey.

B) Bubble plot of gene expression and chromatin accessibility within the promoter region of key TFs and signaling molecules. Increasing size of the bubble indicates a higher signal in gene expression (TPM scaled across all samples) and a darker blue color indicates higher signal in chromatin accessibility (TMM normalized counts scaled across all samples).
C) Gene regulatory networks containing 17 transcription factors and 6 signaling molecules generated from ATAC-seq footprinting and gene expression in bulk RNA-seq data. Genome view shows all connections identified. M1 and M2 panels show the connections specific to each cell type. Each color is specific to a transcription factor that regulates multiple targets.

We merged all time points for M1 and M2 ATAC-seq datasets to achieve >200 million reads needed for chromatin footprinting analysis, as aforementioned. We identified 145,332 footprints in M1 and 148,348 footprints in M2 using the Wellington algorithm (Piper et al., 2013). These footprintings were used to build subtype-specific GRNs (see Methods) focused on our 23 genes of interest represented as circuit diagrams (Figure 2.3C). At the "genome view" level we identified 141 interactions, which includes 48 total detected in M0 (6 specific), 110 total detected in M1 (40 specific) and 88 total detected in M2 (17 specific); 78 of the 141 connections are shared between some combination of M0/M1/M2. We have previously described the M0 GRN (Ramirez et al., 2017), and therefore focused on M1 and M2 interactions (Figure 2.3C "M1" & "M2"). As expected, we captured several well-known interactions, such as the PU.1 auto-regulatory feedback loop, RUNX1 regulation of *PU.1*, and STAT1 regulation of *IRF1* (Zenke et al., 2018; Lie-A-Ling et al., 2014; Laslo et al., 2006) (Table S1). We decided to also incorporate ID2, which is an inhibitor of some basic helix-loop-helix-containing transcription factors such as *TCF3* (*E2A*) and *TCF12* (*HEB*) even though it does not bind directly to DNA and thus does not have a motif (Rautela et al., 2019). Interestingly, MEF2A binds to *ID2* during M2 polarization, but not during M1 (Figure 2.3C). Three out of the five TFs targeting *PU.1* in our model (PU.1, RUNX1, and RELB*)* have been confirmed in previous studies (Table S1) and their links to *PU.1* are detected in both M1 and M2 GRNs. The targeting of *PU.1* by NFκB2 was M1-specific. The binding motifs

for NFκB1 and NFκB2 are nearly identical and we selected *NFκB2* in our networks because it is expressed ~15-fold higher than *NFkB1* in M1. Moreover, *NFkB2* expression is ~18-fold higher in M1 than in M2 and is therefore an M1-specific TF. This indicates that in our system, the *NFkB* pathway is upregulated specifically in the M1 subtype and plays a key role in regulating other transcription factors such as PU.1. In addition, the binding partner of *NFkB2* (p100), *RELB*, is expressed ~1.5-fold higher than *RELA* in M1 and *RELB* expression is ~10-fold higher in M1 than M2. This indicates that in our system, the noncanonical *NFkB* pathway is upregulated specifically in the M1 subtype and plays a key role in regulating other transcription factors such as PU.1 (Figure 2.3C).

2.3.5 Single-cell heterogeneity during macrophage polarization reveals distinct activation trajectories

We isolated and sequenced single cells representing each polarization time point seen in Figure 2.1A using the microfluidic Bio-Rad ddSEQ platform (see Methods) to examine how individual macrophages respond to stimuli. After filtering out low-quality cells, our final dataset contained 18,363 single cells representing subtypes of HL-60 and M0 as well as cells from M1 and M2 polarization time courses (Table S2). A UMAP of 9,993 cells that passed the threshold for the RNA velocity analysis described below showed clear subtype-specific clustering with six distinct cell populations or "Paths" (Figure 2.4A). HL-60 and M0 cells were enriched in Paths 1 and 2, respectively. Path 3 contained subsets of M1 and M2 time points, whereas Path 4 mainly contained subsets of M0, M1, and M2 cells (Figure 2.4B). Paths 5 and 6 were enriched for terminally polarized M1 and M2, respectively. Next, we used Monocle to identify a pseudotime course of macrophage polarization (X. Qiu et al., 2017) to further verify our clustering and

reconstruct the main trajectories of these populations (Figure 2.4C). Paths 5 and 6 were located at the end of two distinct trajectories, thus constituting terminally polarized M1 and M2, respectively. The terminally polarized M1 population contained subsets of all M1 time points (3-, 6-, 12- and 24-hours post-stimuli). Similarly, the terminally polarized M2 population contained subsets of all M2 time points. We thus found that subsets of macrophages respond rapidly to stimuli and our time points contain mixtures of cells at different degrees of polarization.

Paths 3 and 4 were located between M0-M1 and M0-M2 trajectories, suggesting that these cells are transitional cell types (Figure 2.4C). In addition, we applied RNA velocity (see Methods, Figure S2.3A) which uses the ratio of unspliced to spliced reads to infer differentiation trajectories represented as a vector whose amplitude and direction depict the future transcriptional state of each cell or group of cells (Figure 2.4A). This analysis revealed that Path 3 displayed long velocity vectors pointing back towards Path 2 (M0-specific). Moreover, Path 3's unspliced signal for M1 and M2 markers were similar to Path 2's (M0) unspliced signal for those markers, indicating that Path 3 was regressing towards the naïve M0 state (Figure 2.4D). This suggests that Path 3 represented macrophages that do not respond to stimuli and tend to maintain a naïve state. We observed that a subset of Path 4 cells was progressing towards Path 5 (M1-specific) and another subset was moving towards Path 6 (M2-specific) based on arrow directions and cluster proximity. Path 4 also showed unspliced reads signal of both M1 and M2 markers (Figure 2.4D). This suggested that Path 4 represented macrophages that could become either M1 or M2. Interestingly, Path 4 showed higher *ATF3* and *ZNF384* TFs activity compared to other paths (Figure 2.4E). Paths 5 and 6 showed higher signal of unspliced reads for M1 and M2 markers, respectively, corroborating that these cells are likely terminally polarized M1 and M2. Our results indicated that there is cell to cell variability in response to microenvironmental stimuli and that our macrophage

subpopulations are heterogeneous. In particular, we found a subpopulation that does not respond to stimulus and tends to maintain an M0 state, a very plastic subpopulation that can polarize

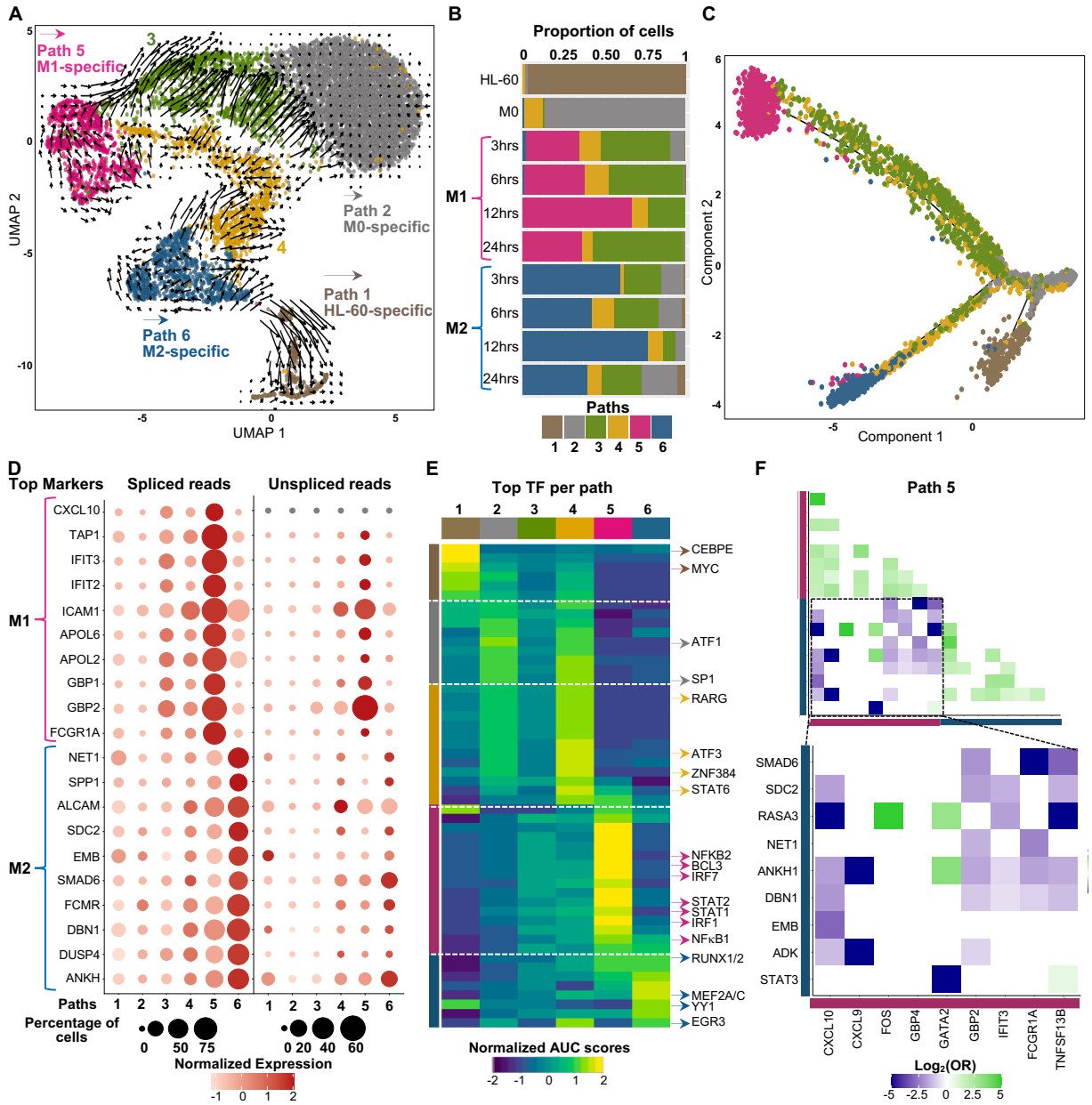

Figure 2.4 Single-cell RNA-seq and pseudotime analysis identify heterogeneous subpopulations of polarizing macrophages

A) UMAP embedding representation of single-cell RNA-seq polarization time course annotated by clusters of subpopulations (Paths). RNA velocity vectors were projected onto the UMAP and indicate future cellular trajectories.

B) Bar plot of the relative proportion of cell subtypes per cluster (Path).

C) Pseudotime trajectory of macrophage polarization colored by clusters. Colors are as noted in B.
D) Bubble chart depicting spliced and unspliced reads for a given gene (row) per Path (column). Circle sizes represent the percentage of cells expressing the gene. Color key represents normalized average expression.
E) Heatmap of AUC scores of transcription factors' activity per cluster estimated by SCENIC. Columns represent clusters and rows represent top transcription factors that are active per cluster.
F) Pairwise odds-ratios (OR) for M1 genes (pink) and M2 genes (blue) detected in Path 5. Odds-ratios that present a p value > 0.05 (calculated by Fisher's exact test) are set to 0. Data shown as $\log_2$(odds-ratio).

towards both M1 and M2, and a subset that responds to microenvironmental stimuli and terminally polarizes towards either M1 or M2.

2.3.6 Subpopulation of terminally polarized M2 macrophages express proliferation genes not observed in the M1 population

We sought to characterize the identity of our single-cell populations (Figure 2.4A) based upon expression of unique HL-60, M0, M1, and M2 markers obtained from our bulk RNA-seq analysis and from the literature. As expected, only Path 1 (HL-60-specific) presented high expression of *TOP2A*, which is a marker of aberrant cellular proliferation in cancer cells, and high levels of *TYMS*, which is known to be highly expressed in HL-60 cells (Pei et al., 2018; Ulger et al., 2003) (Figure S2.3B). M1 stimulation induced *PARP9* that has been shown to promote expression of pro-inflammatory genes (Iwata et al., 2016). Importantly, *P2RY14* gene that is involved in inflammatory signaling and induces cell cycle dormancy was present only in terminally polarized M1/Path 5, corroborating our findings that M1 cells do not continue cycling (Cho et al., 2014). M2 stimulation induced expression of genes *SLA* and *RASA3* which are involved in progression of cell cycle (Dulmovits et al., 2015) (Figure S2.3A). In addition, TF YY1 increases cell proliferation and is more active in M2 (Figure 2.4E). These results combined with ontology

analysis of M2-specific genes identified in our bulk experiments (Figure 2.1E) suggest that M2 macrophages are capable of proliferating, whereas M1 macrophages might not be.

2.3.7 M1 macrophages more strongly express polarization markers than M2

After quantification of spliced and unspliced single-cell reads, we observed that Path 5 (M1) expresses strong signals for both spliced and unspliced M1 markers, while Path 6 (M2) expresses weaker unspliced signals for M2 markers (Figure 2.4D). In addition, M1 showed more active TFs compared to M2 (Figure 2.4E). M1 stimulus led to increased activity of canonical M1 TFs STAT1, STAT2, IRF1, IRF7, NFκB1, and NFκB2. M2 stimulus promoted increased activity of TFs YY1, RUNX1/2 and MEF2A/C. These results suggest that M1 and M2 polarization are regulated by a distinct subset of TFs that is reflected at the single-cell level.

We explored orthogonal expression of M1 and M2 markers in individual single cells by calculating Odds-Ratio (OR) (see Methods) to further survey cell to cell variability in response to stimuli. For instance, we inquired whether a cell expressing a M1 marker X would have reduced probability (Negative OR, p value < 0.05) or increased probability (High/Positive OR, p value < 0.05) of expressing a M2 marker Y. We also investigated which pair of M1 and M2 markers are more likely to be expressed in the same cell (Figures 2.4F & S2.3C). We observed that M1 cells (Path 5) expressing M1-specific chemokines *CXCL10, CXCL9* and signaling molecule *TNFSF13B* are significantly less likely to express M2 markers (Figure 2.4F). Similarly, M1 cells that express M1-specific genes *GBP2*, *IFIT3,* and *FCGR1A* are less likely to express M2 markers (Figure 2.4F). When it comes to M2 cells (Path 6), the pair-wise expression correlations are not as strong (Figure S2.3C), as previously reported (Muñoz-Rojas et al., 2021). This suggests that terminally polarized M1 present a stronger phenotype and are less likely to express M2 markers.

2.3.8 M2 repolarized towards M1 presents a unique transcriptome profile

We addressed whether a polarization switch from M1 to M2 or from M2 to M1 was possible to further evaluate macrophage plasticity and ability to repolarize. Remarkably, we were able to repolarize M2 cells towards an M1 subtype but were unable to repolarize M1 towards an M2 subtype, likely due to a stronger M1 phenotype and low likelihood of expressing M2 genes (Figure 2.4F). We applied fluorescence-activated cell sorting (FACS) to select terminally polarized M2, CD163 high M2 macrophages (SM2) in order to obtain a homogeneous M2 population (Hu et al., 2017). We further repolarized these cells with M1 stimuli LPS and IFN-γ (see Methods). We performed single-cell RNA-seq on M2 repolarized M1 (M2M1). We compared the transcriptome profiles of M2M1 cells with HL-60, M0 in addition to M1, M2 and SM2 (24 hours post-stimuli) and observed the clustering of subpopulations using UMAP (Figure 2.5A). We identified four distinct cell populations or paths (Figures 2.5A & S2.3D). As expected, HL-60 cells were enriched in a unique Path 1R and M0 cells were enriched in Path 2R (Figures 2.5B & S2.3E). Path 3R was mainly enriched in M1 and M2M1 cells and Path 4R was enriched in M2 and SM2. Next, we visualized the main markers identified in each population (Figure 2.5C). M2M1 showed a similar expression pattern as M1 macrophages, suggesting that the populations are transcriptionally very similar. Correspondingly, M2 and SM2 presented similar expression patterns. Unsupervised *in-silico* trajectory reconstruction by Monocle demonstrated that M0 bifurcated into two distinct trajectories that contained mainly M2M1 and M1 or mainly M2 and SM2 (Figure 2.5D). Based on the number of M2M1 cells that clustered with M1 (Figure S2.3E) we determined that approximately 90% of terminally polarized M2 cells repolarized towards an M1 subtype upon LPS and IFN-γ activation. M2M1 expressed M1-specific markers very similarly to M1 macrophages (Figures 2.5E & 2.5F). In addition, M2M1 showed high signal of unspliced M1 markers,

suggesting that their future state is more M1-like (Figure 2.5F). Although M2M1 expressed M1-specific markers, they retained some unique transcriptional differences. M2M1 cells still expressed M2 genes associated with proliferation, such as *CDK1, MCM2,* and *MKI67* (Figure 2.5F). In our model, we observed that M2M1 macrophages acquired an M1-like transcriptome profile but likely maintained M2's ability to proliferate.

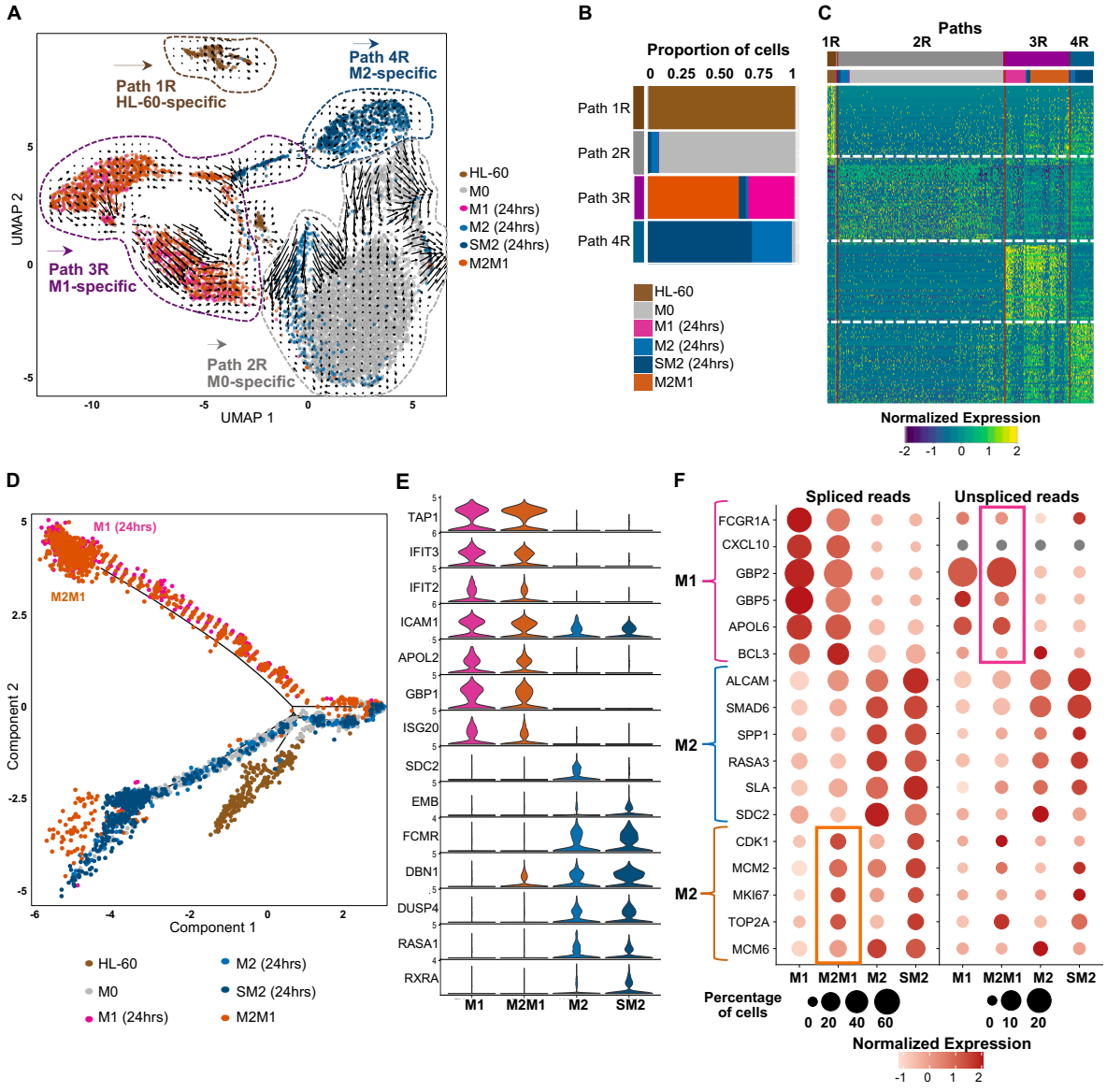

Figure 2.5 M2 repolarized towards M1 presents a unique transcriptome profile
A) UMAP embedding representation of single-cell RNA-seq repolarization time course annotated by time points and clusters of subpopulations (Paths). RNA velocity vectors were projected onto

the UMAP and indicate future cellular trajectories. Brown, grey, pink, light blue, dark blue, and orange represent HL-60, M0, M1, M2, sorted M2 (SM2), and M2 repolarized towards M1 (M2M1) populations, respectively.
B) Bar plot of the relative proportion of cell subtypes per cluster (Path).
C) Heatmap of top differentially expressed genes per cluster. Each column represents a cluster of cells (Path), and each row represents a gene. Expression is row normalized. Column colors are as noted in B.
D) Pseudotime trajectory of macrophage repolarization colored by time points
E) Stacked violin plots of selected M1 and M2 markers. Plot shows markers' expression per cluster.
F) Bubble chart depicting spliced and unspliced reads for a given gene (row) per Path (column). M1- and M2-specific markers were highlighted in pink and blue, respectively. Orange brace highlights proliferation genes expressed in the M2, sorted M2 (SM2), and M2 repolarized towards M1 (M2M1) populations. Circle sizes represent the percentage of cells expressing the given gene. Color key represents normalized average expression.

2.3.9 Single-cell GRN provides additional potential network connections

We built scATAC-seq libraries of subsets of M0, as well as 24-hour polarized M1 and M2 macrophages using the Bio-Rad ddSEQ platform to construct a single-cell GRN using scRNA-seq and scATAC-seq data sets (see Methods). We used the linked self-organizing maps (SOM) strategy (Jansen et al., 2019) to provide additional networking analysis from the single-cell data and compare the results to our bulk GRN. We built separate SOMs and performed metaclustering for each of the scRNA and scATAC datasets separately (Figure S2.4A). Metaclusters were linked by finding the closest gene within 1Mb for each genome region to create a multiclustering (see Methods). These linked metaclusters were each searched for motifs via FIMO (q-value < 0.05) and the motifs were filtered by linked metacluster enrichment (p value < 0.05). This provided a total of ~500,000 unique network connections of which ~36,000 were TF-TF interactions. We identified 135 connections between the 23 genes of our core network (Figure 2.6A). We recovered previously studied interactions including E2F4 regulation of *PU.1*/*SPI1* (Lachmann et al., 2010), PU.1 regulation of *CSF1* (Smith et al., 1996), as well as IRF7*'s* and MEF2A's auto-regulatory loops (Ning et al., 2005; Ramachandran et al., 2008) (Table S1). The predicted auto-regulatory

loop for *IRF1* was also an interesting finding considering the well-known feed-forward loop behavior seen in the IRF1-*STAT1* regulatory system (Michalska et al., 2018).

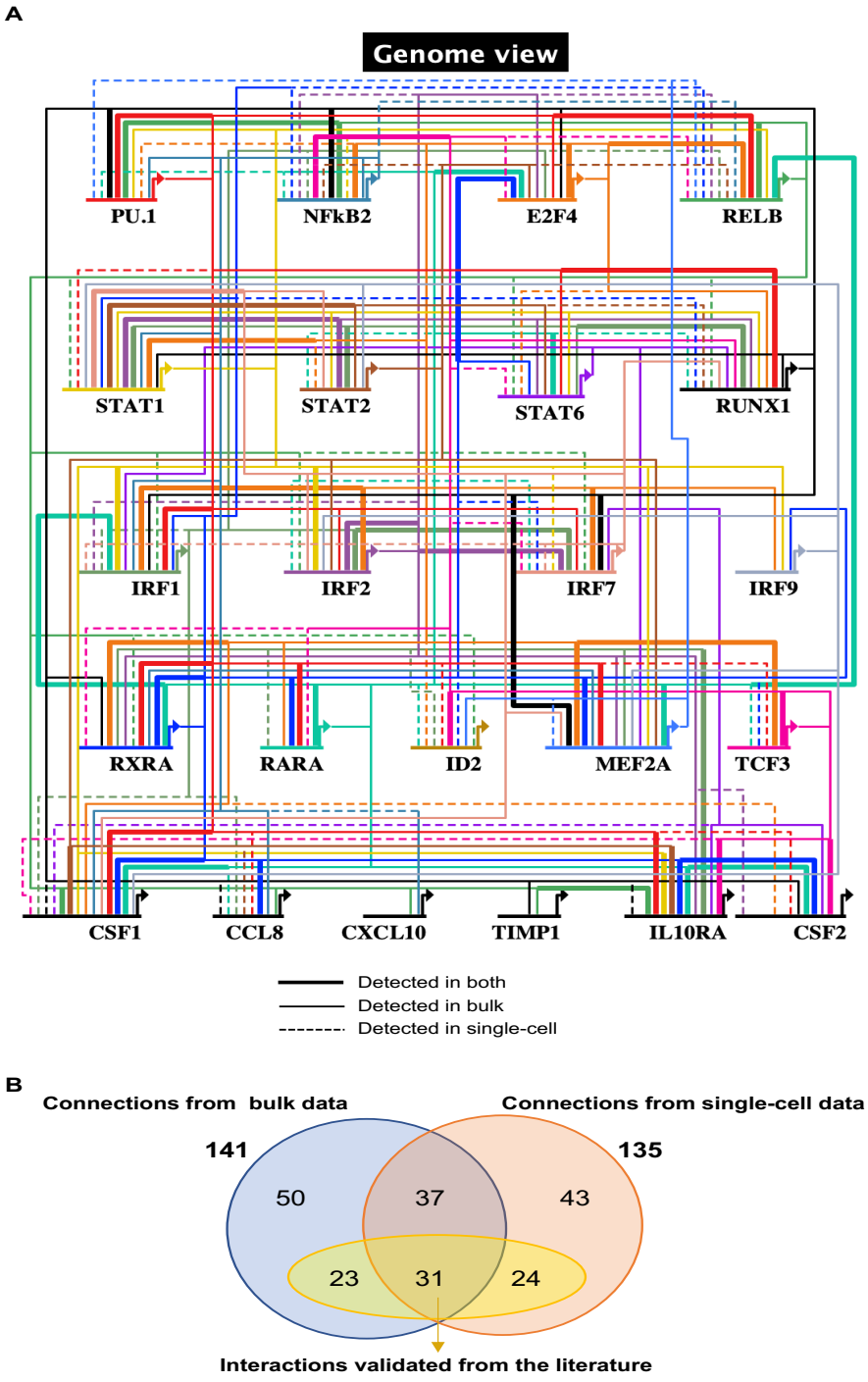

Figure 2.6 Comparison of single-cell-derived connections and bulk-derived connections
A) Gene regulatory networks containing 17 transcription factors and 6 signaling molecules. Genome view shows connections identified in the single-cell GRN, in the bulk GRN and

connections identified by both methods. Solid bold lines indicate connections detected using both single-cell and bulk methods; solid lines indicate connections detected using the bulk method only; dashed lines indicate connections identified using the single-cell method only. Each color is specific to a transcription factor that regulates multiple targets.
B) Venn diagram of total number of connections detected using bulk analysis (blue) and single-cell analysis (orange) as well as the overlaps between both methods. Yellow diagram highlights the connections confirmed by previous studies.

Footprinting analysis of bulk data identified a total of 141 connections, whereas SOM linking analysis of single-cell data identified 135 connections (Figure 2.6B). Comparison of the SOM linking-derived connections to those identified from the bulk analysis found that around half of these connections (68) overlapped. Overall, our single-cell-derived GRN identified 55 known interactions and 80 novel candidate interactions that regulate macrophage polarization, whereas our bulk-derived GRN identified 54 known interactions and 87 novel candidate interactions that regulate macrophage polarization. However, neither approach recovered all previously validated interactions from the literature, and the combined network is more complete than either strategy alone.

2.3.10 Validation of GRN connections using siRNA in M2 polarization

We decided to confirm some of our M2 polarization GRN predictions using siRNA knockdown (KD) of four transcription factors of interest – IRF1, IRF7, IRF9, and ID2 (Figure 2.7A). We chose to perturb M2 since it has been less studied, and our predicted targets presented unique links that are M2-specific. For instance, *IRF1* is targeted by RARA only in M2; *IRF7* is targeted by PU.1, IRF1, and IRF2 only in M2 (Figures 2.3C & 2.6A). Therefore, we perturbed IRF1, IRF7, and IRF9 to explore their regulatory roles during M2 polarization. Moreover, we sought to explore which genes were affected by $ID2^{KD}$ since our results showed that it might play an important role in M2 polarization.

We profiled bulk gene expression and chromatin accessibility after 24 hours of siRNA and M2 polarization stimuli (see Methods). We observed that chromatin became significantly less accessible in genomic regions associated with our KD targets *IRF1*, *IRF7*, *IRF9* and *ID2* (Figures 2.7B & S2.5A). Similarly, the expression of *IRF1*, *IRF7*, *IRF9*, and *ID2* was reduced compared to controls, confirming the successful knockdown (Figures 2.7C & S2.5B). $ID2^{KD}$ downregulated 927 genes and upregulated 110 genes (Figure S2.5C). ID2 is known to repress *TCF3* and its expression increased in $ID2^{KD}$ M2 (Figure 2.7C). Importantly, $ID2^{KD}$ led to overexpression of M1-specific genes, such as *STAT1*, *STAT2*, and *NFκB2* suggesting that ID2 might repress important M1 markers during M2 polarization (Figures 2.7C & S2.5B). Differential motif enrichment calculated in regions whose chromatin accessibility changed upon knockdown showed that $ID2^{KD}$ and $IRF9^{KD}$ affected regions that contain similar motifs (Figures 2.7D & 2.7E). The chromatin regions that became less open upon ID2 reduction or IRF9 reduction were enriched in JUNB/C, ATF3, and BATF3 motifs (Figure 2.7E).

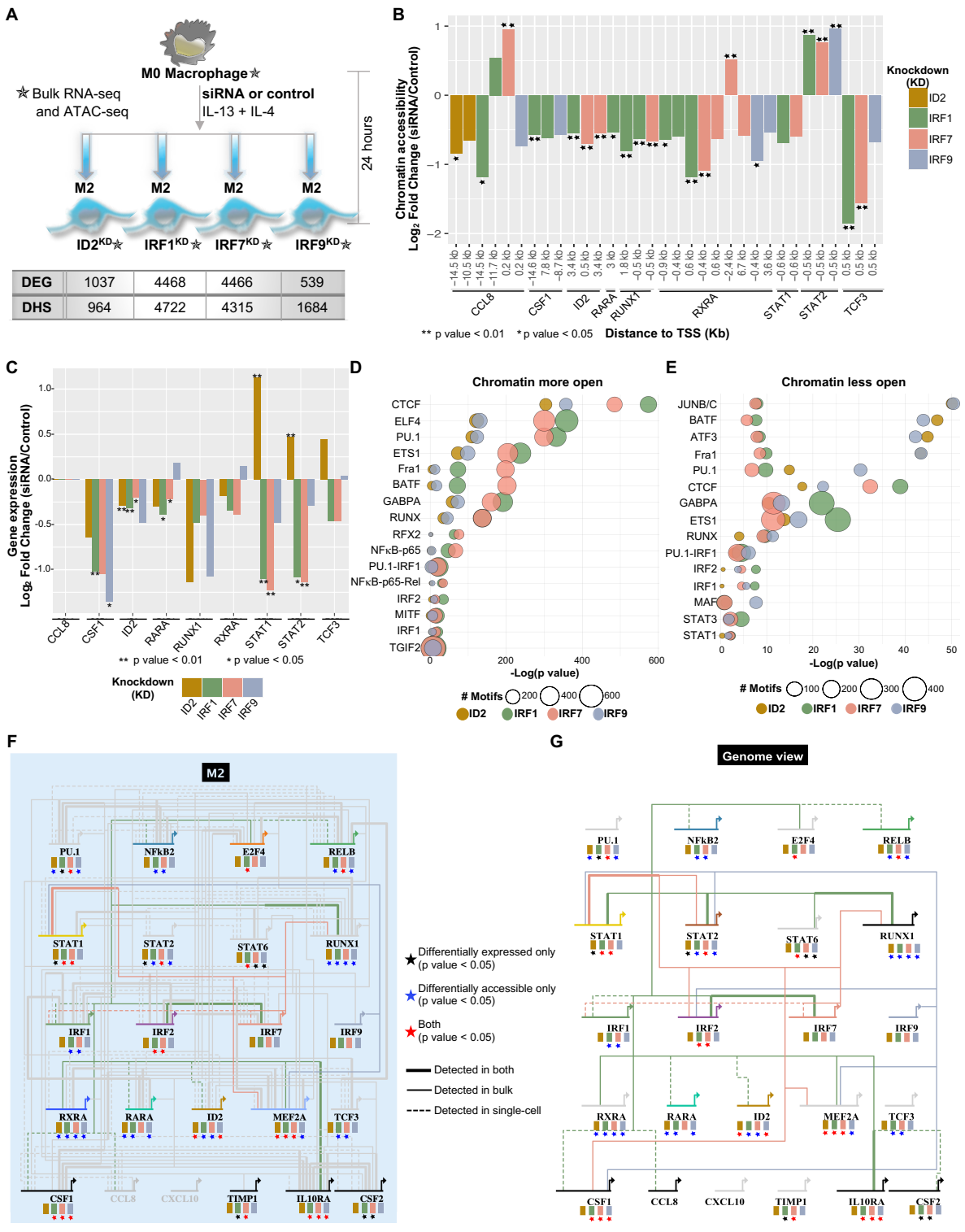

Figure 2.7 IRF1, IRF7, IRF9, and ID2 regulate distinct subsets of transcription factors during M2 polarization

A) Perturbation assays pipeline: M0 macrophages were treated with IRF1, IRF7, IRF9, ID2, or control siRNAs combined with M2-specific stimuli (IL-13 and IL-4). Cells were harvested 24

hours post-siRNA treatment. Table indicates the number of differentially expressed genes (DEG) and the number of differentially open regions of chromatin (DNase I hypersensitive sites - DHS) per knockdown.
B) Chromatin accessibility fold change (log_2) between $ID2^{KD}$, $IRF1^{KD}$, $IRF7^{KD}$, $IRF9^{KD}$, and control conditions ($log_2FC > 0.5$) is shown for a partial list of regions associated with genes (15kb+/-) depicted in the gene regulatory networks of macrophage polarization. The distance from the chromatin element to the start of each gene is indicated. Differential accessibility is indicated $*p$ value < 0.05, $**p$ value < 0.01.
C) Gene expression fold change (log_2) between knockdowns and control is shown for a partial list of genes depicted in the gene regulatory networks of macrophage polarization. Differential expression significance was calculated using biological replicates (see Methods). $*p$ value < 0.05, $**p$ value < 0.01.
D) Motif enrichment in regions that became more accessible upon $ID2^{KD}$, $IRF1^{KD}$, $IRF7^{KD}$, and $IRF9^{KD}$. Circle sizes represent the number of motifs for the given transcription factor (y axis). Each color represents the TF that was knocked down.
E) Motif enrichment in regions that became less accessible upon $ID2^{KD}$, $IRF1^{KD}$, $IRF7^{KD}$, and $IRF9^{KD}$. Circle sizes represent the number of motifs for the given transcription factor (y axis). Each color represents the TF that was knocked down.
F) Bulk M2-focused GRN (Figure 2.3C) centered on knockdown TFs. Links originating directly from IRF1, IRF7, or IRF9 are colored by green, pink, or blue, respectively, while all other links are in grey for simplicity. Target genes are colored if the single-cell analysis predicted a regulatory connection between the knockdown TF and the target gene. Any link present in both the bulk and the single-cell networks is in bold. The banners underneath each gene correspond to each knockdown (ID2 in gold, IRF1 in green, IRF7 in pink, IRF9 in blue). The stars represent the significance of the knockdown in both RNA-seq and ATAC-seq for that gene. Black stars indicate the gene is differentially expressed upon knockdown ($p < 0.05$), blue stars indicate differential chromatin accessibility determined by at least 1 region in 15kb+/- TSS (p value <0.05), and red stars indicate the gene is both differentially expressed and accessible.
G) Single-cell-focused GRN (Figure 2.6A) centered on knockdown TFs. Target genes are colored if the single-cell analysis predicted a regulatory connection between the knockdown TF and the target gene. Differential expression and accessibility for each gene are noted as in F. Regulatory connection lines and colors are in the same style as in F.

The number of chromatin regions that became more or less open upon $IRF1^{KD}$ was very similar to the number for $IRF7^{KD}$ (Figure S2.5D). In addition, chromatin regions that became more open upon $IRF1^{KD}$ or $IRF7^{KD}$ contained similar motifs, such as CTCF, ELF4, and PU.1 (Figure 2.7D). These results suggest that IRF1 and IRF7 might have similar regulatory roles during M2 macrophage polarization (Figures 2.7D & 2.7E). We found that several predicted IRF1 targets identified in our GRN showed significant changes in expression and/or chromatin accessibility

upon *IRF1* knockdown. Such potentially confirmed targets include *IRF2, IRF7, RUNX1,* and *IL10RA,* which were predicted to be IRF1 targets in M2 in both bulk and single-cell GRNs, as well as *RXRA* and *MEF2A* (detected in the bulk GRN), and *CSF1* and *ID2* (detected in the single-cell GRN) (Figures 2.7F & 2.7G). Similarly, IRF7 was predicted to target *RUNX1* (detected in the bulk GRN) and *IRF1* (detected in the single-cell GRN), which both showed changes in chromatin accessibility and/or gene expression upon IRF7 reduction. Some differences in expression and chromatin accessibility upon knockdown of our targets can also be explained by indirect TF regulation. *PU.1* expression significantly changes upon *IRF1* knockdown (Figure 2.7F). Although we did not identify *PU.1* as a direct IRF1 target, MEF2A is a predicted IRF1 target (detected in the bulk GRN) that seems to regulate *PU.1* expression (detected in the single-cell GRN) (Figures 2.6A & 2.7F). *MEF2A* expression significantly decreased in our IRF1^{KD} in M2, thus potentially explaining *PU.1* expression changes. Also, IRF7^{KD} led to changes in gene expression and chromatin accessibility in *IL10RA*, which is not a direct IRF7 target. However, STAT1 is a potential IRF7 target whose expression and chromatin accessibility change in IRF7^{KD} and therefore likely explains the expression changes of the STAT1 predicted target *IL10RA* (Figure 2.7F). In summary, our perturbations provided significant evidence to key connections identified in our bulk and single-cell GRNs by direct or indirect TF interactions.

2.4 Discussion

Defining the gene regulatory networks that underlie cellular maturation in response to stimuli is a challenging task. A previous study used network modeling software on published gene expression data to identify macrophage polarization regulators (Palma et al., 2018). Although it highlighted important players in the M1/M2 activation, it did not identify the main TF-target

interactions that underlie the process. Our bulk footprinting-derived GRN revealed distinct and subtype-specific TF-target connections between 23 polarization genes. M1 had 40 unique connections, and M2 had 17 unique connections; 63 connections were shared between M1 and M2, suggesting a large concordance between the M1 and M2 polarization pathways. In addition, some polarization markers seem to play distinct roles in both M1 and M2 GRNs. We captured the known activation of *IRF1* by STAT6 in the M1 GRN, but not in M2 (Miller et al., 2019). *STAT6* is a well-known marker of M2, while *IRF1* is a pro-inflammatory marker of M1. Our identified connections implied that STAT6 may still have a regulatory role in driving a pro-inflammatory response in M1 that is absent in M2. Around 32% (23 of 73) of our bulk-specific interactions have been confirmed in previous studies, and 68% are novel candidate interactions.

As regulatory genomics is rapidly adopting single-cell methods, we sought to verify whether single-cell techniques would reproduce or improve our bulk RNA-seq and ATAC-seq derived networks. Our single-cell GRN identified 135 connections, of which 68 overlapped our bulk GRN. It identified 67 connections not found using bulk data, whereas bulk analysis identified 73 connections not found in the single-cell GRN. Similar to our bulk GRN, around 36% (24 of 67) of our single-cell-specific interactions have been confirmed by the literature and 64% are novel candidate interactions. Around 46% (31 of 68) of the links predicted by both methods have been confirmed in previous studies, which is a higher percentage compared to each method separately.

Using our bulk data sets, we detected rapid changes in gene expression as early as 3 hours post polarization. Large chromatin accessibility changes during polarization were detected later in the time course, similar to results seen during macrophage differentiation (Ramirez et al., 2017). *FCGR1A*, whose expression is increased in immuno-inflammatory syndromes (Minar et al., 2014), reacted to M1, but not M2 stimuli as early as 3 hours of polarization. Therefore, *FCGR1A* is a

possible target to modulate M1 polarization for therapeutics of inflammatory disorders (Thepen et al., 2009). In turn, *CSF2* reacted to M2 stimuli but not M1 as early as 3 hours. *CSF2* is a potential candidate target to alter M2 polarization through modulation of autophagy and could possibly be a target for cancer therapeutics (P. Chen et al., 2014). Overall, our results provide early, intermediary and late polarization markers that could facilitate the manipulation of macrophages to desired polarized states and could therefore reveal novel therapeutic targets for cancers and immune diseases.

ID2 is an important regulator of macrophage development *in vivo* and *in vitro*. $ID2^{KD}$ mice lacked specialized skin macrophages, called Langerhans cells (Hacker et al., 2003). However, ID2 has never been explored as a macrophage polarization marker. Given its increased expression and chromatin accessibility during our M2 polarization time course, we suggest that it can be a novel marker of M2 polarization. Additionally, we found that $ID2^{KD}$ led to overexpression of M1 markers suggesting it may induce the M2 lineage by suppressing M1 markers.

M0 macrophages' ability to proliferate has been well explored (Daems & De Bakker, 1982), but it is less clear whether M1 or M2 can proliferate. Skin resident macrophages are able to proliferate in order to maintain the tissue population throughout life (Hacker et al., 2003). However, during inflammatory conditions, macrophages were unable to proliferate and were instead replaced by circulating monocytes (Dieu-Nosjean et al., 2000). In our model, M1 expressed genes linked to cell cycle dormancy suggesting that M1 did not enter the cell cycle, similar to what has been seen in inflammatory contexts. On the other hand, our M2 cells expressed proliferation genes not seen in M1 and thus seemed to proliferate. A previous study has shown that macrophage proliferation is a hallmark of T Helper 2 signaling and is linked to IL-4, which corroborates our findings (Jenkins et al., 2011). These results suggested that macrophage

proliferation is directly linked to microenvironmental stimuli. Thus, naïve M0 and M2 stimulated by IL-4 are able to proliferate, whereas M1 stimulated by inflammatory signals are not. Notably, despite acquiring an M1-like transcriptome, our M1 cells that repolarized from M2 maintained expression of proliferative genes. Therefore, M1 cells that were once M2 may inherit proliferative capabilities.

Both bulk and single-cell functional genomics methods used in our studies have advantages and limitations that will shape the resulting networks. The bulk footprinting method we used is known to show high efficiency, but it relies on protein occupancy, which may not detect TFs with short-lived binding. Hence, important polarization TFs such as NFκB, which are very dynamic, do not always leave footprints in bulk chromatin (Sung et al., 2016). In contrast, single-cell assays face technical challenges, including resolution, sparsity and number of genes detected. This last limitation is present in our analysis due to 3' tagmentation methods that produce dropouts. For example, we were unable to detect *PU.1* reliably in our scRNA-seq experiments, which severely restricted our ability to detect its connections in the single-cell GRN. Therefore, neither method alone was able to predict all known interactions, and more complete results were obtained by a combination of both bulk and single-cell GRNs.

In summary, our findings provide a clearer understanding of the heterogeneity of the cells that undergo M1 and M2 polarization and M2 to M1 repolarization. We identified transient polarization markers and found that ID2 is a novel M2 TF. We constructed *de novo* GRNs containing both known and novel interactions that underlie M1 and M2 polarization. It will be interesting to investigate how much of this polarization network is conserved across heterogeneous tissue-resident macrophages in health and disease, especially in the context of microglial polarization in AD. In conclusion, we believe that despite the revolution and the great potential of

single-cell biology, bulk results are still needed for building more comprehensive and accurate GRNs where practical, i.e., where we can isolate relatively pure cell types for bulk assays. We expect that insights gained from this work will provide experimental and computational guidelines for building GRNs of cellular maturation in response to microenvironmental stimuli.

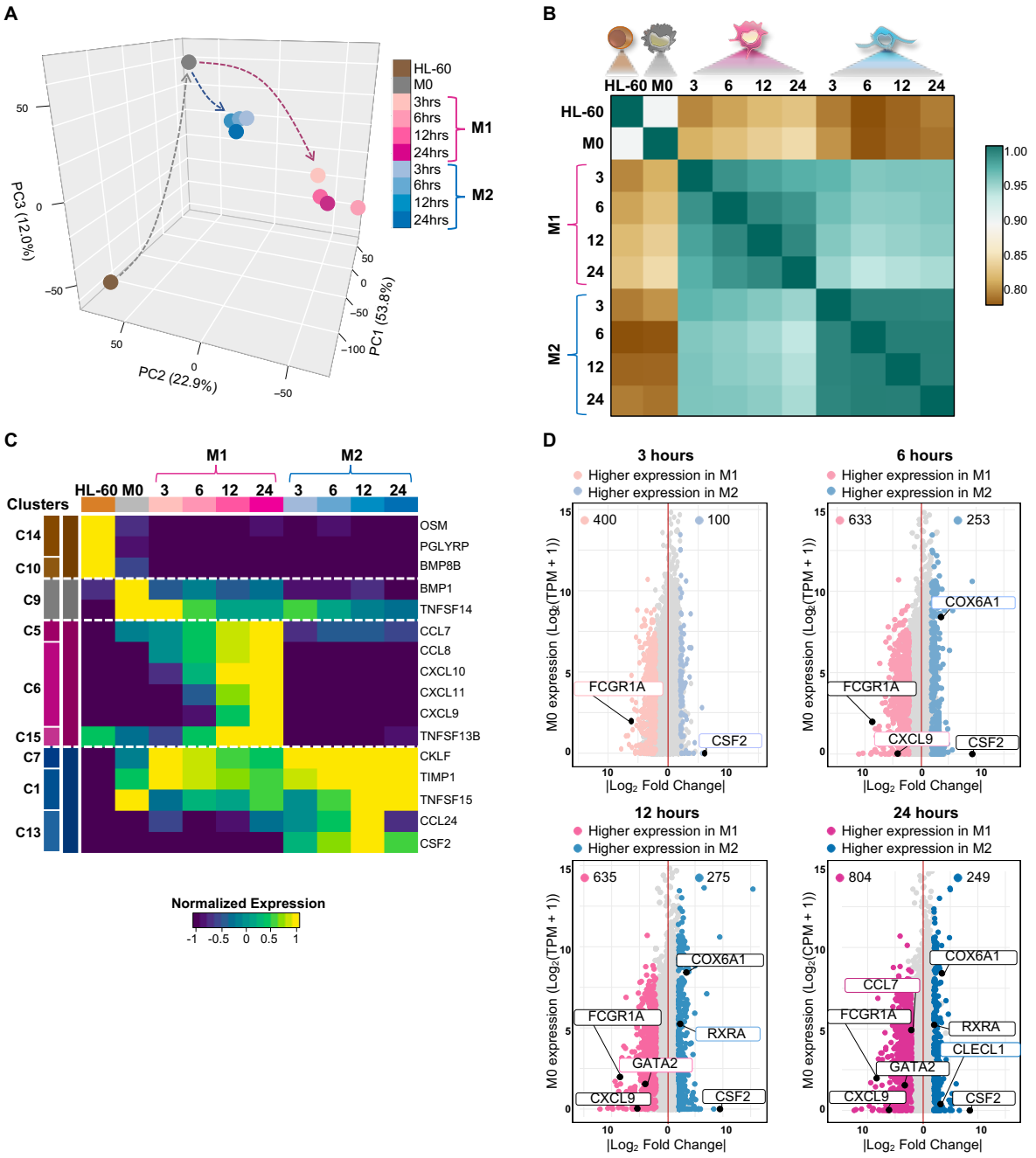

Figure S2.1 Characterizing temporal changes in gene expression during macrophage polarization

A) Principal component analysis of the RNA-seq time course of macrophage polarization. Time points were connected to illustrate subtype-specific trajectories. Cell types are depicted in distinct colored points.

B) Pearson correlation analysis of the RNA-seq time course of macrophage polarization**.**

C) Heatmap of signaling molecules included in HL-60-, M0-, M1- or M2-specific clusters identified by MaSigPro. Each column represents the average expression for a time point and each row represents a signaling molecule. RNA-seq data is row-mean normalized.

D) Genes differentially expressed between M1 and M2 time points ($log_2FC > 1$, FDR < 0.05) compared to normalized M0. M1- and M2-specific genes FCGR1A, CSF2, CXCL9, COX6A1, GATA2, RXRA, CCL7, and CLECL1 are indicated.

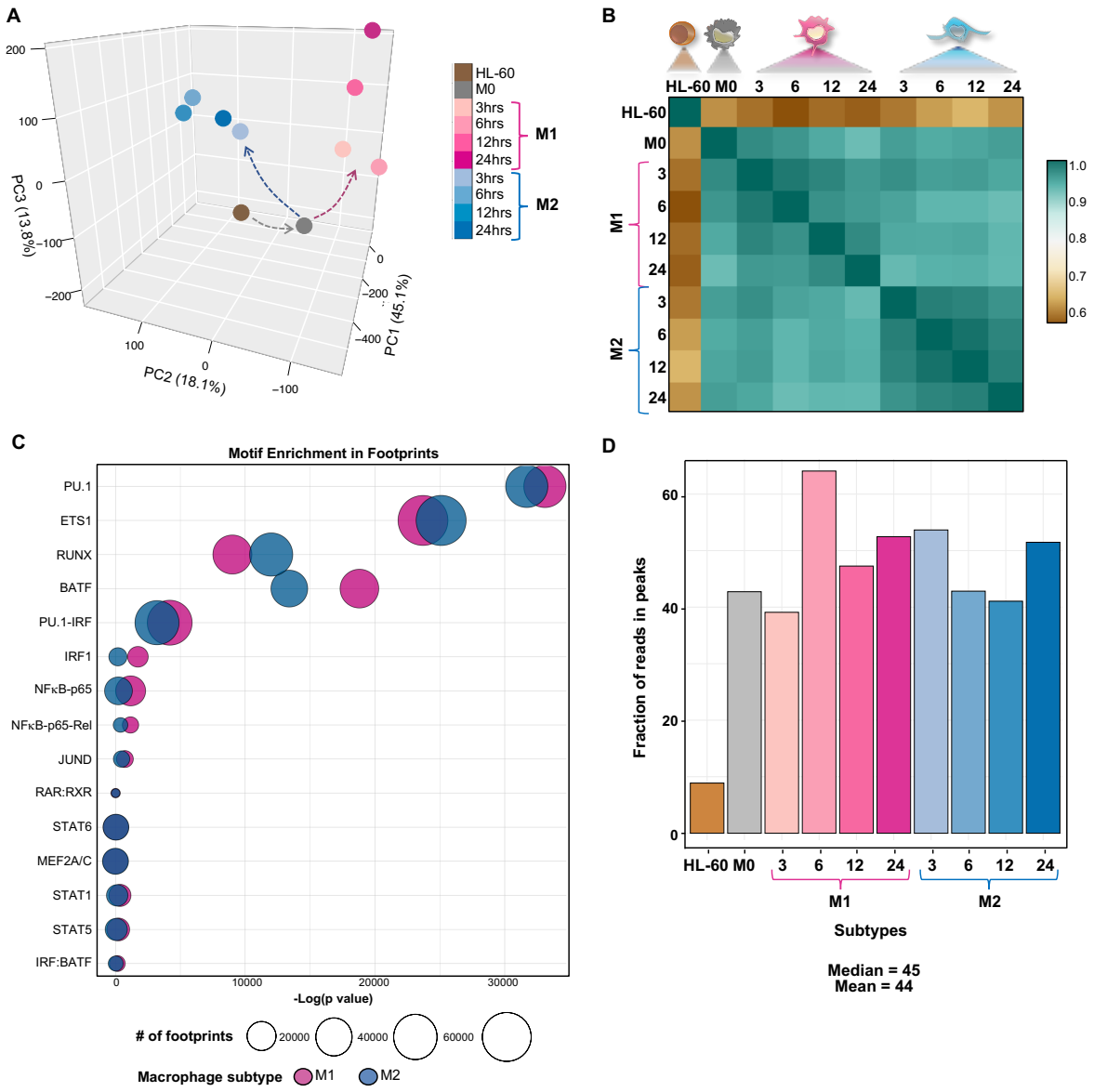

Figure S2.2 Quality assessment of bulk ATAC-seq data

A) Principal component analysis of the ATAC-seq time course of macrophage polarization. Time points were connected to illustrate subtype-specific trajectories. Cell types are depicted in distinctly colored points.

B) Pearson correlation analysis of the ATAC-seq time course of macrophage polarization.

C) Differential motif enrichment between chromatin accessibility footprints in M1 and M2 subtypes compared to each other. Circle sizes represent the number of footprintings for the given transcription factor.

D) Distribution of ATAC-seq fraction of reads in peaks (FRiP). Mean = 44, median = 45.

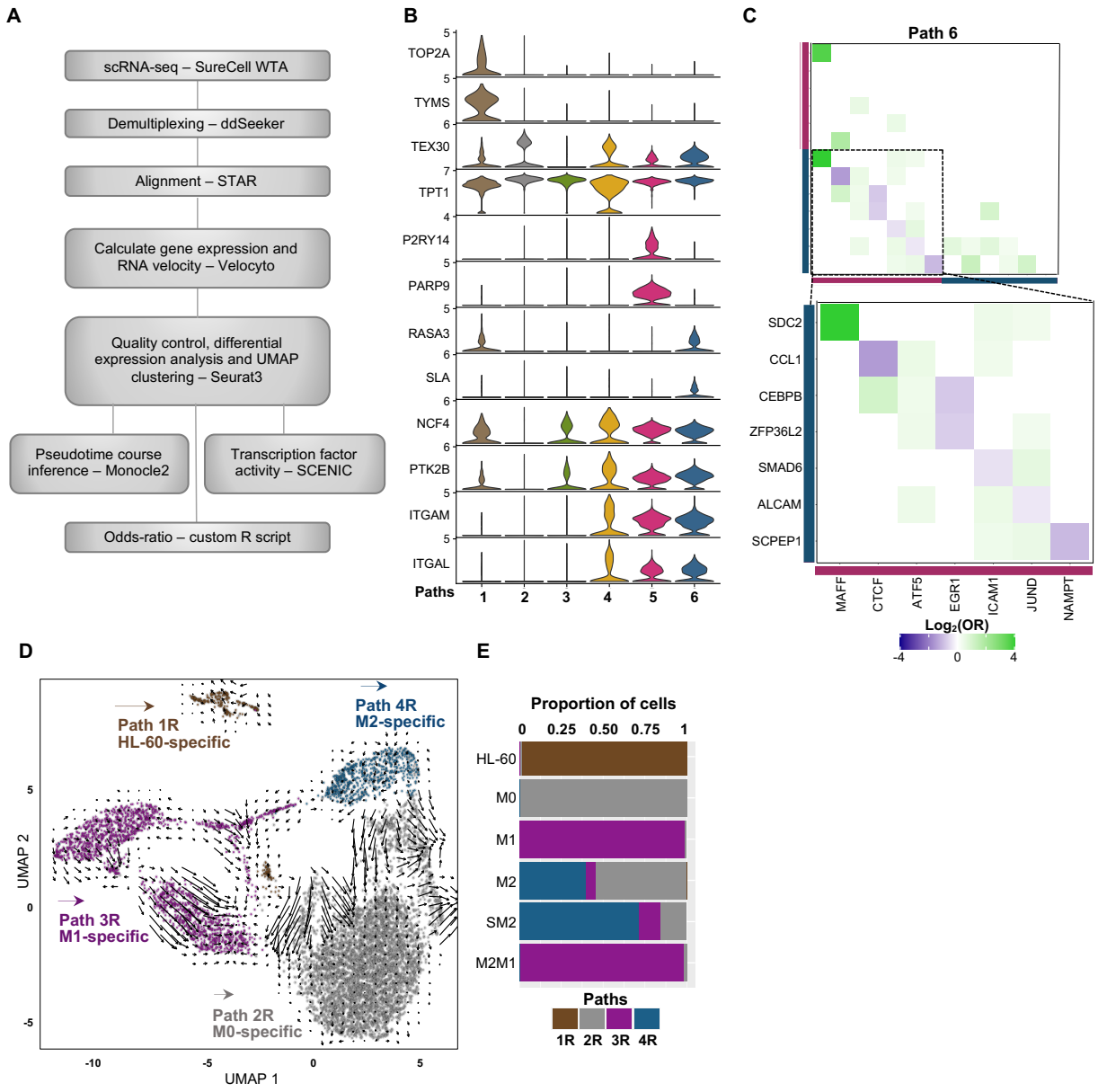

Figure S2.3 Single-cell RNA-seq of macrophage polarization and repolarization
A) Single-cell RNA-seq data analysis pipeline.
B) Stacked violin plots of selected markers' expression per cluster (Path).
C) Pairwise odds-ratios (OR) for M1 genes (pink) and M2 genes (blue) detected in Path 6. Odds-ratios that present a p value > 0.05 (calculated by Fisher's exact test) are set to 0. Data shown as $\log_2$(odds-ratio).
D) UMAP embedding representation of the single-cell RNA sequencing repolarization time course annotated by clusters of subpopulations. RNA velocity vectors were projected onto the UMAP and indicate future cellular trajectories.

E) Bar plot of the relative proportion of cell subtypes per cluster.

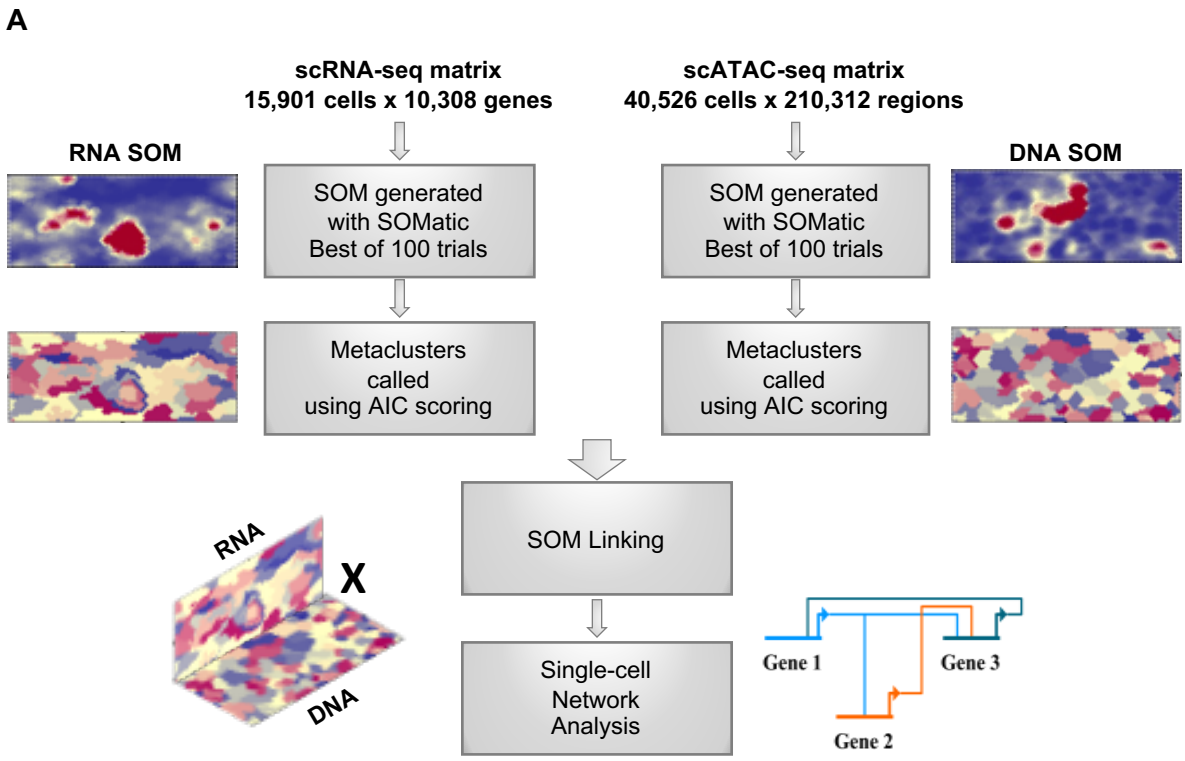

Figure S2.4. Single-cell RNA-seq and ATAC-seq data integration using SOM linking
A) SOM linking data analysis pipeline used to build the single-cell gene regulatory networks.

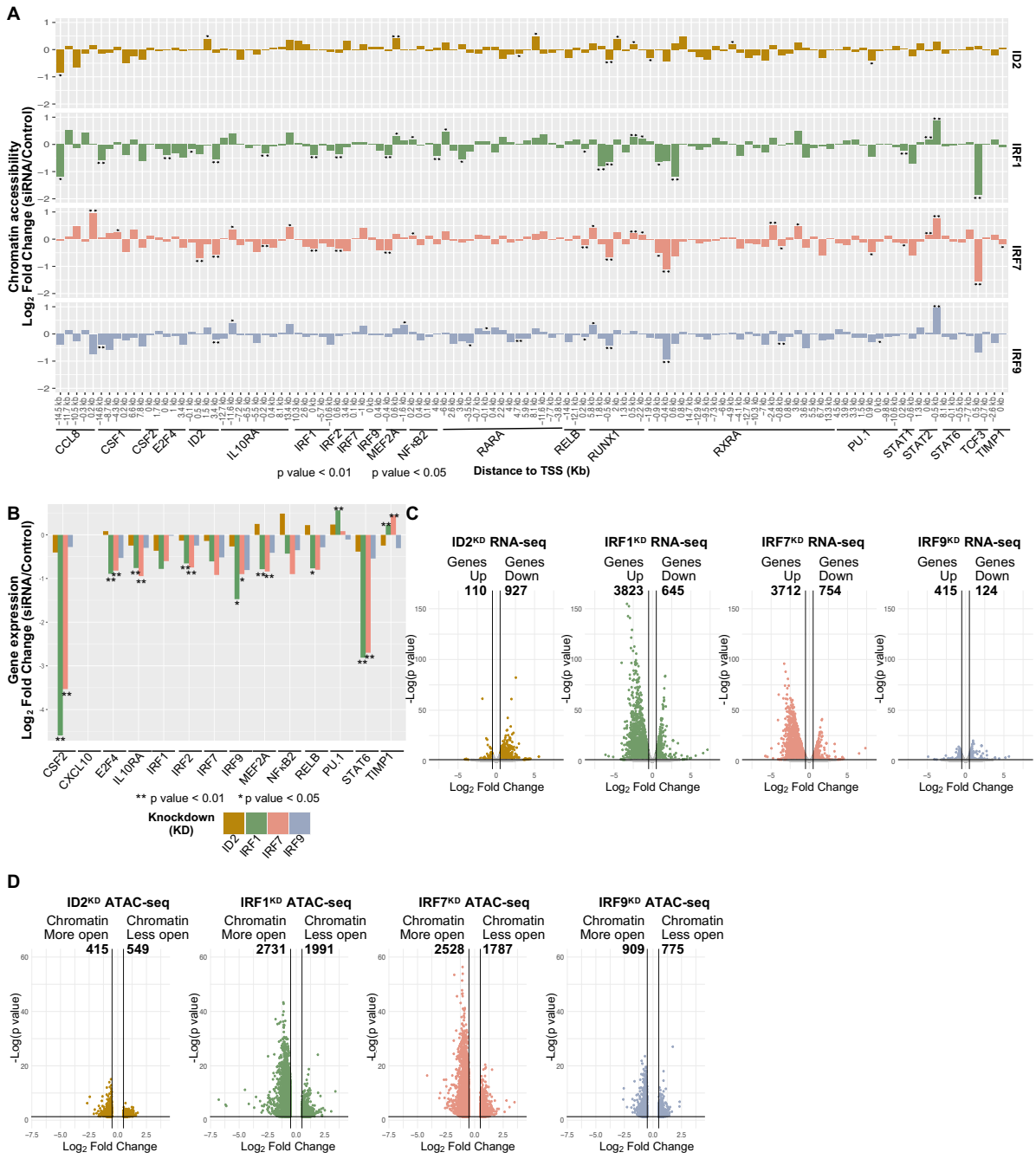

Figure S2.5 Differential gene expression and chromatin accessibility upon IRF1^{KD}, IRF7^{KD}, IRF9^{KD}, and ID2^{KD}

A) Chromatin accessibility fold change (log_2) between ID2^{KD}, IRF1^{KD}, IRF7^{KD}, IRF9^{KD}, and control conditions is shown for regions associated with genes (15kb+/-) depicted in the gene regulatory networks of macrophage polarization. The distance from the chromatin element to the start of each gene is indicated. Differential accessibility is indicated ∗p value < 0.05, ∗∗p value < 0.01.

B) Gene expression fold change (log_2) between knockdowns and control is shown for a partial list of genes depicted in the gene regulatory networks of macrophage polarization. Differential

expression significance was calculated using biological replicates (see Methods). ∗p value < 0.05, ∗∗p value < 0.01.
C) Volcano plot highlighting genes upregulated or downregulated in $ID2^{KD}$, $IRF1^{KD}$, $IRF7^{KD}$, $IRF9^{KD}$. Differentially expressed genes are colored in gold, green, orange, and blue, respectively. p value < 0.05, $|\log_2 FC| > 0.5$.
D) Differential chromatin accessibility between $ID2^{KD}$, $IRF1^{KD}$, $IRF7^{KD}$, $IRF9^{KD}$, and control conditions. Differentially open regions are colored in gold, green, orange, and blue, respectively. p value < 0.05, $|\log_2 FC| > 0.5$.

Table S2.1 Regulatory interactions that were previously studied

Citations	Interactions	Identified in our data
Bonizzi, G., Bebien, M., Otero, D. C., Johnson-Vroom, K. E., Cao, Y., Vu, D., … Karin, M. (2004). Activation of IKKα target genes depends on recognition of specific κB binding sites by RelB:p52 dimers. EMBO Journal, 23(21), 4202–4210. https://doi.org/10.1038/sj.emboj.760039	RELB auto-regulatory loop	Both
Bren, G. D., Solan, N. J., Miyoshi, H., Pennington, K. N., Pobst, L. J., & Paya, C. V. (2001). Transcription of the RelB gene is regulated by NF-κB. Oncogene, 20(53), 7722–7733. https://doi.org/10.1038/sj.onc.1204868	RELB->IRF7	Single-cell
De Silva, N. S., Anderson, M. M., Carette, A., Silva, K., Heise, N., Bhagat, G., & Klein, U. (2016). Transcription factors of the alternative NF-kB pathway are required for germinal center B-cell development. Proceedings of the National Academy of Sciences of the United States of America, 113(32), 9063–9068. https://doi.org/10.1073/pnas.1602728113; Lovas, A., Radke, D., Albrecht, D., Buket, Z. B., Möller, U., Habenicht, A. J. R., & Weih, F. (2008). Differential RelA- and RelB-dependent gene transcription in LTβR-stimulated mouse embryonic fibroblasts. BMC Genomics, 9, 606. https://doi.org/10.1186/1471-2164-9-606	RELB->STAT6	Single-cell
Dong, X., Craig, T., Xing, N., Bachman, L. A., Paya, C. V, Weih, F., … Griffin, M. D. (2003). Direct transcriptional regulation of RelB by 1α,25-dihydroxyvitamin D3 and its analogs: physiologic and therapeutic implications for dendritic cell function. Biochemistry, (33).	RXRA->NFkB2	Single-cell
El Zein, R. M., Soria, A. H., Golib Dzib, J. F., Rickard, A. J., Fernandes-Rosa, F. L., Samson-Couterie, B., … Boulkroun, S. (2019). Retinoic acid receptor α as a novel contributor to adrenal cortex structure and function through interactions with Wnt and Vegfa signalling. Scientific Reports, 9(1), 14677. https://doi.org/10.1038/s41598-019-50988-2	RARA->TCF3	Single-cell
Fijneman, R. J. A., Anderson, R. A., Richards, E., Liu, J., Tijssen, M., Meijer, G. A., … Cormier, R. T. (2012). Runx1 is a tumor suppressor gene in the mouse gastrointestinal tract. Cancer Science, 103(3), 593–599. https://doi.org/10.1111/j.1349-7006.2011.02189.x	RUNX1->CCL8	Single-cell
Ho, J., Pelzel, C., Begitt, A., Mee, M., Elsheikha, H. M., Scott, D. J., & Vinkemeier, U. (2016). STAT2 Is a Pervasive Cytokine Regulator due to Its Inhibition of STAT1 in Multiple Signaling Pathways. PLOS Biology, 14(10), e2000117. https://doi.org/10.1371/journal.pbio.2000117	STAT2->STAT1	Both
Hohaus, S., Petrovick, M. S., Voso, M. T., Sun, Z., Zhang, D. E., & Tenen, D. G. (1995). PU. 1 (Spi-1) and C/EBP alpha regulate expression of the granulocyte-macrophage colony-stimulating factor receptor alpha gene. Molecular and cellular biology, 15(10), 5830-5845. DOI: 10.1128/MCB.15.10.5830	PU.1->CSF2	Single-cell
I, A., WY, Y., A, F., JJ, C., EA, W., & MR, H. (2014). p75NTR is highly expressed in vestibular schwannomas and promotes cell survival by activating nuclear transcription factor κB. Glia, 62(10). https://doi.org/10.1002/GLIA.22709	TCF3->NFkB2	Both
Ji, M., Li, H., Suh, H. C., Klarmann, K. D., Yokota, Y., & Keller, J. R. (2008). Id2 intrinsically regulates lymphoid and erythroid development via interaction with different target proteins. Blood, The Journal of the American Society of Hematology, 112(4), 1068-1077. https://doi.org/10.1182/blood-2008-01-133504	PU.1->ID2	Single-cell
Koh, C.P., Wang, C.Q., Ng, C.E.L., Ito, Y., Araki, M., Tergaonkar, V., Huang, G., and Osato, M. (2013). RUNX1 meets MLL: epigenetic regulation of hematopoiesis by two leukemia genes. Leukemia 27, 1793–1802.	RUNX1->MEF2A	Both
Kwon, G., & Kang, K. (2020). Transcriptional regulation of IL10 gene in human macrophages.	PU.1->IL10RA	Both
Lachmann, A et al. (2010) ChEA: transcription factor regulation inferred from integrating genome-wide ChIP-X experiments. Bioinformatics. 26:2438-44. - Harmonizome - D R, GW G, NF F, Z W, CD M, et al. (2016) The harmonizome: a collection of processed datasets gathered to serve and mine knowledge about genes and proteins. Database(Oxford) Jul 3;2016	E2F4->NFkB2	Both
Laslo, P., Spooner, C.J., Warmflash, A., Lancki, D.W., Lee, H.J., Sciammas, R., Gantner, B.N., Dinner, A.R., and Singh, H. (2006). Multilineage Transcriptional Priming and Determination of Alternate Hematopoietic Cell Fates. Cell 126, 755–766; Kubosaki, A., Tomaru, Y., Tagami, M., Arner, E., Miura, H., Suzuki, T., Suzuki, M., Suzuki, H., and Hayashizaki, Y. (2009). Genome-wide investigation of in vivo EGR-1 binding sites in monocytic differentiation. Genome Biology 10, R41	PU.1 auto-regulatory loop	Both

Lee et al., (2011) Wide-ranging functions of E2F4 in transcriptional activation and repression revealed by genome-wide analysis. Nucleic Acids Research, Volume 39, Issue 9, https://doi.org/10.1093/nar/gkq1313	E2F4->IRF1	Both
	E2F4->IRF2	
	E2F4->IRF7	
	E2F4->MEF2A	
	E2F4->STAT1	
	E2F3->TCF3	
Lie-A-Ling, M., Marinopoulou, E., Li, Y., Patel, R., Stefanska, M., Bonifer, C., … Lacaud, G. (2014). RUNX1 positively regulates a cell adhesion and migration program in murine hemogenic endothelium prior to blood emergence. Blood, 124(11), 11–20. https://doi.org/10.1182/blood-2014-04-572958	RUNX1->PU.1	Both
Lovas, A., Radke, D., Albrecht, D., Buket, Z. B., Möller, U., Habenicht, A. J. R., & Weih, F. (2008). Differential RelA- and RelB-dependent gene transcription in LTβR-stimulated mouse embryonic fibroblasts. BMC Genomics, 9, 606. https://doi.org/10.1186/1471-2164-9-606	RELB->ID2	Single-cell
Mathelier, A et al. (2014) JASPAR 2014: an extensively expanded and updated open-access database of transcription factor binding profiles. Nucleic Acids Res. 42:D142-7. - Harmonizome - D R, GW G, NF F, Z W, CD M, et al. (2016) The harmonizome: a collection of processed datasets gathered to serve and mine knowledge about genes and proteins. Database(Oxford) Jul 3;2016	IRF2->STAT1	Both
Michalska et al., (2018) A Positive Feedback Amplifier Circuit That Regulates Interferon (IFN)-Stimulated Gene Expression and Controls Type I and Type II IFN Responses. Frontiers in Immunology, https://doi.org/10.3389/fimmu.2018.01135	IRF1->STAT1	Both
Minucci, S., Leid, M., Toyama, R., Saint-Jeannet, J. P., Peterson, V. J., Horn, V., ... & Ozato, K. (1997). Retinoid X receptor (RXR) within the RXR-retinoic acid receptor heterodimer binds its ligand and enhances retinoid-dependent gene expression. Molecular and Cellular Biology, 17(2), 644-655. DOI: 10.1128/MCB.17.2.644	RXRA->RARA	Both
Nair, P. M., Starkey, M. R., Haw, T. J., Ruscher, R., Liu, G., Maradana, M. R., … Hansbro, P. M. (2018, March 1). RelB-deficient dendritic cells promote the development of spontaneous allergic airway inflammation. American Journal of Respiratory Cell and Molecular Biology, Vol. 58, pp. 352–365. https://doi.org/10.1165/rcmb.2017-0242OC	RELB->PU.1	Both
Nakagawa, M., Shimabe, M., Watanabe-Okochi, N., Arai, S., Yoshimi, A., Shinohara, A., … Kurokawa, M. (2011). AML1/RUNX1 functions as a cytoplasmic attenuator of NF-κB signaling in the repression of myeloid tumors. Blood, 118(25), 6626–6637. https://doi.org/10.1182/blood-2010-12-326710	RUNX1->IRF7	Both
Nakanishi, M., Tomaru, Y., Miura, H., Hayashizaki, Y., & Suzuki, M. (2008). Identification of transcriptional regulatory cascades in retinoic acid-induced growth arrest of HepG2 cells. Nucleic Acids Research, 36(10), 3443–3454. https://doi.org/10.1093/nar/gkn066	RARA->IRF1	Both
	RARA->STAT6	Both
	RXRA->RUNX1	Single-cell
	RXRA->TCF3	Single-cell
Navarro-Montero, O., Ayllon, V., Lamolda, M., López-Onieva, L., Montes, R., Bueno, C., … Real, P. J. (2017). RUNX1c Regulates Hematopoietic Differentiation of Human Pluripotent Stem Cells Possibly in Cooperation with Proinfla	RUNX1->CSF1	Single-cell
Nigten, J., Nikoloski, G., De Witte, T., Van der Reijden, B. A., & Jansen, J. H. (2004). Id1 and Id2 Are Retinoic Acid Responsive Genes and Induce a G0/G1 Arrest in Acute Promyelocytic Leukemia Cells. https://doi.org/10.1182/blood.V104.11.2029.2029	RARA->ID2	Single-cell
Ning, S., Huye, L. E., & Pagano, J. S. (2005). Regulation of the transcriptional activity of the IRF7 promoter by a pathway independent of interferon signaling. Journal of Biological Chemistry, 280(13), 12262-12270. doi: 10.1074/jbc.M404260200	IRF7 auto-regulatory loop	Single-cell
Orlikova, B., Schnekenburger, M., Zloh, M., Golais, F., Diederich, M., & Tasdemir, D. (2012). Natural chalcones as dual inhibitors of HDACs and NF-κB. Oncology Reports, 28(3), 797. https://doi.org/10.3892/OR.2012.1870	STAT1->NFkB2	Single-cell
Pongubala, J. M. R., & Atchison, M. L. (1997). PU.1 can participate in an active enhancer complex without its transcriptional activation domain. Proceedings of the National Academy of Sciences of the United States of America, 94(1), 127. https://doi.org/10.1073/PNAS.94.1.127	PU.1->TCF3	Single-cell
Ramachandran, B., Yu, G., Li, S., Zhu, B., & Gulick, T. (2008). Myocyte enhancer factor 2A is transcriptionally autoregulated. Journal of Biological Chemistry, 283(16), 10318-10329. doi: 10.1074/jbc.M707623200	MEF2A auto-regulatory loop	Single-cell
Wislet, S., Vandervelden, G., & Rogister, B. (2018). From Neural Crest Development to Cancer and Vice Versa: How p75NTR and (Pro)neurotrophins Could Act on Cell Migration and Invasion?. Frontiers in molecular neuroscience, 11, 244. https://doi.org/10.3389/fnmol.2018.00244	TCF3 auto-regulatory loop	Both
Saeed, S., Logie, C., Stunnenberg, H. G., & Martens, J. H. A. (2011). Genome-wide functions of PML-RARα in acute promyelocytic leukaemia. British Journal of Cancer, 104(4), 554–558. https://doi.org/10.1038/sj.bjc.6606095	RARA->RUNX1	Single-cell
	RARA->PU.1	
Satoh, J. I., Asahina, N., Kitano, S., & Kino, Y. (2014). A comprehensive profile of ChIP-Seq-based PU. 1/Spi1 target genes in microglia. Gene regulation and systems biology, 8, GRSB-S19711. https://doi.org/10.4137/GRSB.S19711	PU.1->CSF1	Both
	PU.1->STAT1	Single-cell

Sin, W.-X., Yeong, J. P.-S., Lim, T. J. F., Su, I.-H., Connolly, J. E., & Chin, K.-C. (2020). IRF-7 Mediates Type I IFN Responses in Endotoxin-Challenged Mice. Frontiers in Immunology, 11, 640. https://doi.org/10.3389/fimmu.2020.00640	STAT1->IRF7	Single-cell
Tallam, A., Perumal, T. M., Antony, P. M., Jäger, C., Fritz, J. V., Vallar, L., ... & Michelucci, A. (2016). Gene regulatory network inference of immunoresponsive gene 1 (IRG1) identifies interferon regulatory factor 1 (IRF1) as its transcriptional regulator in mammalian macrophages. PLoS One, 11(2), e0149050. https://doi.org/10.1371/journal.pone.0149050	IRF1->RUNX1	Both
The FANTOM Consortium., Suzuki, H., Forrest, A. et al. The transcriptional network that controls growth arrest and differentiation in a human myeloid leukemia cell line. Nat Genet 41, 553–562 (2009). https://doi.org/10.1038/ng.375	IRF1->IRF2	Both
	IRF2 auto-regulatory loop	Both
	PU.1->IRF1	Both
	PU.1->RUNX1	Both
Thomsen, I., Kunowska, N., Souza, R. de, Moody, A.-M., Crawford, G., Wang, Y.-F., … Sabbattini, P. (2018). RUNX1 controls the dynamics of cell cycle entry of naïve resting B cells by regulating expression of cell cycle and immunomodulatory genes in response to BCR stimulation. E-Conversion - Proposal for a Cluster of Excellence.; Navarro-Montero, O., Ayllon, V., Lamolda, M., López-Onieva, L., Montes, R., Bueno, C., … Real, P. J. (2017). RUNX1c Regulates Hematopoietic Differentiation of Human Pluripotent Stem Cells Possibly in Cooperation with Proinfla	RUNX1->IL10RA	Single-cell
Tomaru, Y., Simon, C., Forrest, A. R. R., Miura, H., Kubosaki, A., Hayashizaki, Y., & Suzuki, M. (2009). Regulatory interdependence of myeloid transcription factors revealed by matrix RNAi analysis. Genome Biology, 10(11), R121. https://doi.org/10.1186/gb-2009-10-11-r121	RXRA->RELB	Single-cell
Wan, Y. J. Y., Wang, L., & Wu, T. C. J. (1994). The expression of retinoid X receptor genes is regulated by all-trans-and 9-cis-retinoic acid in F9 teratocarcinoma cells. Experimental Cell Research, 210(1), 56–61. https://doi.org/10.1006/excr.1994.1009; Nakanishi, M., Tomaru, Y., Miura, H., Hayashizaki, Y., & Suzuki, M. (2008). Identification of transcriptional regulatory cascades in retinoic acid-induced growth arrest of HepG2 cells. Nucleic Acids Research, 36(10), 3443–3454. https://doi.org/10.1093/nar/gkn066	RARA->RXRA	Both
Waters, M. R., Gupta, A. S., Mockenhaupt, K., Brown, L. S. N., Biswas, D. D., & Kordula, T. (2019). RelB acts as a molecular switch driving chronic inflammation in glioblastoma multiforme. Oncogenesis, 8(6). https://doi.org/10.1038/s41389-019-0146-y	RELB->CSF1	Both
	RELB->IRF2	Single-cell
Wontakal, S. N., Guo, X., Will, B., Shi, M., Raha, D., Mahajan, M. C., ... & Skoultchi, A. I. (2011). A large gene network in immature erythroid cells is controlled by the myeloid and B cell transcriptional regulator PU. 1. PLoS Genet, 7(6), e1001392. ttps://doi.org/10.1371/journal.pgen.1001392	E2F4->PU.1	Single-cell
Zenke, K., Muroi, M., & Tanamoto, K. I. (2018). IRF1 supports DNA binding of STAT1 by promoting its phosphorylation. Immunology and Cell Biology, 96(10), 1095-1103. https://doi.org/10.1111/imcb.12185	STAT1->IRF1	Both

Table S2.2 Statistics for bulk and single-cell experiments

		Bulk RNA-seq		Bulk ATAC-seq			scRNA-seq		scATAC-seq	
Timepoint	Replicate	Mapped reads	Genes > 1TPM	Mapped reads	Homer total peaks	IDR-passing peaks	Cells > 500UMI	Cells >150 genes & <20% MT reads	Cells that pased QC	Avg. TSS Enrichment Score
HL-60	Rep1	9.0M	13,187	21.5M	531,523	49,081	4,123	628	_	_
	Rep2	8.4M	13,124	14.1M	737,361					
Mac_0hrs	Rep1	13.9M	14,436	15.8M	514,659	131,631	4,480	4,145	4,960	42
	Rep2	12.7M	14,374	8M	584,661					
M1_3hrs	Rep1	13.5M	10,369	29.3M	584,661	168,480	635	415	_	_
	Rep2	17.2M	9,250	25.1M	494,114					
M1_6hrs	Rep1	13.5M	10,473	19.7M	431,602	162,497	3,453	475	_	_
	Rep2	13.1M	9,369	13.3M	391,476					
M1_12hrs	Rep1	11.7M	9,744	25.3M	482,322	170,366	571	490	_	_
	Rep2	16.2M	9,820	56.1M	459,273					
M1_24hrs	Rep1	13.2M	9,385	19M	508,889	164,340	597	524	8,425	40
	Rep2	12.9M	11,136	11.7M	423,695					
M2_3hrs	Rep1	8.0M	8,228	15.3M	451,124	157,267	474	435	_	_
	Rep2	12.0M	8,109	15.9M	460,571					
M2_6hrs	Rep1	10.0M	7,722	16.1M	501,319	148,226	507	389	_	_
	Rep2	13.7M	7,510	16.3M	505,241					
M2_12hrs	Rep1	9.5M	7,413	23.1M	462,814	153,577	877	285	_	_
	Rep2	10.7M	7,585	29.4M	549,522					
M2_24hrs	Rep1	9.0M	7,788	20.3M	506,421	187,605	494	418	8,809	37
	Rep2	10.0M	8,123	20.9M	504,361					
M2_24hrs_Sorted	–	–		–	–	–	829	630	–	–
M2M1_Repolarized	–	–		–	–	–	1,323	1,159	329	16
M2_Neg_Ctrl	Rep1	15.5M	11,293	23.9M	459,529	172,866	_	_	_	_
	Rep2	18.3M	12,022	24.4M	459,889					
M2_Pos_Ctrl	Rep1	13.1M	12,373	25.9M	479,147	112,537	_	_	_	_
	Rep2	15.0M	11,674	23.8M	485,730					
M2_IRF1_KD	Rep1	13.3M	10,643	23.3M	471,072	142,157	_	_	_	_
	Rep2	15.5M	10,669	27.3M	514,258					
M2_IRF7_KD	Rep1	13.7M	10,534	27.9M	508,087	166,015	_	_	_	_
	Rep2	13.7M	10,770	23.2M	490,966					
M2_IRF9_KD	Rep1	18.4M	11,125	25.1M	484,455	184,304	_	_	_	_
	Rep2	15.8M	11,545	25.3M	477,066					
M2_ID2_KD	Rep1	20.9M	11,760	22.6M	473,521	181,900	_	_	_	_
	Rep2	10.8M	12,016	23.2M	465,532					

2.5 Methods

2.5.1 Experimental model and subject details

HL-60 cells (ATCC-CC240) were grown in ATCC-recommended media: 20% FBS (Omega Scientific) and 1% penicillin/streptomycin antibiotics (Life Technologies) in Dulbecco's Modification of Eagle's Medium (Corning). They were incubated at 37°C with 5% CO_2. All cell lines were maintained in horizontally oriented 25mL or 75mL Falcon Tissue Culture Treated Flasks (Thermo Fisher Scientific) at a density of 1×10^6 cells/mL in a total of 10mL or 20mL, respectively. Cells were consistently passaged once over 2 to 3-day periods up to differentiation.

2.5.2 Macrophage differentiation and polarization

We performed PMA-induced differentiation of HL-60 cells into M0 macrophages (Murao et al., 1983) in order to obtain M1 and M2 macrophage subtypes for characterization. Approximately 5×10^6 cells at a density of 1×10^6 cells/mL were plated in 60mm cell culture dishes with 10 μM of PMA (Thermo Fisher Scientific). Media was changed every 48 hours and 10μM of PMA was added at every media change. After 120 hours of PMA stimulus, M0 macrophages were polarized by either applying 100ng/mL of IFN-γ and LPS to obtain M1 or 10ng/mL of IL-4 and IL-13 to obtain M2 polarized subtypes (Huang et al., 2018; Wang et al., 2007). Differentiation and polarization were confirmed by fluorescence immunostaining for cell type specific markers (Rőszer, 2015; Yu et al., 2009; Holness & Simmons, 1993) and by observation of markedly distinct cellular morphologies, as M1 cells are characterized by a large cell body with a varied number of pseudopodia and M2 cells are characterized by an elongated shape (McWhorter et al., 2013). Macrophages were collected at 0, 3, 6, 12 and 24 hours after addition of polarization stimuli, along with undifferentiated HL-60 for bulk and single-cell RNA-

seq (Figure 2.1A). We generated a total of 62 bulk data sets, approximately 50,000 single-cells using scRNA-seq, and approximately 40,000 single-nuclei using scATAC-seq.

2.5.3 M2 repolarization towards M1

M0 macrophages were polarized towards M2 for 24 hours according to aforementioned protocol. M2 macrophages were harvested and resuspended in PBS at a concentration of 1×10^4 cells/mL. Non-specific antigens were blocked by 5% BSA in PBS buffer. Cells were then fluorescently labeled using CD163-FITC mouse conjugated monoclonal antibody (Thermo Fisher, MA5-17719). Cells that presented high CD163 levels were sorted using an Aria 2 Flow Cytometer (BD Biosciences) in order to obtain a homogeneous M2 population (Hu et al., 2017). M2 macrophages were repolarized towards M1 by applying 100ng/mL of IFN-γ and LPS during 24 hours. Populations of M2 repolarized towards M1 (M2M1) were harvested in a single-cell suspension and loaded into the ddSEQ single-cell isolator (Bio-Rad). Single-cell libraries were prepared using the SureCell WTA 3′ Library Prep Kit for the ddSEQ System (Illumina). The quality of the libraries was assessed using the Agilent 2100 Bioanalyzer. Single-cell libraries were sequenced using the NextSeq 500 (Illumina). Cell viability (>90%) was confirmed prior to single-cell library preparation.

2.5.4 Bulk RNA-seq and ATAC-seq experiments

Bulk sequencing experiments were conducted in triplicates per time point (Figure 2.1A) per assay. We collected 2 million cells for RNA-seq and 50,000 cells for ATAC-seq. RNA-seq and corresponding ATAC-seq biological replicates were collected from the same dish. Cell viability (>90%) was monitored prior to cell collection. Macrophages were detached from plates

by incubating with 3.5mL of Trypsin-EDTA 0.25% (Life Technologies) at 37°C for 4 minutes. Trypsin was neutralized by adding 14mL of complete media per dish, then the cells were pelleted in a centrifuge at 1,500 RPM for 5 minutes. The cells were washed with PBS and spun down again to remove all traces of Trypsin and media before library preparation. HL-60 cells were collected for RNA-seq by pelleting suspended cells and washing them with PBS. We relied on our previous paper for undifferentiated HL-60 ATAC-seq data (Ramirez et al., 2017). RNA-seq and ATAC-seq libraries were built following the Smart-seq2 protocol (Picelli et al., 2014) and the Omni-ATAC protocol (Corces et al., 2017a), respectively. The Omni-ATAC-seq libraries went through a gel size selection step to enrich for DNA fragments ranging from 150 to 500bp. The quality of all libraries was assessed using the Agilent 2100 Bioanalyzer. Bulk libraries were sequenced using the NextSeq 500 (Illumina) obtaining around 10 million reads per sample for RNA-seq and around 20 million reads per sample for ATAC-seq. Two replicates per time point were used in downstream analyses.

2.5.5 Single-cell RNA-seq experiment

Single-cell libraries were prepared from 12,000 cells per time point (Figure 2.1A) using the SureCell WTA 3′ Library Prep Kit for the ddSEQ System (Illumina). Cells with viability >90% were collected by detaching cells from plates using Trypsin-EDTA 0.25%, as previously described in the "Bulk RNA-seq and ATAC-seq experiments" section. The detached cells were washed in cold PBS + 0.1% BSA and resuspended to reach 2,500 cells/μL. The cells were filtered through a 40 μM strainer and verified to be in single-cell suspensions under the microscope. Cells suspended in a reverse transcription reaction buffer were loaded into the Bio-Rad ddSEQ microfluidic device along with barcoded beads. Single cells were encapsulated in an oil-water emulsion as

nanodroplets and their RNA was reverse transcribed, during which unique molecular identifiers (UMIs) and cell barcodes were added to the cDNA. The first strand cDNA was recovered from the droplets through emulsion breakage and bead cleanup, then the second strand of cDNA was synthesized. The cDNA was cleaned, tagmented, amplified, and cleaned again to produce the final libraries. The concentration and size distribution of the libraries were assessed using the Agilent 2100 Bioanalyzer. Single-cell libraries were sequenced using the NextSeq 500 (Illumina) at 3.1 pM loading concentration using a custom primer.

2.5.6 Single-cell ATAC-seq experiment

The Omni-ATAC version of the Bio-Rad ddSEQ SureCell ATAC-seq (Illumina) workflow was followed, based off of the bulk ATAC-seq protocol of the same name (Lareau et al., 2019; Corces et al., 2017). Single-cell suspensions of M0, as well as 24-hour polarized M1 and M2 samples were prepared as previously described in the "Single-Cell RNA-seq experiment" section. Cells were resuspended to approximated $1x10^6$/mL in PBS + 0.1% BSA, filtered through a 40µM strainer, and verified to be single-cell suspensions under the microscope. Samples of 300,000 cells per biological replicate of M0, M1, and M2 were lysed with ATAC-Lysis buffer containing freshly added digitonin, then the nuclei were washed with ATAC-Tween buffer. Staining with Trypan Blue (Bio-Rad) confirmed cells were lysed with viability <10% and nuclei were verified to be single-nucleus suspensions under the microscope. 60,000 nuclei were used in each Tn5 tagmentation reaction (incubation at 37°C for 30 min) per sample. After tagmentation, nuclei suspended in an amplification reaction were loaded into the Bio-Rad ddSEQ microfluidic device along with barcoded beads. Single nuclei were encapsulated in nanodroplets and the fragments generated by the Tn5 transposase were barcoded by UMIs and cell barcodes and amplified. The

fragments were recovered from the droplets through emulsion breakage, bead cleanup, a second amplification reaction, and a final bead cleanup before quality control using the Agilent 2100 Bioanalyzer. Libraries were assessed by concentration and size distribution before being loaded onto the NextSeq 500 (Illumina) and sequenced at 1.5 pM loading concentration using a custom primer.

2.5.7 IRF1, IRF7, IRF9 knockdown in M2

M0 cells were differentiated from HL-60 then polarized to M2 for 24 hours as previously described in the "Macrophage differentiation and polarization" section. At the same time that polarization reagents were added, siRNAs targeting IRF1, IRF7, IRF9, ID2, positive control (GAPD), and negative (non-targeting) control (Dharmacon) were transfected in 3 biological replicates of M2 per target knockdown. DharmaFECT 4 Transfection Reagent was added at 1:500 final concentration and siRNAs were added at 0.025μM final concentration in 4mL media in 60mm cell culture dishes. The perturbed cells were collected for both bulk RNA-seq and ATAC-seq 24 hours later.

2.5.8 Bulk RNA-seq preprocessing

Bulk RNA-seq reads were mapped to the hg38 reference genome with gene annotations from Gencode release 29 using STAR (version 2.5.1b) and gene level expression was quantified using RSEM (version 1.2.25) (Dobin et al., 2013; Li & Dewey, 2011). Expression represented by counts per gene was normalized utilizing the "weighted" Trimmed Mean of M-values (TMM) approach using edgeR (version 3.28.1) and saved as a matrix of TMM normalized counts per

million (CPM) (Robinson & Oshlack, 2010). Counts were also converted to transcripts per million (TPM).

2.5.9 Bulk RNA-seq analysis

EdgeR (version 3.28.1) also identified genes differentially expressed between selected time points using a false discovery rate (FDR) of 1% and an alpha of 0.05. TMM normalized CPM were then $\log_2$ normalized and used as input for maSigPro (version 1.58.0) to identify gene expression changes over time allowing for k-means clustering of genes that present similar patterns of expression during the time course of polarization.

2.5.10 Bulk ATAC-seq preprocessing

ATAC-seq reads were mapped to the hg38 genome, annotated by Gencode release 29, using Bowtie2 (version 2.2.7) (Langmead & Salzberg, 2012). Reads mapped to the mitochondrial chromosome were discarded from downstream analysis. The resulting bam file was sorted using Picard toolkit (version 2.18.4) and PCR duplicates were removed (https://broadinstitute.github.io/picard/). Using a custom script, the remaining reads aligning to the positive strand were shifted by +4bps and reads aligning to the negative strand were shifted by -5bps to account for the 9bp duplication caused by Tn5 transposition (Berg et al., 1983). We used HOMER (version 4.7) to create a tag directory for each sample using the sorted and shifted bam file (Heinz et al., 2010). To determine the final set of open regions: peaks were called for both "narrow" regions of 150bp and "broad" regions of 500bp using HOMER (version 4.7) and the resulting bed files were merged across replicates for each sample. Biologically reproducible regions across replicates were identified by irreproducible discovery rate analysis (IDR), then

ENCODE “blacklist” regions were removed in order to generate the final set of open regions (Amemiya et al., 2019; Li et al., 2011). We used HOMER (version 4.7) to estimate read coverage across the final set of open regions using the tag directories generated for each sample, and to annotate each region.

2.5.11 Bulk ATAC-seq analysis

ATAC-seq read counts were corrected for TMM and library size (represented as CPM) using edgeR (version 3.28.1) to normalize the data. EdgeR was also used to identify differentially open chromatin regions within gene promoters at each of the differentiation time points. TMM normalized counts were then $\log_2$ transformed and maSigPro (version 1.58.0) was used to cluster regions based on changes in accessibility during the polarization time course (Nueda et al., 2014). All clusters were converted into bed files of genomic regions and HOMER (version 4.7) findMotifsGenome.pl was used to find which known motifs were most enriched in each cluster.

2.5.12 Bulk data integration and gene regulatory network construction

We applied Pearson’s $\chi 2$ test from the R Stats Package (version 3.6.2) to determine p values of enrichment between ATAC-seq clusters and RNA-seq clusters. A final list of TFs was manually curated by combining TFs found in RNA clusters, linked RNA-ATAC cluster pairs, results from scRNA-seq analysis, motif enrichment in ATAC clusters, and differentially expressed TFs across the time course. ATAC-seq data across all the M1 or M2 replicates from 3 hours to 24 hours were pooled in order to achieve >200 million reads to mine the open regions for transcription factor footprints. We used the Wellington algorithm from the pyDNase library (version 0.2.4) and the HINT-ATAC tool to identify chromatin footprints with an FDR of 1%, with footprint sizes of 8 to

31bp with a 1bp step size (Li et al., 2019; Piper et al., 2013). We then used FIMO (version 4.12.0) to identify footprint regions with enriched HOCOMOCO (version 11) transcription factor motifs, using a p value cutoff of 0.0001 and hg38 background (Kulakovskiy et al., 2013). We used bedtools intersect to determine the target genes for each footprint using the HOMER-annotated bulk ATAC-seq regions. We finally used footprints <50kb away from the TSSs of the target genes to build bulk GRNs with our TFs and signaling molecules of interest.

2.5.13 Single-Cell RNA-seq preprocessing

Single-cell RNA-seq reads were demultiplexed using ddSeeker, which extracts cell barcodes and UMIs and produces a demultiplexed bam file (Romagnoli et al., 2018). From the bam file, we used a custom script to extract one fastq file per cell. Each cell was mapped to the hg38 reference genome with gene annotations from Gencode release 29 using STAR (version 2.5.1b). Spliced and unspliced reads were calculated using velocyto (version 0.17.16) and expression was also quantified using RSEM (version 1.2.25) (La Manno et al., 2018). Low quality cells with less than 500 UMI counts, more than 20% mitochondrial reads, and less than 150 genes detected were removed from further analysis. We also removed cells with more than 4,000 genes detected to avoid possible doublets.

2.5.14 Single-cell RNA-seq analysis

Each cell that passed the initial quality control filters was used as input for Velocyto (La Manno et al., 2018). Velocyto (version 0.17.16) only considers uniquely mapped reads that align to both exonic and intronic regions and removes reads mapped to repeat masked regions. The new UMI count matrices were exported from a loom file format to a Seurat object (V3.1.5) (Satija et

al., 2015). Downstream normalization, differential expression and Leiden clustering were implemented using Seurat (Traag et al, 2019). RNA velocities calculated by Velocyto were then overlaid onto the Seurat UMAP dimensionality reduction. To further investigate cell trajectories we used the R package Monocle (version 2.8.0) to order cells within a pseudotime utilizing an unsupervised clustering method (X. Qiu et al., 2017). We then applied Single-Cell Regulatory Network Inference And Clustering (SCENIC, version 1.1.2-2) to estimate the transcription factors that regulate gene expression on cell populations identified using Seurat (Aibar et al., 2017). We finally applied the Odds-Ratio (OR) analysis to investigate orthogonal expression of M1 and M2 markers in individual cells. The odds-ratio was calculated from the spliced counts. Genes with greater than 2 counts were considered "expressed". The odds-ratio was calculated as the product of the number of cells expressing both genes (YY) and the number of cells expressing neither gene (NN) divided by the product of the number of cells expressing only one gene (YN) and the number of cells expressing only the other gene (NY). OR=(YYxNN)/(YNxNY). Plots use $\log_2$ of the odds-ratio with any infinite values set to the positive or negative absolute maximum value. All odds-ratio values with a p value > 0.05 were set to 0.

2.5.15 Single-cell ATAC-seq preprocessing

The average number of nuclei collected and average number of unique fragments per nucleus between technical replicates of M0 were 2,480 and 4,104, respectively. For two sets of biological replicates with two technical replicates each (4 libraries) of M1, we recovered 3,860 nuclei and 8,102 unique fragments per cell on average. For two sets of biological replicates with two technical replicates of M2, we recovered 4,404 nuclei and 8,839 unique fragments on average. Raw sequencing data were primarily processed using the Bio-Rad ATAC-seq Analysis Toolkit

(version 1.0.0) in order to generate mapped reads. We installed the Bio-Rad Docker containers on our lab's server and followed the steps to perform fastq QC, debarcoding of fastq files, alignment to hg38 using BWA with blacklist regions removed, and alignment QC using Picard Tools (Li & Durbin, 2009). Next, the Bio-Rad Toolkit used Jaccard indexing to determine bead duplicates and remove cell-free droplets, then BAP to "deconvolute" or merge bead duplicates. The mapped reads for UMI-passing cells and the peaks called by MACS2 (Zhang et al., 2008) were used in a custom python script (found here: https://github.com/fairliereese/lab_pipelines/tree/master/sc_atac_pipeline) to generate peaks-by-cells counts matrices for each sample for use in SOM analysis.

2.5.16 Single-cell SOM analysis

To analyze the single-cell data, we trained a self-organizing map on the read counts for each of the 210,312 fragments for each cell/nucleus. For this, we used our SOMatic tool (Jansen & Ramirez et al., 2019) with a 40x60 map for 5 epochs and 100 trials. This process resulted in 114 DNA metaclusters. Similarly, we built a 40x60 map on the scRNA data with the same options and received 52 RNA metaclusters. Then, these 2 sets of metaclusters were linked, generating 5928 (114 x 52) linked metaclusters. The regions in these linked metaclusters were sent through the same network analysis pipeline as our previous work (above) using the HOCOMOCOv11 motif database (p value < 0.05, q-value < 0.05). The pipeline can be found here: https://github.com/csjansen/SOMatic-Network-Analysis. This generated a total of 8,904,925 potential network connections or 833,114 TF-TF interactions.

2.5.17 Data and software availability

The accession number for the sequencing data reported in this paper is GEO: GSE164498.

CHAPTER 3

Complement C5aR1 signaling promotes inflammatory cascades and modulates the expression of select glial activation genes in a mouse model of Alzheimer's disease

Notes:
(1) Dr. Nicole Schartz and I equally contributed to the material in this chapter. She performed the behavioral experiments, immunohistochemistry, and interpretation of the results. I performed tissue lysis, RNA extraction, RNA-seq library preparation, data analysis, and interpretation
(2) Heidi Liang performed RNA-seq library sequencing
(3) Gabriela Balderrama-Gutierrez contributed to results interpretation
(4) Shu-Hui Chu performed mice perfusion and tissue dissection
(5) Purnika Selvan performed immunohistochemistry experiments
(6) Angela Gomez-Arboledas performed immunohistochemistry experiments
(7) Dr. Ali Mortazavi and Dr. Andrea Tenner conceived the study and provided continued support and guidance throughout the project

3.1 Abstract

The complement system is part of the innate immune system that works to clear pathogens and cellular debris. In the central nervous system (CNS), complement activation can promote synaptic pruning, clearance of neuronal blebs, and recruitment of phagocytes. However, in the inflammatory environment of the Alzheimer's disease (AD) brain, complement activation may contribute to inflammatory pathways, neuronal loss, and cognitive decline. Importantly, activation of downstream complement via engagement of C5a with its receptor C5aR1 can instigate a feed-forward loop of inflammation, injury, and neuronal death, thus making this molecule a potential target for modulation in AD therapeutics. To further elucidate the role of complement C5a in AD pathogenesis, we crossed the Arctic AD mouse model, known to rapidly accumulate fibrillar amyloid plaques, to a transgenic mouse that overexpresses C5a under the GFAP promoter (C5a+) or a model that lacks the receptor for C5a (C5aR1KO). Bulk RNA-sequencing and immunohistochemistry were used to identify pathways and molecular markers, respectively, that were altered with different C5a–C5aR1 activity throughout disease progression. Furthermore, we used the object location memory (OLM) test to determine the effects of C5a on AD-associated hippocampal-dependent memory loss. ArcticC5a mice showed advanced disease progression compared to Arctic mice, as shown in poor spatial discrimination in OLM and hippocampal neuronal loss compared to Arctic mice. Eliminating C5aR1 in Arctic mice did not alter amyloid plaque accumulation but either delayed or prevented the expression of important AD genes in hippocampi, indicating a separation between those genes induced by amyloid plaques and those influenced by C5a-C5aR1 signaling. C5ar1 deletion reduced the expression of select pan-reactive and A1 reactive astrocyte genes. The ArcticC5aR1KO group also showed delayed expression of genes enriched for biological processes that are significant in the AD context, such as regulation

of inflammatory signaling, microglial cell activation, astrocyte migration, and lysosome pathway. Immunohistochemical assays further confirmed that ablation of C5aR1 either delayed or reduced some reactive microglial markers in the Arctic hippocampus, including Cd11b. Our results suggest that C5a-C5aR1 signaling enhance AD pathways and alter microglial pathology. Thus, pharmacological inhibition of this pathway may be a promising therapeutic strategy to treat AD.

3.2 Introduction

Alzheimer's disease (AD) is the most common form of dementia and is characterized by the accumulation of extracellular amyloid beta (Aβ) plaques, hyperphosphorylated tau, synaptic loss, eventual neuronal death, and ultimately cognitive decline (DeTure & Dickson, 2019). Evidence suggests that inflammatory pathways are induced by amyloid plaques and tau but also contribute to these AD pathologies, exacerbating neuronal injury and cognitive decline (Yang et al., 2020; Hur et al., 2020; Griffin et al., 1989).

The complement system is a powerful effector of the innate immune system that is activated via three distinct pathways, classical, lectin, and alternative, all of which converge on proteolytic cleavage of C3 into the chemoattractant C3a and opsonin C3b. C3b also forms part of the C5 convertase, which cleaves C5 into C5a, a potent pro-inflammatory chemoattractant, and C5b, the initiating molecule of the lytic membrane attack complex (MAC) (Schartz & Tenner, 2020). C1q, the recognition molecule of the classical pathway, can bind to apoptotic neurons to promote clearance by microglia to maintain neuronal homeostasis (Fraser et al., 2010). However, the association of C1q with the proteases C1r/C1s enables synaptic pruning as well as complement activation by fibrillar amyloid which can lead to the generation of C3a and, if C5 is present, C5a, both of which produce potent proinflammatory responses (Tenner, 2020). These inflammatory

responses can lead to neuronal death and promote neurodegeneration (Pavlovski et al., 2012; Hernandez et al., 2017).

Ablation of complement C5a receptor 1 (C5aR1) alters microglial gene expression in the Arctic mouse model of AD resulting in decreased inflammatory gene expression and enhanced expression of genes associated with pathways involved in debris clearance (Hernandez et al., 2017). Ablation of C5aR1 in Arctic mice is also associated with attenuation of cognitive decline and loss of neuronal complexity in the CA1 region of the hippocampus. In addition, administration of C5a to neurons *in vitro* is neurotoxic (Hernandez, et al., 2017). In two other mouse models of AD, treatment with the C5aR1 inhibitor PMX205 reduced activated microglia and astrocytes, and protected mice against hippocampal synaptic loss and cognitive decline (Fonseca et al., 2009). Inhibition or ablation of C5a-C5aR1 activity has also been demonstrated to increase survival and lower motor deficits in models of amyotrophic lateral sclerosis (ALS) (Wang et al., 2017; Woodruff et al., 2008), reduce seizure susceptibility and inflammation in experimental epilepsy, and speed up functional recovery after spinal cord injury (Biggins et al., 2017). These data are consistent with detrimental consequences of C5a-C5aR1 activity in neurodegenerative diseases, including AD, and support that inhibition of C5a-C5aR1 signaling may slow or prevent the progression of these diseases. Importantly, C5aR1 receptor antagonists have been shown to be nontoxic in human clinical trials and case studies (Ennis et al., 2020; Tesar & Hruskova, 2018; Vergunst et al., 2007).

To begin to define the mechanistic pathways from altered C5a-C5aR1 signaling to effects on neurons and thus cognition, bulk RNA-sequencing of microglia isolated from half brains (hippocampus and cortex combined) was previously analyzed over the course of disease progression. Arctic mice lacking C5aR1 (ArcticC5aR1KO) (Hernandez, et al., 2017) had higher

expression of genes associated with phagocytosis (e.g. Trem2, Tyrobp) and lysosomal proteins (e.g. Lamp1, Ncp2, Cts) relative to Arctic mice as early as 5 months of age, long before the onset of hippocampal-dependent cognitive decline that is evident in Arctic mice at 10 months of age (Hernandez et al., 2017). At the same time, other studies showed that microglial activation can influence the reactive state of astrocytes (Liddelow et al., 2017a). To further elucidate the role of C5a-C5aR1 signaling in amyloid-associated cognitive decline, and to expand on our previous behavioral studies examining the role of C5a-C5aR1 signaling on cognitive decline in the Arctic mouse, we crossed the Arctic mouse to a model that overexpresses C5a under the control of the GFAP promoter (ArcticC5a+) and tested spatial memory with the object location memory (OLM) test (Vogel-Ciernia & Wood, 2014). We used immunohistochemistry to assess morphological and molecular changes in microglia and astrocytes in the hippocampus and cortex relative to fibrillar amyloid plaques in Arctic, ArcticC5aR1KO, and ArcticC5a+ mice. In our previous study, astrocytic and other cell-specific genes were missing from the analyses. In this study, we microdissected the hippocampus and cortex of mice at different ages for bulk RNA-sequencing to identify region-, age-, and amyloid-specific transcriptomic changes. We aim to identify the dynamic roles of excess of C5a or C5aR1 depletion in the aging Arctic mice.

Our approach profiled the dynamic changes in the transcriptomes of all 6 mice cohorts (WT, C5aR1KO, C5a+, Arctic, ArcticC5aR1KO, and ArcticC5a+) at 2.7, 5, 7, and 10 months of age. We identified more abundant changes in expression in hippocampi compared to cortices, correlating with higher amyloid pathology localization. We detected either decreased or delayed expression of AD-associated, DAM-associated, and reactive astrocyte-associated genes upon C5aR1 knockout. C5aR1 ablation also led to delayed expression of genes enriched for inflammation, microglial activation, phagocytosis, and cholesterol biosynthesis. On the other

hand, C5a overexpression induced genes associated with synapse assembly, transcription, and GABAergic synapse. Additionally, we did not identify significant sex-specific changes in expression in the Arctic mice besides known sexually dysmorphic genes. We also observed cognitive decline and loss of NeuN in the ArcticC5a+ at 7 months, supporting the hypothesis that C5aR1 ablation is neuroprotective. However, C5a increase did not result in robust inflammatory gene profile as expected.

3.3 Results

3.3.1 C5a-C5aR1 signaling accelerates hippocampal-dependent memory deficits and promotes hippocampal cell loss in Arctic mice

We previously reported that ablation of C5aR1 in Arctic mice prevents memory deficits assessed with the OLM test at 10 months of age (Hernandez, et al., 2017), suggesting that binding of C5a to C5aR1 induces a response that contributes to the cognitive decline observed in the Arctic mouse model. The C5a+ transgene results in elevated levels of C5a in the cortex and hippocampus in both wild type and Arctic mice (Figure S3.1) without increasing plasma levels, as expected, since it is under the control of the GFAP promoter. Since elevated C5a production could result in greater engagement of C5a with C5aR1, we assessed whether that transgene accelerates the effects of this receptor. Arctic and ArcticC5a+ mice and their WT controls were tested at 5 and 7 months to determine if overexpression of C5a in brain would accelerate memory decline in the presence (ArcticC5a+ cohort) or absence (C5a+ cohort) of amyloid pathology. First, analysis of open field and the familiarization trial of OLM (Vogel-Ciernia & Wood, 2014) revealed that there were no gross abnormalities in locomotion or differences in side preference for two novel objects or total object exploration (Figure S3.2**)**. Twenty-four hours after the OLM training (Figure 3.1a), one of

the objects was moved to a new location, and exploration time of each object assessed. At 5 months of age, Arctic mice did not show a deficit in object location memory compared to WT. As hypothesized, ArcticC5a+ mice had a lower discrimination index (DI) compared to Arctic mice ($p = 0.005$). The DI of ArcticC5a+ mice were also significantly lower than the C5a+ controls ($p = 0.001$), while the DI of C5a+ mice did not differ from WT mice (Figure 3.1B). Similarly, ArcticC5a+ mice had diminished cognitive performance compared to Arctic mice at 7 months of age ($p = 0.001$). Still, at this age there was no difference in behavior between WT and Arctic mice ($p = 0.52$) or the WT and the C5a+ mice ($p = 0.35$) (Figure 3.1C). These data suggest that the cognitive deficit accelerated by overexpression of C5a is dependent on co-existing amyloid pathology or some consequence of the overexpression of the hAPP mutant transgene. Taken together, and with the data published in 2017, these data are consistent with the hypothesis that chronic stimulation of the C5a-C5aR1 accelerating memory decline in Arctic mice, whereas ablation of C5aR1 protects against it.

Neuronal loss and cognitive decline are common features of Alzheimer's disease (DeTure & Dickson, 2019). In the Arctic model, mice show significant memory deficits and loss of neuronal integrity (neurite branching in CA1) by 10 months of age (Hernandez, et al., 2017). Therefore, to determine the effects of enhanced C5a-C5aR1 signaling and ablation of C5aR1 on neuronal loss, we used immunohistochemistry and semi-quantitative densitometry analysis to compare the levels of neuronal nuclei (NeuN) in the CA1, CA3, and dentate gyrus (DG) at 7 and 10 months of age in these mice (Figure S3.3). Percent field area was normalized to WT levels for each age. At 7 months, NeuN levels were comparable between WT and C5a+ mice and between WT and Arctic mice in all regions of the hippocampus, consistent with previous findings using Sholl analysis in the CA1 (Hernandez et al., 2017). However, ArcticC5a+ mice had a trend towards lower NeuN

immunoreactivity in the CA1 (p = 0.06) and a significant loss in the DG (p = 0.02) compared to Arctic mice (no loss was detected in the CA3 (p = 0.17)) at 7 months, suggesting an accelerated neuropathology in these mice, which correlates with the early onset of cognitive deficits. By 10 months of age, NeuN levels in the Arctic mice were significantly reduced in the CA1 (p = 0.02), CA3 (p = 0.001), and in the DG (p = 0.01) compared to WT mice. However, ablation of C5aR1 did not protect against this neuronal loss as Arctic/C5aR1KO mice had reduced levels of NeuN compared to C5aR1KO hippocampus (CA1, p = 0.0004; CA3, p < 0.0001; DG, p = 0.06), similar to the reduced level of C5aR1 sufficient Arctic mice. No differences were observed between WT and C5aR1KO at 10 months.

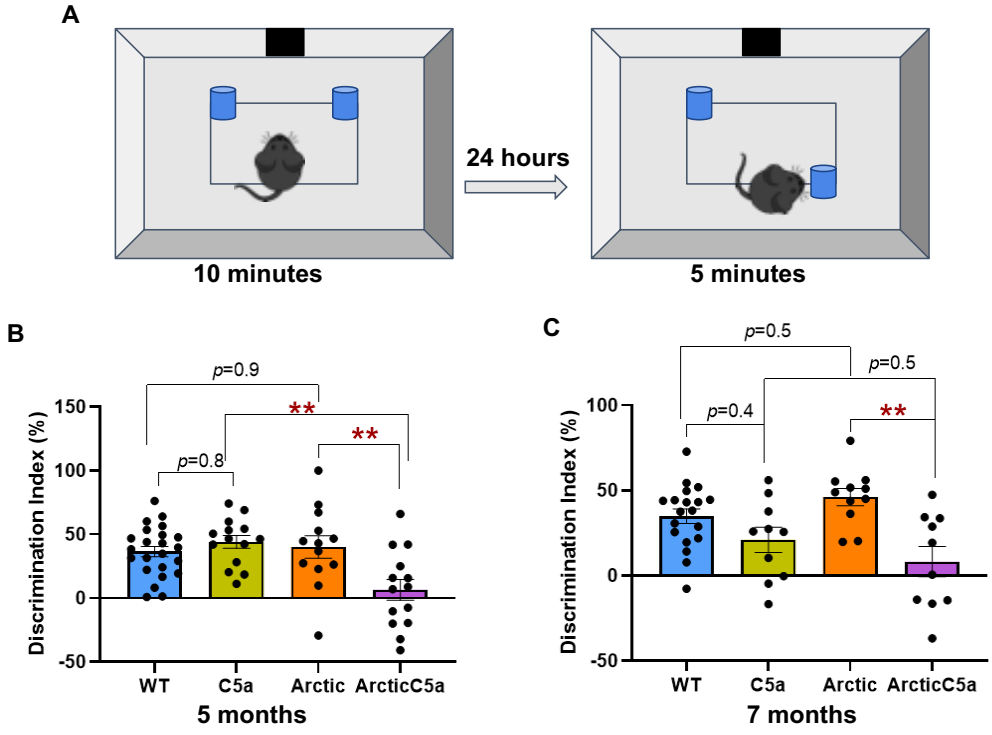

Figure 3.1 Overproduction of C5a accelerates memory decline in Arctic mice at 5 and 7 months

A) Overview of experimental design for object location memory (OLM) test. ArcticC5a mice had a significant deficit in OLM at 5 (B) and 7 (C) months of age. Data shown as Mean ± SEM. ** p < 0.01. Two-way ANOVA with Tukey's post hoc test. For 5 months, N = 23 (WT), 14 (C5a+), 13 (Arctic), 14 (ArcticC5a+). For 7 months, N = 19 (WT), 10 (C5a+), 11 (Arctic), 10 (ArcticC5a+).

3.3.2 Distinct subsets of genes are affected by C5ar1 knockout or C5a overexpression

We dissected 372 cortices and hippocampi of mice representing six distinct genotypes (WT, C5aR1KO, C5a+, Arctic, ArcticC5aR1KO, and ArcticC5a+) throughout disease progression at 2.7, 5, 7, and 10 months of age (see Methods) in order to build RNA-seq libraries and thus identify transcriptome changes in different cohorts (Figure 3.2A). UMAP dimensionality reduction showed clear tissue-specific clustering characterized by the separation of cortices from hippocampi samples on UMAP 1. UMAP 2 showed a subtle separation of tissues from younger mice located at the top and tissues of older mice located towards the bottom of the axis in cortex samples, and left to right in hippocampus samples, highlighted by the gradient of colors with age from light to dark, respectively (Figure 3.2B). We used edgeR (Robinson et al., 2010) to identify differentially expressed genes between male and female Arctic mice. Genes up-regulated in females were mainly known sexually dysmorphic genes (Armoskus et al., 2014; X. Yang et al., 2006), such as Xist and Tsix, which are X-chromosome located genes, whereas males presented upregulation of genes known to be male-specific, such as Eif2s3y, and Ddx3y genes, which are located in the Chromosome Y (Figures S3.4A & S3.4B). Therefore, differential expression analyses show lack of sex-specific changes in the Arctic mice.

We assessed the gene expression patterns of the maSigPro generated clusters (Nueda et al., 2014) to identify differences in gene expression between all the six cohorts (WT, C5aR1KO, C5a+, Arctic, ArcticC5aR1KO, and ArcticC5a+). We identified 1,763 genes whose expressions varied in a time-specific fashion (Figure S3.5A). These genes grouped into 15 clusters with distinct patterns of expression (Figure 3.2C). Clusters RNA cluster (Rc)6, Rc7 Rc1, and Rc2 represent genes whose expression changes were mainly driven by the knockout of C5ar1 and are represented in shades of brown. Clusters Rc4, Rc3, Rc5, and Rc8 to Rc15 represent genes whose expression

changed mainly in response to C5a overexpression and thus are represented in shades of lilac. Each cluster contains distinct subsets of complement pathway (CP) genes, as well as distinct subsets of astrocyte-associated (Ast) (Liddelow et al., 2017b), Arctic microglia-associated (Hernandez, Jiang, et al., 2017) and AD-associated genes elevated in the 5xFAD mouse model with pathology (5xFAD up) (Forner et al., 2021) (Figure 3.2C). Expression of C5ar1 gene was lowest (essentially non detectable) in the C5aR1KO and ArcticC5aR1KO cohorts, confirming its genetic ablation (Figure 3.2D). Correspondingly, expression of C5ar2 also decreased in the C5aR1KO and ArcticC5aR1KO cohorts, consistent with previous studies showing a correspondence in expression of those genes (Klos et al., 2013; Lee et al., 2019). The C5a+- and C5aR1KO-dependent expression changes were more abundant in the hippocampus compared to cortex, correlating with the relative concentration of amyloid pathology localization in the Arctic mice (Hernandez et al., 2017; Cheng et al., 2007).

Expression of genes of some of the early complement pathway components were induced in the Arctic mice peaking at 7 month of age and suppressed in the absence of C5ar1 (Figure 3.2D). Notably, cluster Rc6 contained most of the complement genes identified using maSigPro, including C1qa, C1qb, C1qc (known to be coordinately expressed) (Chen et al., 2011; Lattin et al., 2009), and C4b, as well as the receptor for the C3a activation fragment, C3ar1, and the inhibitor Serping1 (inhibitor of C1, as well as bradykinin formation), all of which showed higher expression in the Arctic mice at 5 months and increasing with age. While C1q was the most robust early induced component, consistent with the rapid increase in multiple injury models, increases in expression of the genes for C4 (required for synaptic pruning) and Serping1 were slower in the

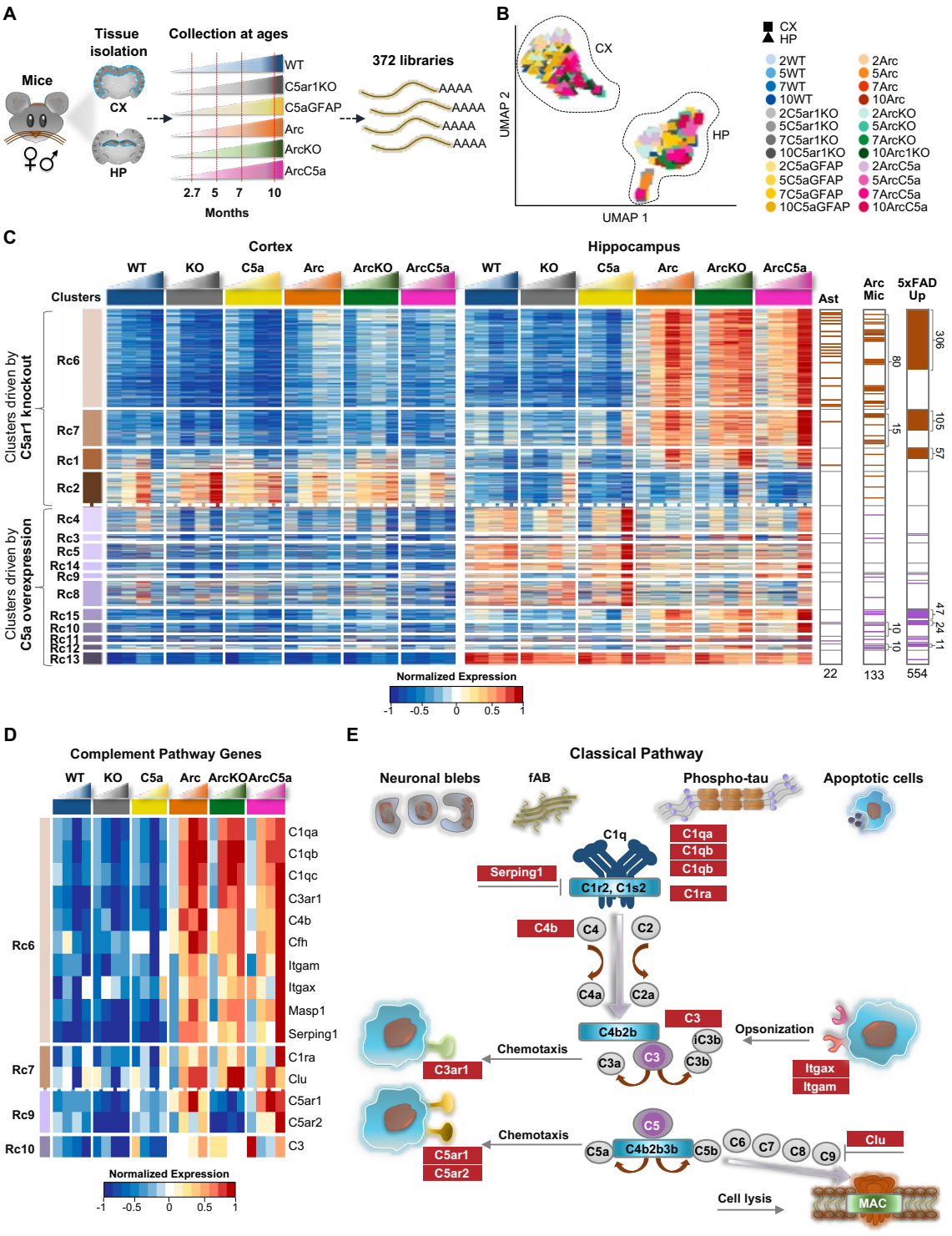

Figure 3.2 Distinct subsets of genes are affected by C5ar1 knockout or C5a overexpression
A) Schematic diagram of experimental design highlighting 372 RNA-seq samples processed from cortices and hippocampi of 6 mice genotypes during disease progression at 2.7, 5, 7, and 10 months of age.

B) UMAP embedding representation of 372 RNA-seq samples represented in panel A. Samples from WT mice are represented in shades of blue, from the C5ar1KO cohort in shades of gray, from the C5aGFAP cohort in shades of yellow, from the Arctic cohort in shades of orange, from the ArcC5ar1KO cohort in shades of green, and samples from the ArcC5aGFAP cohort in shades of pink.
C) Heatmap of 1,763 genes with dynamic temporal profiles identified by maSigPro clustering (alpha < 0.05, FDR < 0.05%). Each column represents the average expression for a time point and each row represents a gene. Each cluster represents a subset of genes that show a similar pattern of expression along the time course. Clusters shown in brown gradient and lilac gradient represent genes whose expression changes are driven by C5ar1KO or C5a overexpression, respectively. RNA-seq data (TPM) is row-mean normalized. Astrocyte-associated genes (Ast), Arctic mice isolated microglia-associated genes (Arc Mic), and genes upregulated with pathology progression in the 5xFAD mice (5xFAD Up) present in each cluster are shown.
D) Heatmap of 15 genes of the complement pathway that were present in maSigPro identified clusters. RNA-seq data (TPM) is row-mean normalized.
E) Representative diagram of the Classical pathway activation of the complement cascade, highlighting complement-associated genes present in the maSigPro identified clusters (as seen in panel D).

ArcticC5ar1KO as seen in the previous analysis of isolated microglia in this model (Hernandez, Jiang, et al., 2017). Interestingly, delayed increases in these components were also seen in ArcC5a+ with highest expression at 10 months. We also investigated changes in expression of genes of the complement pathway that were driven by an increase in C5a from the transgene. Complement genes Cfh, Masp1, and C1ra, inhibitor Clu and the α chains Itgam (CD11b) and Itgax (CD11c) of CR3 and CR4 were up regulated by the presence of the Arc APP transgene but showed striking increased expression in the ArcticC5a+ hippocampus at 10 months (Figure 3.2D). Thus, the knockout of receptor C5ar1 and the overexpression of C5a affected genes that act in multiple arms of the complement cascade, including complement factors, receptors, and inhibitors (Figure 3.2E**).**

We investigated changes in expression of genes found in our previous reports of isolated microglia from Arctic and ArcticC5aKO at the same ages (Hernandez et al., 2017), as well as changes in expression of genes known to be associated with AD pathology progression in the

5xFAD mice model (Forner et al., 2021), and human AD genes (Bertram & Tanzi, 2019; Verheijen & Sleegers, 2018; Efthymiou & Goate, 2017; Tanzi, 2012) in order to understand the effects of C5a-C5ar1 signaling on gene expression in AD (Figure 3.2C & Figure S3.5B). Most of the genes upregulated in microglia isolated from the Arctic mice (Hernandez, Jiang, et al., 2017) were part of clusters Rc6 (80 of them) and Rc7 (15 of them), which are clusters linked to inflammation and cholesterol metabolism, respectively (Figure 3.2C). Similarly, most of the genes upregulated in the 5xFAD mouse model are part of Rc6 (306 of them) and Rc7 (105 of them). Interestingly, AD genes Cd33, Trem2, Cst7, and Tyrobp showed increased expression in the Arctic cohort with a peak at 7 months of age, while in the ArcticC5aR1KO cohort the expression did not increase until 10 months of age. Genes Inpp5d, S100a6, Stat3 showed lower expression at all ages in the ArcticC5aR1KO. Thus, C5ar1 deletion either delayed or prevented the expression of several genes upregulated in the Arctic and 5xFAD mouse models, as well as genes upregulated in human AD. Apoe, which is one of the main genetic risk factors for AD (Gottschalk et al., 2016) increased in both Arctic and ArcticC5aR1KO, (but showed decreased expression in the ArcticC5a+ mice) at 10 months of age. In summary, eliminating C5ar1 in the Arctic AD model results in either decreased or delayed expression of many but not all important AD genes, indicating a separation between those genes induced by amyloid plaques and those requiring the C5a-C5aR1 signaling.

While many of the above genes are considered predominantly microglial genes, we sought to determine the changes in expression of astrocyte-associated genes, given that our libraries were built from whole cortex or whole hippocampus tissues which included mainly neurons, astrocytes, and oligodendrocytes, and given the evidence for altered astrocyte states in AD (Habib et al., 2020; Jha et al., 2019; Liddelow et al., 2017). Rc6 contained 18 astrocyte-associated genes, including Pan-reactive astrocyte genes Cd44, Lcn2, Osmr, Vim, and Serpina3n and A1 reactive astrocyte

genes Ggta1, H2-T23, Serping1, and Srgn (Liddelow et al., 2017b) whose expression was higher in the Arctic cohort and ablation of C5ar1 reduced or delayed the activation of those genes. Therefore, C5ar1 deletion may reduce the activation of neurotoxic reactive astrocytes (Figure S3.5C). The overexpression of C5a led to increased expression of those Pan-reactive and A1 genes at 10 months suggesting that an increase in C5a may lead to activation of reactive astrocytes. In contrast, GFAP (pan-reactive), as well as Psmb8 and Aspg (A1), are all highly upregulated in the presence of amyloid plaques regardless of C5aR1 presence or overexpression of C5a, indicating a subset of astrocyte genes that are responsive to insult, but not influenced by C5aR1 signaling (Figure S3.5C**).**

3.3.3 Gene ontology analysis of Rc6 revealed reduced expression of inflammation- and DAM-associated genes in the ArcticC5aR1KO mice

We performed gene ontology analysis to identify relevant biological processes and pathways associated with differentially expressed genes present in each maSigPro cluster. Cluster 6 (Rc6) mainly consisted of genes whose expression was increased in the hippocampus of the Arctic cohort peaking at 7 months while in the ArcticC5aR1KO cohort their expression did not increase until 10 months of age. Rc6 was enriched for DAM genes, such as Trem2, Tyrobp, Cybb, Cst7, Ctss, and Spp1 whose activation was delayed in the ArcticC5aR1KO hippocampus (Figures 3.3C & 3.3A). Rc6 contained inflammatory chemokine genes such as Ccl3, Ccl2, Cxcl9, and Cxcl10, whose signal was also delayed in the Arctic mice in response to C5ar1 ablation. Additionally, gene ontology and pathway analysis showed enrichment for biological processes that are significant in the AD context, for instance regulation of inflammatory signaling including IFN-γ and IL-6 production, as well as microglial cell activation and lysosome pathway, all of which

were likely delayed in the ArcticC5aR1KO cohort (Figure 3.3B). Our results suggested that the ablation of C5ar1 delayed DAM activation, phagocytosis, astrocyte migration, and inflammation (Figure 3.3C).

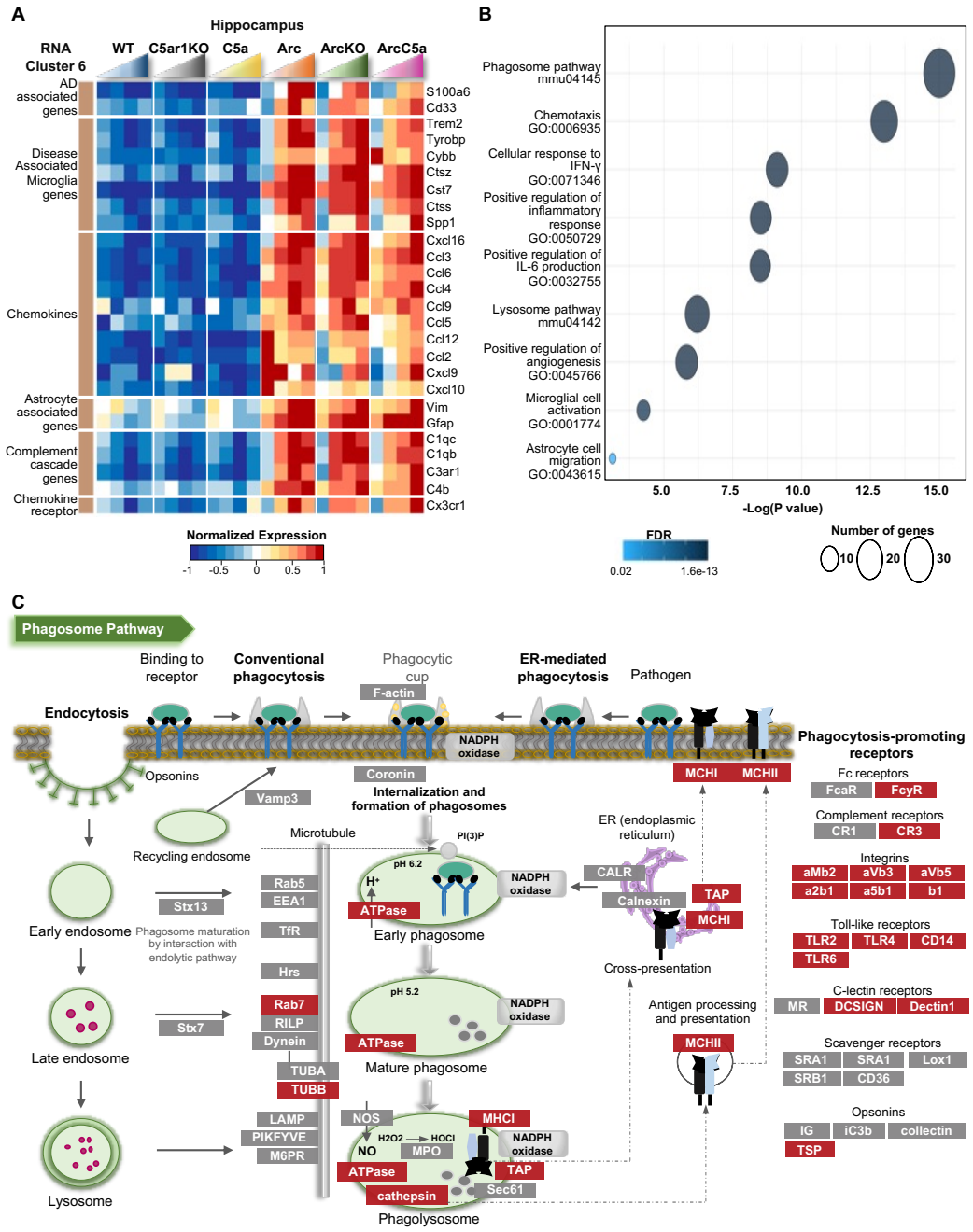

Figure 3.3. Reduction of inflammation- and DAM-associated genes in the ArcticC5aR1KO mice

A) Heatmap of selected genes present in RNA cluster 6. Genes were clustered based on AD study findings and molecular functions: AD-associated genes, disease-associated microglia genes, chemokines, astrocyte-associated genes, complement cascade-associated genes, and chemokine receptors. RNA-seq data (TPM) is row-mean normalized.
B) Gene ontology (GO) and pathway enrichment analyses of genes present in Rc6.
C) Representative diagram of the Phagosome pathway (mmu04145) with select genes present in the panel B heatmap highlighted.

3.3.4 Gene ontology analysis of Rc7 revealed reduced expression of genes associated with cholesterol biosynthesis in the ArcticC5aR1KO mice

Cluster 7 mainly consisted of genes whose expression was increased in the Arctic peaking at 7 months while in the ArcticC5aR1KO their expression did not increase. Rc7 was also dominantly driven by the Arctic mutations and further increased by the overexpression of C5a in the ArcticC5a+ mice at 10 months (Figure 3.4A). Rc7 contained genes associated with inflammatory response, such as Csf1, Icam1, Tnfsf1b, Akna, Sbno2, and Nrros, whose expression was reduced in the Arctic mice at 7 months in response to C5ar1 ablation and further increased in response to C5a overexpression at 10 months. Gene ontology and pathway analysis showed enrichment for lipid metabolic processes, inflammatory response, and cholesterol biosynthesis, suggesting that those processes were reduced upon C5ar1 deletion in the Arctic model and recovered when C5a is overexpressed (Figures 3.4A & 3.4B). Cholesterol cannot cross the blood brain barrier, and almost all brain cholesterol is synthesized locally. Early studies have shown that human AD brain plaques were highly enriched in cholesterol (Panchal et al., 2010) and that reduction of brain cholesterol biosynthesis increased longevity in Alzheimer's disease mice (Strittmatter et al., 2009). Our results suggest that ablation of C5ar1 may be beneficial to AD by reducing brain cholesterol metabolic processes (Figure 3.4C).

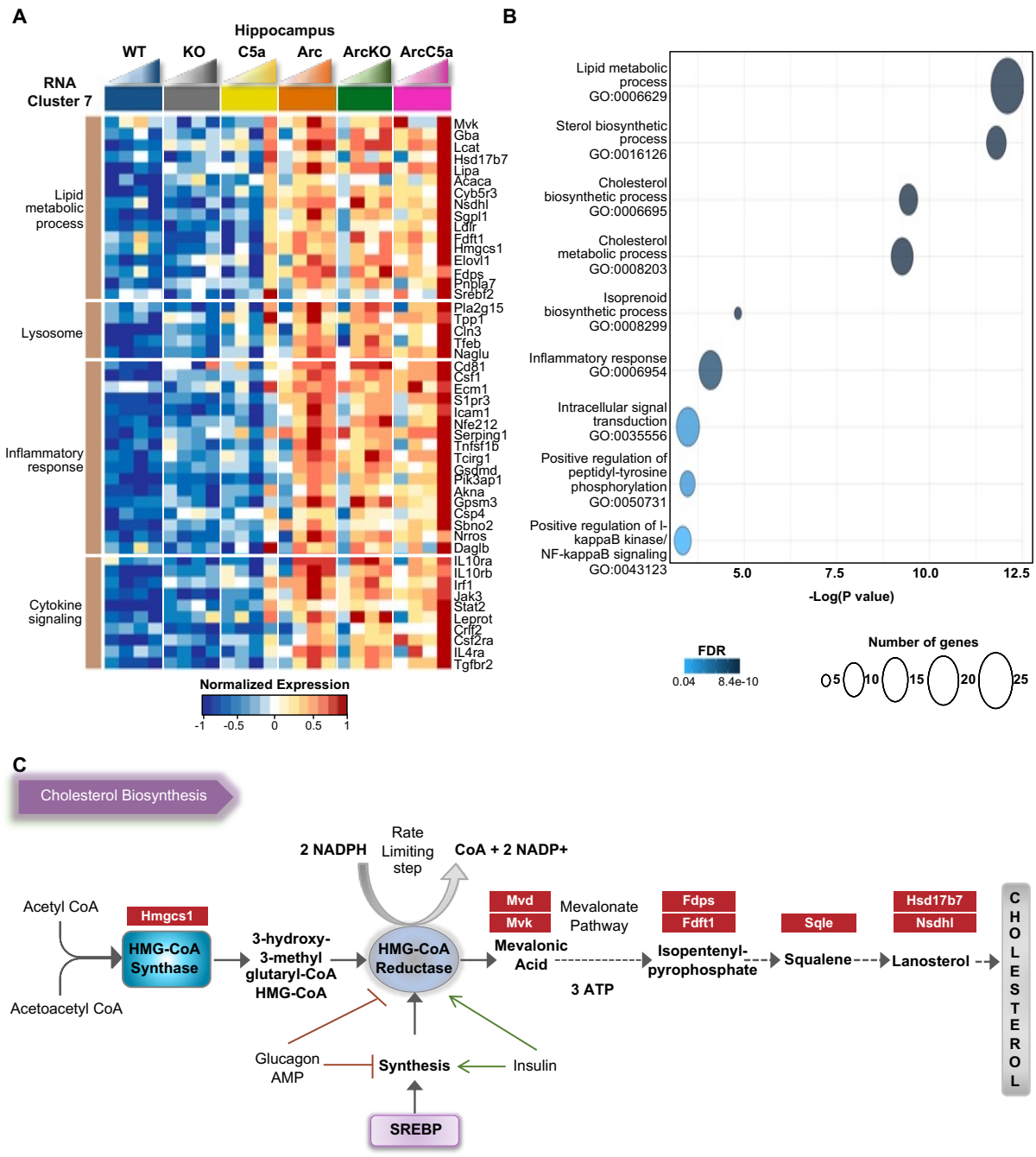

Figure 3.4 Reduced cholesterol biosynthesis-associated genes in the ArcticC5aR1KO mice
A) Heatmap of selected genes present in RNA cluster 7. Genes were clustered based on biological processes and molecular functions: lipid metabolic process, lysosome, inflammatory response, and cytokine signaling. RNA-seq data (TPM) is row-mean normalized.
B) Gene ontology (GO) and pathway enrichment analyses of genes present in Rc7.
C) Representative diagram of the Phagosome biosynthesis pathway with select genes present in the panel B heatmap highlighted.

3.3.5 C5a overexpression leads to increase in expression of genes associated with synapse transmission and assembly

C5a increase has been shown to promote neuronal damage in vitro, and enhance Aβ-associated damage (Hernandez et al., 2017b), although it plays a positive role in neurogenesis during early development (Coulthard et al., 2017)**.** We thus sought to explore effects of C5a overexpression in our mice in the presence and absence of amyloid pathology, given the accelerated deficiency in behavior (Figure 3.1). Genes in clusters 4 and 3 showed increased expression in the C5a+ mice at 10 months in the absence of the amyloid transgene, but also showed less but substantial increases in expression in the ArcticC5a+ cohort at 10 months. These results suggested that Rc4 and Rc3 expression changes were markedly driven by overexpression of C5a (Figure 3.5A). Interestingly, C5a overexpression seems to promote ion transport, synapse assembly, axogenesis, and transcription (Figure 3.5B). Specifically, C5a overexpression is associated with an increase of genes that regulate GABAergic synapse processes (Figure 3.5C). It has been shown that alterations of GABAergic neurotransmission may contribute to AD pathology (Yanfang Li et al., 2016). Therefore, C5a overexpression might contribute to alterations of GABAergic transmissions that may be detrimental to AD prognosis.

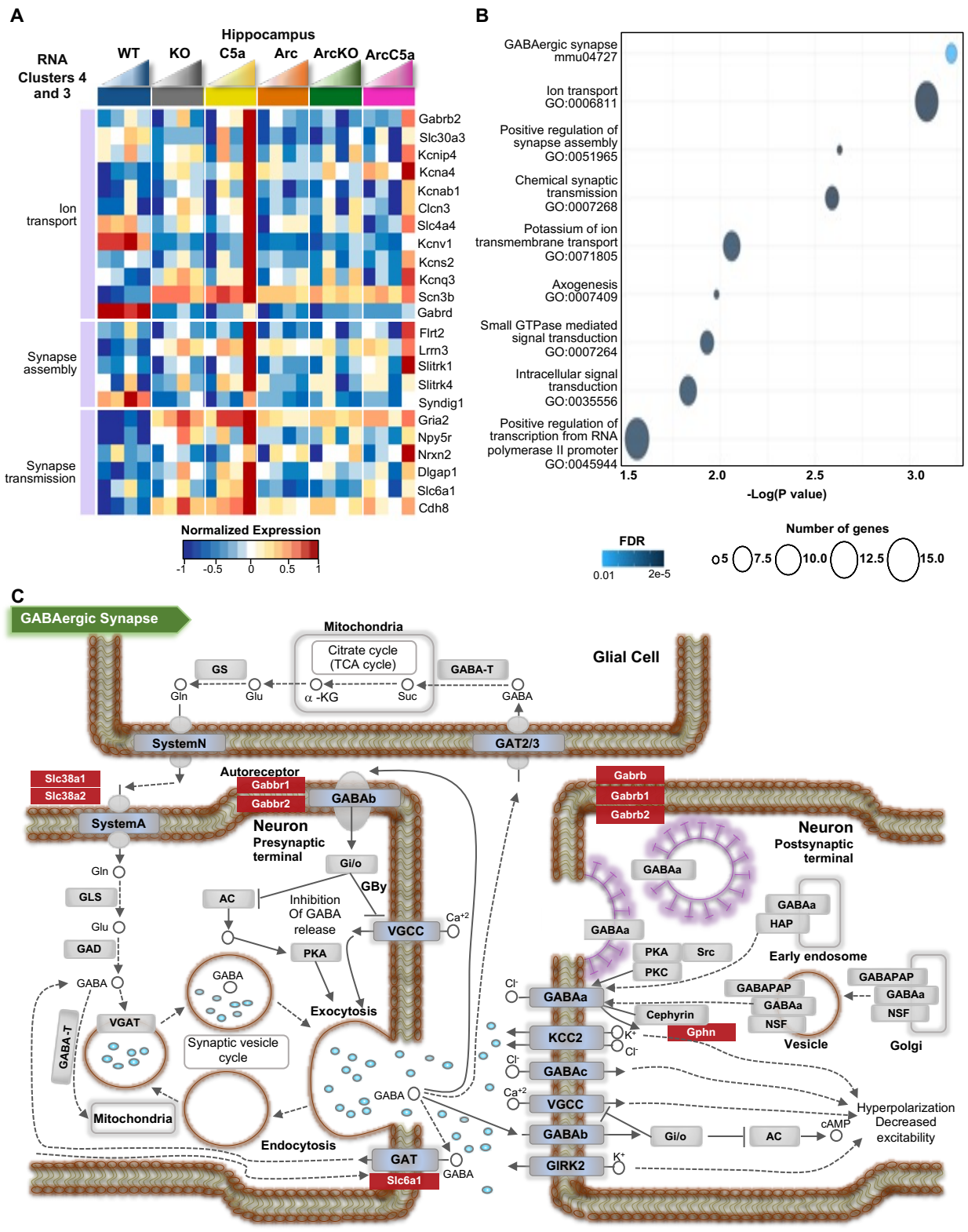

Figure 3.5 C5a overexpression leads to increase in expression of genes associated with synapse transmission and assembly

A) Heatmap of selected genes present in RNA clusters 3 and 4. Genes were clustered based on biological processes: ion transport, synapse assembly, and synapse transmission. RNA-seq data (TPM) is row-mean normalized.
B) Gene ontology (GO) and pathway enrichment analyses of genes present in Rc6.
C) Representative diagram of the GABAergic synapse pathway with select genes present in the panel B heatmap highlighted.

3.3.6 Ablation of C5aR1 reduces microglial activation in the Arctic mouse.

Amyloid pathology in humans and animal models can activate microglia to an inflammatory and disease-enhancing state (Dani et al., 2018; Sarlus & Heneka, 2017). Thus, we characterized the age- and pathology-dependent changes of several microglial markers in the Arctic and ArcticC5aR1KO mice alongside their controls (Figure 3.6). We assessed the hippocampus and cortex separately as amyloid deposition and glial activation are first seen in the hippocampus in the Arctic model.

The ionized calcium binding adaptor molecule 1 (Iba1) is a macrophage- and microglia-specific marker that is expressed on most microglia and has been shown to increase in expression after injury or in neurodegenerative diseases (Ohsawa et al., 2004). As expected, percent field area of Iba1 was greater in Arctic and ArcticC5aR1KO hippocampus and cortex compared to WT and C5aR1KO controls (Figure 3.6A) At 7 months of age, both Arctic and ArcticC5aR1KO mice had elevated levels of Iba1 in the hippocampus ($p < 0.0001$) and in the cortex ($p < 0.01$) compared to WT and C5aR1KO controls. By 10 months, Iba1 levels increased in the WT and C5aR1KO, supporting a primed state, as expected with age (Harry, 2013). However, Arctic levels were still higher relative to WT ($p < 0.01$) in the hippocampus. Interestingly, Iba1 field area was lower in the ArcticC5aR1KO hippocampus at 10 months compared to Arctic ($p < 0.01$) and comparable to C5aR1KO control levels (Figure 3.6B). In the cortex, Iba1 was higher at 7 months in the Arctic

and ArcticC5aR1KO compared to controls ($p < 0.001$), but by 10 months, no significant differences were observed (Figure 3.6C).

Although we observed significant changes in Iba1 in the Arctic brain that were partially mitigated by the deletion of C5aR1, Iba1 is considered a pan-reactive microglial marker, and thus to further define the disease-associated status of the microglia, we assessed several markers that are either associated with phagocytosis or inflammation. CD68 is a lysosomal marker that is present in microglia is indicative of clearance of ingested material (Walker & Lue, 2015; Zotova et al., 2013). In Arctic mice, CD68 was significantly elevated at 7 months in the hippocampus compared to WT ($p < 0.01$) and at 10 months in both the hippocampus ($p < 0.0001$) and cortex ($p < 0.001$) (Figures 3.6D-F). CD68 expression was similar in ArcticC5aR1KO mice compared to the Arctic mice, suggesting that although ArcticC5aR1KO mice may have slightly fewer Iba1-postive microglia, these microglia have a proportionally greater phagocytic and degradative capacity than Arctic mice, particularly in the hippocampus. This may have an important impact on plaque clearance and degradation.

CD11b is part of the integrin receptor, CR3, for iC3b/C3b that is expressed exclusively on microglia in the CNS (Czirr et al., 2017). While detectable levels of CD11b were consistently low in WT and C5aR1KO mice, there was a significant increase in Arctic and ArcticC5aR1KO observed as early as 5 months of age in the hippocampus and 7 months in the cortex (Figures 3.6G-I). By 10 months of age, CD11b field area was reduced in ArcticC5aR1KO compared to Arctic in the hippocampus ($p < 0.001$) and cortex ($p < 0.05$), and were comparable to WT and C5aR1KO levels. Microglia high in CD11b in AD are typically associated with plaques and worsening pathology (Hickman et al., 2018). It is possible that ArcticC5aR1KO mice have an early yet mild

DAM response at 7 months of age and subsides at 10 months. Therefore, C5aR1 ablation might prevent amyloid-associated cognitive decline that is observed in the Arctic mice at this later age.

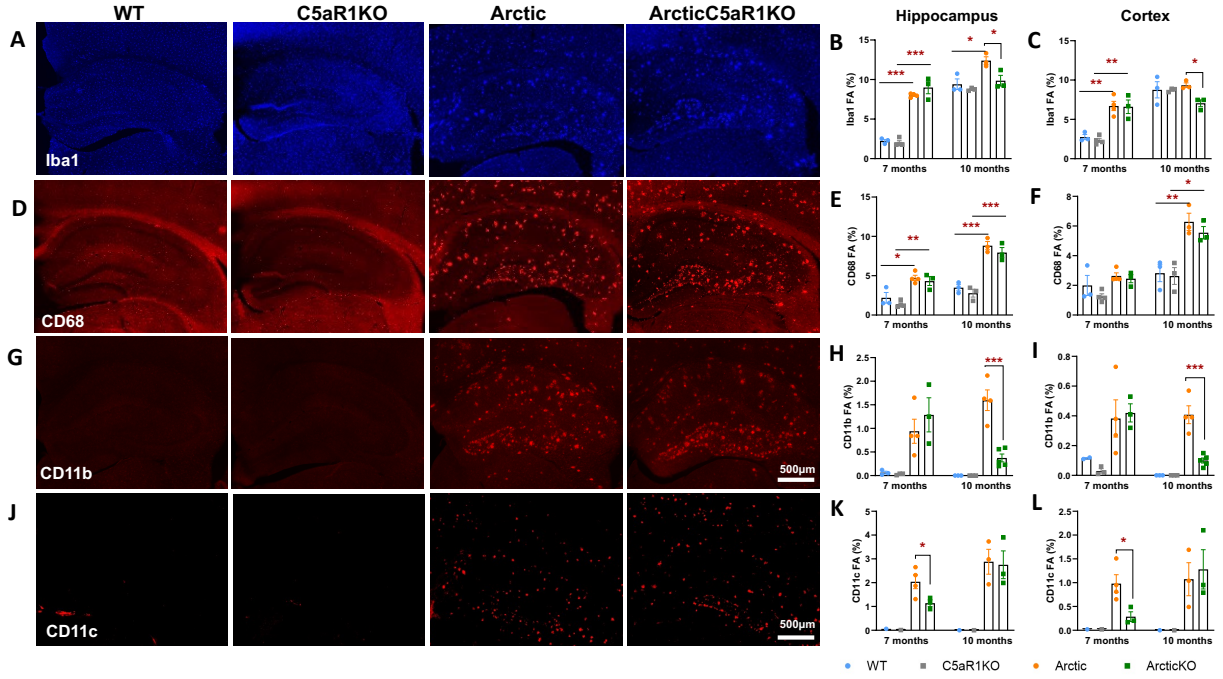

Figure 3.6 Microglial activation in ArcticC5aR1KO
Immunoreactive staining of Iba1 (A), CD68- (D), CD11b- (G), and CD11c-positive (J) microglia in WT, C5aR1KO, Arctic, and ArcticC5aR1KO. Representative images from 10 months; N=2-6 mice per genotype, 4 sections per mouse.
Quantification of Iba1 (B and C), CD68 (E and F), CD11b (H and I), and CD11c (K and J) percent field area (%FA) in cortex and hippocampus. T-test (Arctic vs ArcticKO) *p<0.05; **p<0.01; ***p<0.001; ****p<0.0001; One-way ANOVA w/ turkey's post hoc for comparisons of genotypes within one age.

CD11c-positive microglia appear relatively early in response to plaque deposition and continue to increase with disease progression around plaques in APP/PS1 mice (Kamphuis et al., 2016). To determine if CD11c protein expression was influenced by C5a-C5aR1 signaling in the Arctic model, a time-course of CD11c expression was analyzed (Figure 3.6C). While expression was absent in the WT and C5aR1KO genotypes, CD11c levels increased with age/disease progression in the hippocampus and cortex of Arctic ($p < 0.001$) and ArcticC5aR1KO ($p < 0.001$) mice (Figures 3.6J-L). CD11c was lower in the ArcticC5aR1KO hippocampus ($p = 0.05$) and

cortex ($p = 0.03$) compared to the Arctic. However, while the levels of CD11c plateaued in the Arctic hippocampus and cortex at 10 months, levels continued to steadily rise in the ArcticC5aR1KO, resulting in comparable levels at this later age.

3.3.7 GFAP+ astrocytes are largely unaltered by C5aR1 engagement in the hippocampus.

A recent study demonstrated that inflammatory cytokines released by microglia can trigger a shift towards neurotoxic reactivity in astrocytes. Thus, in order to characterize changes in astrocyte function with disease progression and modulation of C5a-C5aR1 signaling, we used immunohistochemistry for the pan-reactive astrocyte marker GFAP (Figure 3.7A**)** and the "A1" astrocyte marker C3 (Figure 3.7B**)** throughout the progression of AD. As expected, we observed a significant increase in GFAP percent field area in all three Arctic groups compared to their respective controls in the hippocampus and cortex (Figures 3.7C-D). However, we were surprised to find that neither overproduction of C5a nor ablation of C5aR1 altered GFAP levels in the hippocampi of Arctic mice. Interestingly, ablation of C5aR1 did result in reduced levels of GFAP in the Arctic cortex at 7 months ($p < 0.05$). Similarly, C3 levels were elevated in the brains of Arctic, ArcticC5aR1KO, and ArcticC5a+ mice compared to WT, C5aR1KO, and C5a+ controls, particularly at 7 and 10 months of age, and levels tended to increase with age in the three Arctic groups but not in the controls (Figures 3.7E-F**)**. However, C3 levels were not different between Arctic, ArcticC5aR1KO, or ArcticC5a+ in the hippocampus, while there was a decrease in C3 in the cortex of ArcticC5aR1KO and ArcticC5a+ compared to Arctic mice ($p < 0.05$). These data suggest that there is a region-specificity to the profiles of astrocytes in the Arctic mouse. Furthermore, these data support that C5a-C5aR1 engagement does not influence the microglia-mediated programing of neurotoxic astrocytes. Lastly, our negative findings in hippocampal

astrocyte characterization suggest that microglial pathology are more influential in neurodegeneration and cognitive decline in the Arctic mouse model of AD.

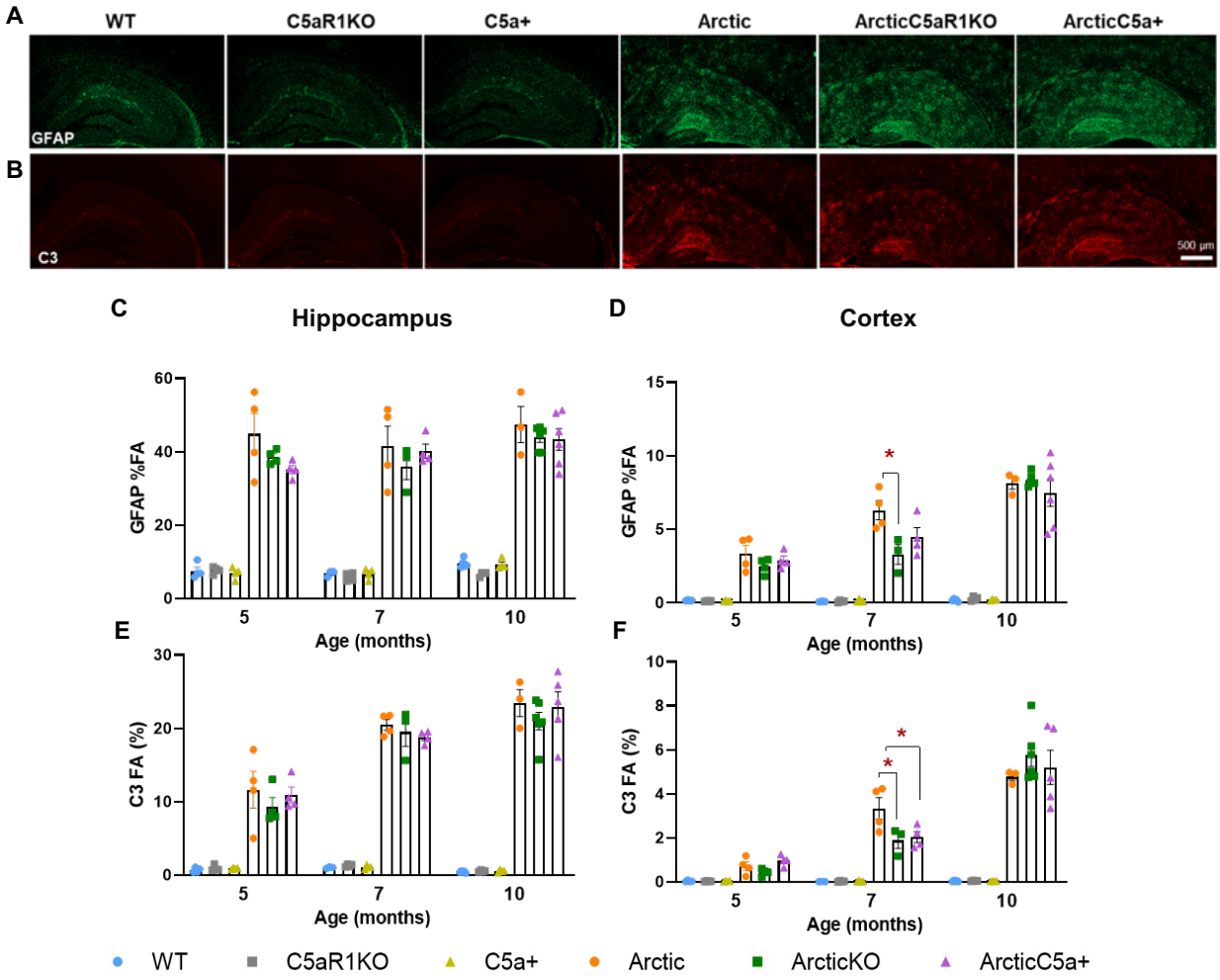

Figure 3.7 Astrocyte pathology in Arctic, ArcticC5aR1KO, and ArcticC5a+ mice
A) and B) Immunoreactive staining of GFAP-positive (A) and C3-positive (B) astrocytes in WT, C5aR1KO, C5a+, Arctic, ArcticC5aR1KO, and ArcticC5a+ hippocampus and cortex.
C) and D) Quantification of GFAP percent field area (%FA) showed an increase in expression in all Arctic genotypes compared to the non-Arctic controls. GFAP %FA was significantly reduced in the ArcticC5aR1KO cortex compared to Arctic mice at 7 months of age (D).
E) and F) Quantification of C3 %FA showed an increase in expression in all Arctic genotypes compared to the non-Arctic controls. C3 %FA was significantly reduced in the ArcticC5aR1KO and ArcticC5a+ cortex compared to Arctic mice at 7 months of age (F). All data shown as mean ± SEM. *$p < 0.05$ One-way ANOVA, Tukey's post hoc test. N = 3-6 per genotype

3.4 Discussion

For the past decade or so, the role of the complement pathway on synaptic pruning, neuronal injury, and cognitive decline has been heavily studied. In the healthy brain, complement proteins tag extranumerary synapses or cellular debris for clearance by microglia. However, aberrant complement activity may result in the removal of stressed but otherwise healthy neurons. Complement proteins are upregulated in the mouse brain with normal aging and are further increased in models of AD. Since inhibition of upstream complement components (such as C1, C3 and CR3) would also impair the immunoprotective functions of the complement pathway, we have explored the effects of C5a, whose inhibition or ablation will not affect upstream complement signaling. Additionally, C5aR1 inhibition still allows for the formation of the downstream membrane attack complex. Our lab has shown that pharmacologic inhibition or genetic ablation of C5aR1 prevents learning and memory deficits in multiple models of AD.

The early spread of human AD pathology is not uniform throughout different brain regions, with the frontal and temporal regions of the cortex showing amyloid deposits in early human AD. Interestingly, early amyloid pathology in the Arctic model is observed first and more severely in the hippocampus, and only spreads to the cortex in later disease stages. Interestingly, our RNA-seq data confirmed that changes in gene expression in consequence of C5aR1 ablation or C5a overexpression were more prominent in hippocampi compared to cortex in the Arctic mice. In addition, the Arctic mouse model did not present significant changes in hippocampal or cortical gene expression between males and females, suggesting that sex-specific differences seen in other AD mouse models may be due to their transgenes. Therefore, the Arctic mouse model has the advantage of revealing pathways common to Alzheimer's disease in both sexes.

Our RNA-seq results suggested that overexpression of C5a in the Arctic mice was not as deleterious as expected, with inflammatory genes being delayed until later in pathology (10 months), and genes associated with synaptic transmission being upregulated in both C5a+ and ArcticC5a+ hippocampi. This may suggest some off-target activity of C5a that may counteract or attenuate the toxic effects of C5a ligation to C5aR1. C5aR2 is an alternative receptor for C5a and its functions are not well elucidated. In vitro studies have confirmed that C5a and a metabolized fragment of C5a (C5a-des Arg) bind to C5aR1 and C5aR2 with similar affinities. C5aR2 has been hypothesized to be a regulatory receptor for C5a. Furthermore, C5aR2 can interact with C5aR1, which promotes C5aR1 internalization via recruitment of β-arrestin and downregulation of ERK signaling, suggesting that C5aR2 is a negative regulator of C5a-C5aR1 activity. A recent study using primary human macrophages demonstrated further evidence that C5aR2 activation attenuates C5aR1-mediated signaling and reduces inflammation in a C5a-dependent manner (Li et al., 2020). C5aR2 seems to bind to extra C5a that is available to regulate its effects. Furthermore, C5aR2 agonism reduces C5a-C5aR1- mediated inflammatory response to toll-like receptors, c-type lectin receptors, or cytosolic DNA sensor stimulator of IFN genes. Therefore, the reduced expression of inflammatory genes seen in the C5a+ and ArcticC5a+ cohorts at 5 and 7 months might be due to excess of C5a and its binding to C5aR2.

We didn't identify significant differences in CD11c expression between ArcticC5aR1KO and Arctic at 5 months, which indicates that knocking out C5aR1 does not affect CD11c expression at this early age. Later at 7 months we observed a steeper increase in CD11c expression in the Arctic compared the ArcticC5aR1KO mice. This difference is no longer seen at 10 months, suggesting a continued increase in CD11c expression in the ArcticC5aR1KO, while in the Arctic mice a plateau maybe reached. Thus, the data suggested that ablating C5aR1 from Arctic mice

may delay or alter expression of specific microglial activation states during the early ages of 5-7 months, which is overcome at later ages (between 7-10 months).

Here, we provide a characterization of behavioral, cellular, molecular, and genetic changes that occur throughout disease progression and that are modulated by C5aR1 activation in the Arctic mouse model of AD. We demonstrated further support of a detrimental role of C5a-C5aR1 signaling in the Arctic mouse, wherein overexpression of C5a in this model resulted in an acceleration of hippocampal-dependent spatial memory deficits that were accompanied by a loss of neuronal marker (NeuN) in the hippocampus. We identified a trend towards increasing select microglial and astrocyte markers with age in the ArcticC5a cohort, suggesting that this molecule enhances the glial response to Aβ-induced injury. C5a overexpression is also associated with increased inflammatory and DAM-associated markers while ablation of the receptor C5aR1 reduced these markers, supporting a detrimental role of C5a-C5aR1 signaling in AD. These data support that inhibition of the potent anaphylatoxin C5a, while leaving C1q and C3 intact, has neuroprotective effects, marking C5a-C5aR1 signaling as a promising therapeutic target for AD.

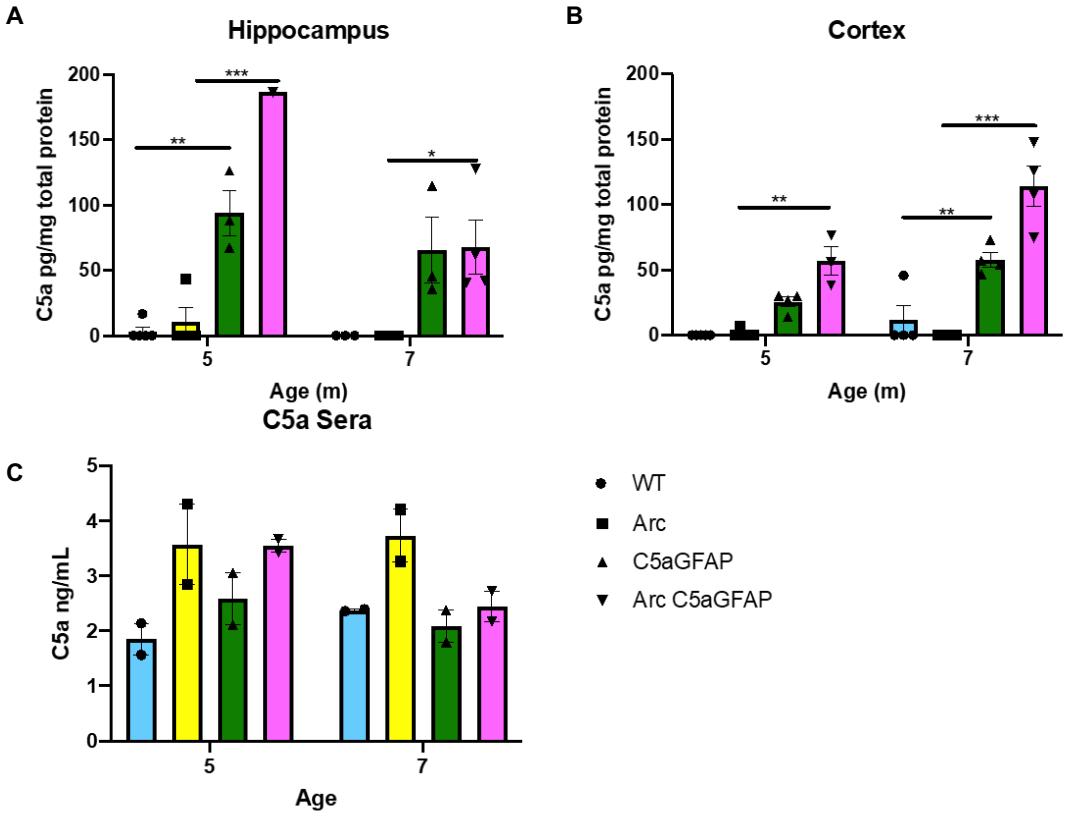

Figure S3.1 Brain and sera levels of C5a
C5a levels detected via enzyme-linked immunosorbent assay (ELISA) of half hippocampi (A), cortices (B), and sera (C) in WT, C5a, Arctic, and ArcticC5a mice at 5, 7, and 10 months of age. Data shown as Mean ± SEM. *$p < 0.05$; **$p < 0.001$; *** $p < 0.0001$; Two-way ANOVA with Tukey's post hoc test. N= X-X per genotype

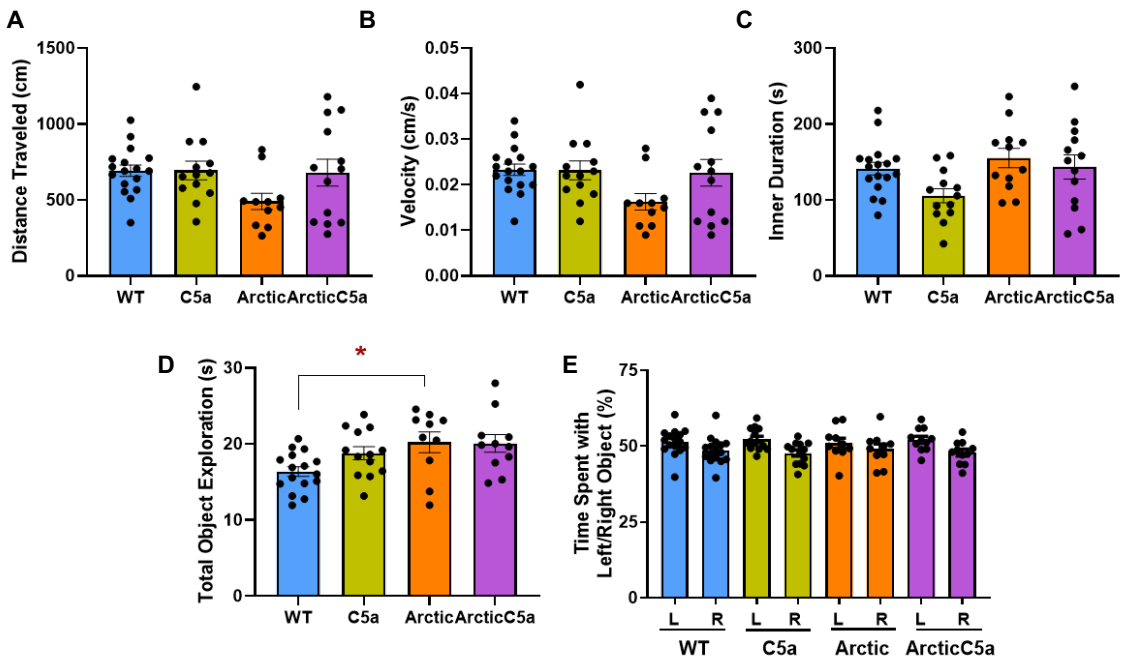

Figure S3.2 Locomotion and exploration during open field (OF) and object location memory (OLM) training at 7 months

A-C) During OF, mice were recorded and distance travelled (A), velocity (B), and inner duration (C) were measured to account for possible changes in locomotion or anxiety-like behaviors.

D-E) During OLM training, total object exploration and preference of the left (L) or right (R) objects was assessed. Data shown as Mean ± SEM. *p < 0.05. Two-way ANOVA with Tukey's post hoc test. Object preference compared with paired t-test. For Open Field N = 17 (WT), 13 (C5a+), 12 (Arctic), 13 (ArcticC5a+). For OLM training N = 16 (WT), 13 (C5a+), 10 (Arctic), 11 (ArcticC5a+).

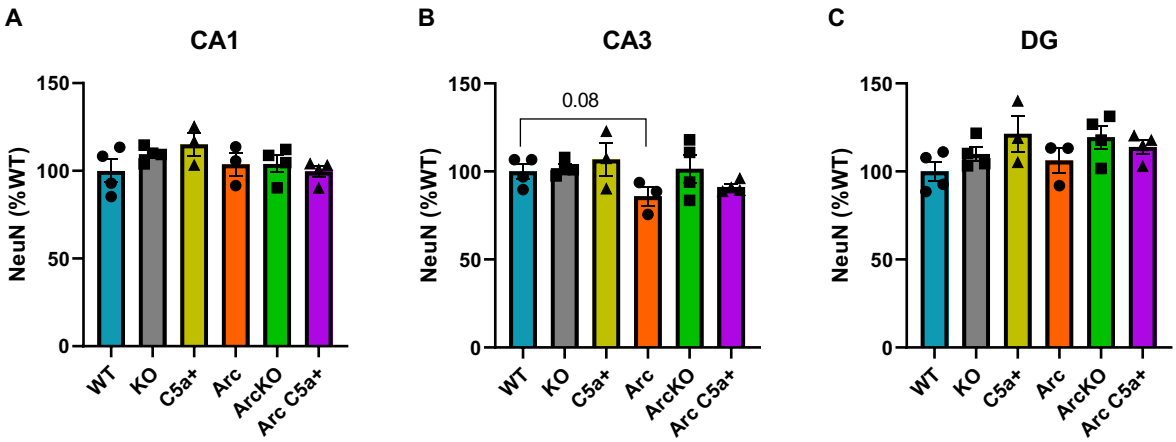

Figure S3.3 Loss of NeuN in the CA3 is attenuated in ArcticKO

NeuN levels detected in hippocampal regions CA1 (A), CA3 (B), and DG (C). NeuN levels are slightly decreased (15%) in the CA3 of Arctic mice compared to WT. WT, KO, C5a+, Arctic, ArcKO, and ArcticC5a+ mice at 10 months of age.

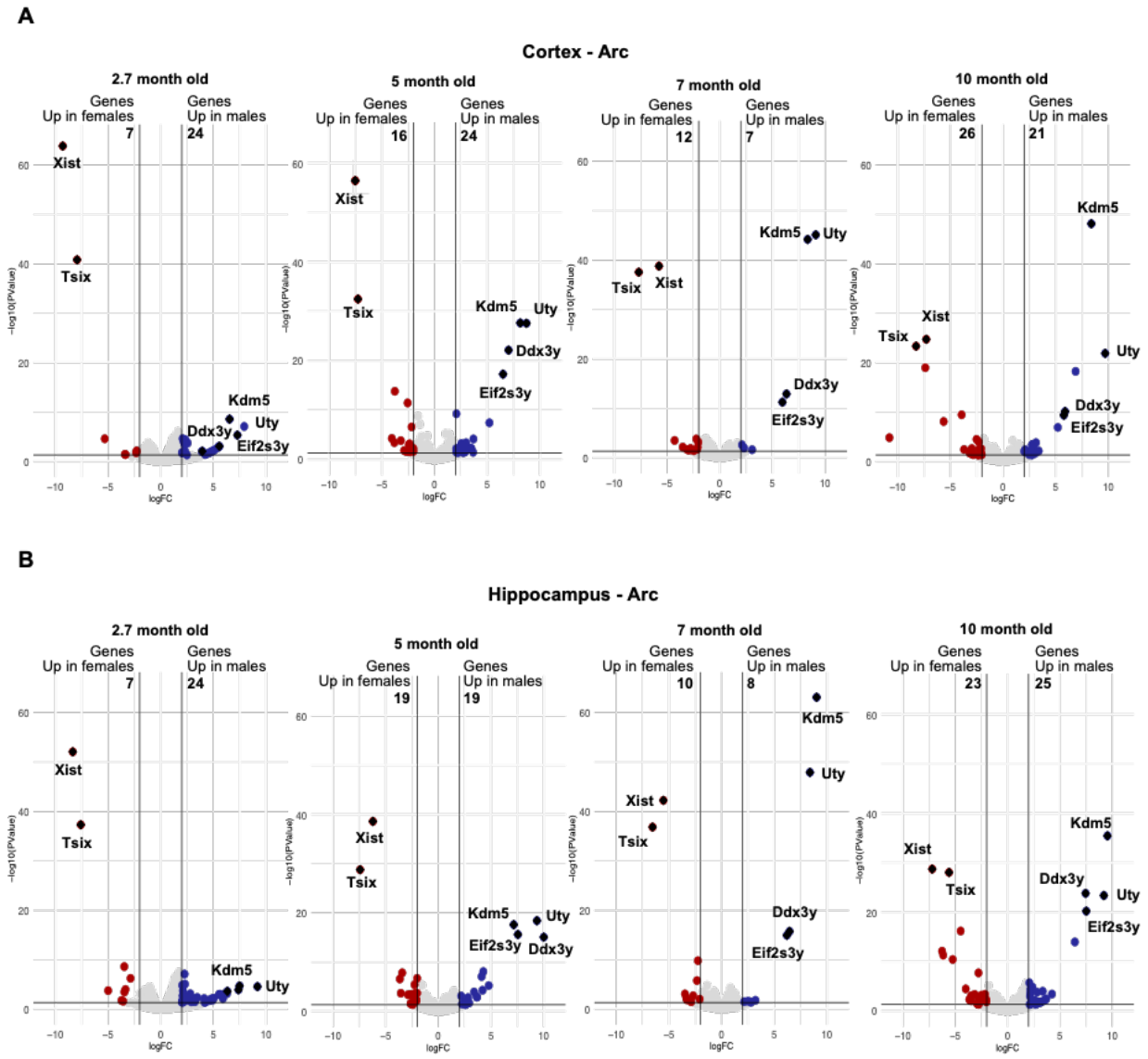

Figure S3.4 Differential expression analysis show lack of sex-specific changes in gene expression in the Arctic mice

A) Volcano plot highlighting genes upregulated in cortices of Arctic female mice (left) and genes upregulated in cortices of Arctic male mice (right) at 2.7, 5, 7 and 10 months of age. Differentially expressed genes are colored in gold, green, orange, and blue, respectively. p value < 0.05, |log2FC| > 2. Genes highlighted are known sexually dysmorphic genes.

B) Volcano plot highlighting genes upregulated in cortices of Arctic female mice (left) and genes upregulated in cortices of Arctic male mice (right) at 2.7, 5, 7 and 10 months of age. Differentially expressed genes are colored in gold, green, orange, and blue, respectively. p value < 0.05, |log2FC| > 2. Genes highlighted are known sexually dysmorphic genes.

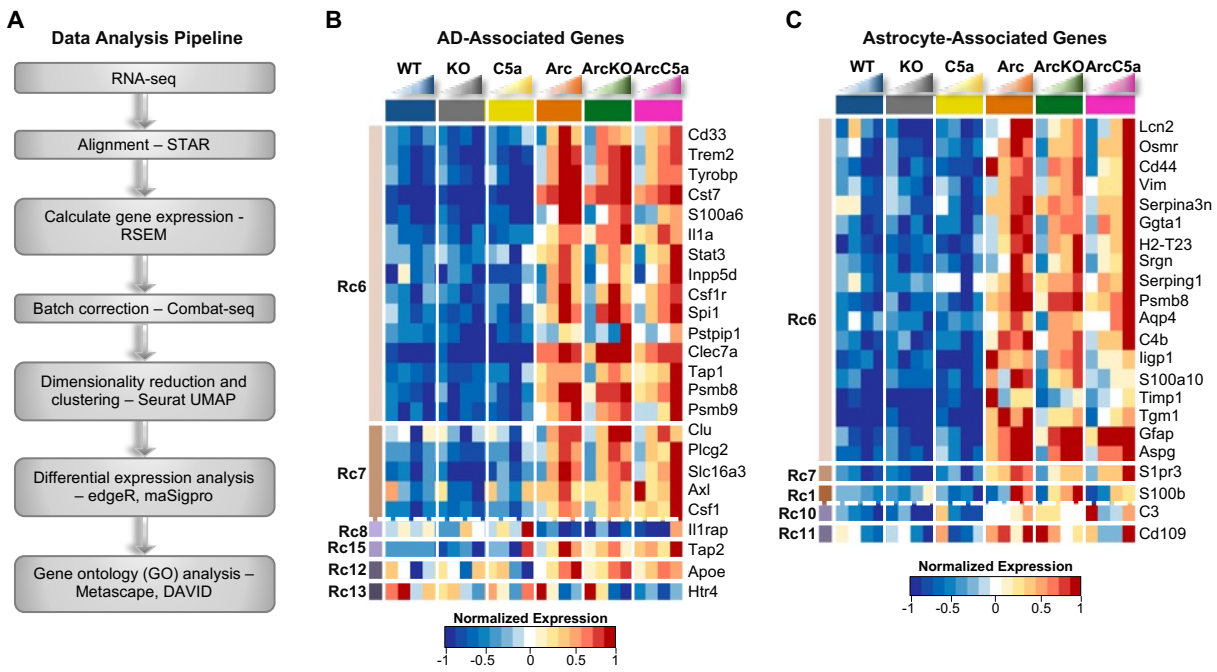

Figure S3.5 C5ar1 knockout in the Arctic AD model results in a decrease or delay of expression of some important AD and astrocyte-associated genes
A) RNA-seq data analysis pipeline
B) Heatmap of 24 genes linked to Alzheimer's disease progression that were present in maSigPro identified clusters. RNA-seq data (TPM) is row-mean normalized.
C) Heatmap of 22 astrocyte-associated genes that were present in maSigPro identified clusters. RNA-seq data (TPM) is row-mean normalized.

3.5 Methods

3.5.1 Animals

The Institutional Animal Care and Use Committee of University of California at Irvine approved all the animal procedures performed and experiments were performed according to the NIH Guide for the Care and Use of laboratory animals. Mice were grouped housed in ambient temperature and given access to food and water ad libitum. The Arctic48 mouse model of Alzheimer's disease on a C57BL6/J background (hereafter referred to as Arctic), which carries the human APP transgene with three mutations – the Indiana (V717F), the Swedish (K670 N + M671 L), and the Arctic (E22G), was originally provided by Dr. Lennart Mucke (Gladstone Institute,

San Francisco, CA). This hemizygous mouse model produces fibrillar plaques as early as 2 to 4 months of age (Cheng et al., 2004). C5a-overexpressing mice, created by cloning the coding region for the C5a fragment of C5 plus a signal sequence into a construct containing the GFAP promoter to induce production and secretion of C5a as a function of induction of GFAP (Reiman et al., 2005), were crossed to Arctic+/- mice generating WT, Arctic, C5a+ and ArcticC5a+ mice. C5aR1KO mice, created by targeted deletion of the C5a receptor 1 gene (Hollmann et al., 2008), were crossed to Arctic+/- mice to generate mice homozygous for C5aR1 deletion with and without the Arctic transgene. These mice were used to assess the effect of C5a overexpression on amyloid-associated cognitive decline, as well as the effects of C5a overexpression or C5aR1 ablation on microglial and astrocytic gene expression in wild type and Arctic mice from 2.7 months to 10 months of age. Both male and female mice were used in all experiments.

3.5.2 Object Location Memory

Object location memory (OLM) took place in dim lighting (50-70 Lux) in testing arenas (37.3 X 30.8 X 21.6 cm) covered with approximately 1 cm of sawdust bedding as previously described (Hernandez et al., 2017; Vogel-Ciernia & Wood, 2014). Briefly, mice were handled for 2 minutes each per day over 5 days in the testing room and were acclimated to the testing arena for 5 minutes per day over 6 days. The last two days of handling overlapped with the first two days of habituation. The first day of habituation was used as an open field test for measures of locomotion and anxiety-like behaviors. On the training day, two identical objects (e.g. 100 mL glass beakers, blue Legos, or opaque light bulbs) were placed in opposite and symmetrical locations in the testing arena and mice were allowed to freely explore the objects over 10 minutes for the familiarization trial. Twenty-four hours later, one of the objects was moved to the opposite

corner from its original placement and mice were again allowed to explore the objects for 5 minutes. Exploration of objects was calculated per minute and was determined to peak by the end of 2 minutes, dropping thereafter. Therefore, subsequent analyses were done on the first two minutes of the OLM test trial as previously described (Hernandez et al., 2017). To prevent olfactory distractions, all objects and arena were cleaned with ethanol and bedding was stirred after each trial (different bedding was used for males and females). Training and testing sessions were recorded by mounted cameras from above and exploration of both objects was scored manually by 2 blinded experimenters using stopwatches. Discrimination indices were calculated with the formula (time spent with moved object minus time spent with unmoved object)/time spent with both objects) x 100 to obtain a percent (%) discrimination index (DI) (Vogel-Ciernia & Wood, 2014). Results were compared with two-way ANOVA followed by Tukey's post hoc tests. Differences were considered significant when p was < 0.05. Mice were removed from the analysis if they spent less than 1 second/minute with the objects during training and/or testing or if the performance of mice was ± 2 standard deviations from the mean. (Data are presented ± SEM).

3.5.3 Immunohistochemistry (IHC)

Mice were deeply anesthetized with isoflurane and perfused transcardially with cold phosphate buffered saline (PBS; 137 mM NaCl, 2.7 mM KCl, 4.3 mM Na_2HPO_4, 1.47 mM KH_2PO_4, pH 7.4). Half brains were quickly dissected and fixed in 4% paraformaldehyde for 24 hours, then stored PBS with 0.02% sodium azide at 4°C. 30-40 μm coronal sections were obtained.

For colorimetric IHC, tissues were briefly washed with PBS, then incubated in 3% hydrogen peroxide (in H_2O) for 30 minutes, followed by 20 minutes incubation in PBS with 3% Triton-x (Tx) (Sigma #T8787), and then incubated for at least one hour in immunobuffer (5%

normal horse serum, 2% BSA (Sigma #A2153) in PBS+0.1%Tx). Tissues were incubated in mouse anti-NeuN (1:1000, Millipore #MAB377) or goat ant-mouse CD45 (0.2 µg/mL, R&D systems #AF114), or rat anti-mouse CD45 (1 µg/mL, Biorad, #MCA1031G) in immunobuffer overnight at 4°C. Following primary antibody incubation, tissues were washed, then incubated in biotinylated secondary antibodies against the corresponding species followed by incubation in avidin-biotin complex (Vector #PK-6100), and stain was developed with DAB (Vector #SK-4100). Tissues were then mounted on glass slides, dehydrated in ascending ethanol concentrations, cleared with xylene, and coverslipped with permount (Fisher #SP15-100). Images were acquired with a ZEISS Axio Scan.Z1 Digital Slide Scanner at 10X magnification, and percent field area was measured in the CA1, CA3, and DG with ImageJ.

For immunofluorescence, sections were incubated in blocking solution (2% BSA, 10% NGS, and 0.1% TxPBS) for 1 hour on a shaker at RT. Tissues were then incubated with primary antibody diluted in blocking solution overnight on a shaker at 4°C. Primary antibodies used were rabbit anti-Iba1 (1:1000, Wako #019-19741), rat anti-CD68 (1:700 Biolegend #137001), rat anti-CD11b (Biorad #MCA74G), hamster anti-CD11c (1:400, Biorad #MCA1369), rat anti-mouse C3 (1:50, Hycult #HM1045), rabbit anti-GFAP (1:2900, Dako #Z0334). Alexa Fluor secondary antibodies were diluted 1:500 in blocking solution and included 568 Goat anti-Armenian hamster (Abcam, # ab175716), 555 goat anti-rat (Invitrogen #A21434), 488 goat anti-rabbit (Invitrogen #A-11070), and 647 goat anti-rabbit (Invitrogen #A21244). To counterstain with Thioflavin-S (ThioS), sections were incubated in 0.1% ThioS in ddH2O for 10 min after secondary antibody. To stain with Amylo-Glo (1:100 in PBS, Biosensis #TR-300-AG), tissues were incubated for 10 min before the first blocking step, washed in PBS for 5 min, and quickly rinsed with ddH_2O before continuing with the IHC protocol. Sections were mounted and coverslipped with Vectashield

(VECTOR). Low magnification images (10X) were acquired using ZEISS Axio Scan.Z1 Digital Slide Scanner. The mean areas of C3, GFAP, CD11b, CD11c, CD68, Iba1, and plaques were quantified in the hippocampal regions CA1, CA3, and DG and in the cortex using the Surfaces feature of Imarisx64 (version 9.5.0). Quantitative comparisons between groups were always carried out on comparable sections of each animal processed at the same time with same batches of solutions.

3.5.4 Enzyme-linked immunosorbent assay

To confirm that mice expressing the C5aGFAP+/- transgene produce higher quantities of C5a protein, we performed enzyme-linked immunosorbent assay (ELISA) on pulverized hippocampus and cortex and on plasma taken from WT, Arctic, C5a, and ArcticC5a mice at 5 and 7 months.

3.5.5 RNA extraction

Mice were perfused with PBS and dissected cortex and hippocampus were stored at -80°C prior to RNA extraction. Hippocampus and cortex were lysed separately in RLT (Qiagen # 80204) buffer with 1% β-Mercaptoethanol by the QIAGEN TissueLyser. We extracted total RNA of each tissue using the QIAGEN RNeasy mini kit (Qiagen # 80204) and quantified it using the NanoDrop ND-1000 spectrophotometer. The RNA integrity number (RIN) was assessed using the Agilent 2100 Bioanalyzer and the samples with RIN > 8.0 were used for library preparation.

3.5.6 RNA-seq library preparation

Bulk sequencing experiments were conducted utilizing between 5 and 8 mice per genotype per age (usually with equal numbers of M and F). RNA-seq libraries were built following the Smart-seq2 protocol using the Nextera library preparation kit (Picelli et al., 2014). In brief, polyadenylated RNA is reverse transcribed and a template-switching oligo (TSO) is added, which carries 2 riboguanosines and a modified guanine to induce a locked nucleic acid (LNA). cDNA is then amplified, and the resulting fragments are tagmented. Fragments between 150 and 600 nucleotides are finally selected using Ampure XP beads. The quality of all libraries was assessed using the Agilent 2100 Bioanalyzer. Bulk libraries were sequenced using the NextSeq 500 (Illumina) obtaining at least 10 million reads per RNA-seq sample.

3.5.7 RNA-seq processing and data analysis

Paired-end RNA-seq reads were aligned to mm10 reference genome and annotated to Gencode v21 transcriptome using STAR v.5.1 (Dobin et al., 2013). Gene expression was calculated using RSEM v1.2.25 (B. Li & Dewey, 2011). Possible noise introduced by batch effects was corrected by the R (version 3.6.2) package Combat-seq (Zhang et al., 2020). Data was then normalized using edgeR trimmed mean of M-values (TMM) function (Mark D Robinson & Oshlack, 2010). TPM was calculated utilizing a custom script and ComBat-seq batch corrected counts as input. Two statistical outliers were removed based on dimensionality reduction by PCA and Pearson correlation coefficient (Mukaka, 2012). A total of 372 RNA-seq data sets were generated.

3.5.8 Differential expression analysis

The R package maSigPro (version 1.58.0) was used to identify gene expression changes over time allowing for k-means clustering of genes that present similar patterns of expression during the time course (Nueda et al., 2014). In addition, edgeR (version 3.28.1) was used to identify genes differentially expressed between selected ages and genotypes (Robinson et al., 2010) using a false discovery rate (FDR) of 1% and an alpha of 0.05. We utilized expression as TMM normalized counts represented as a count per million (CPM) matrix in both aforementioned packages.

3.5.9 Gene ontology and pathway analysis

Gene ontology enrichment analysis was performed using Metascape and DAVID online tools computing gene-set overlaps between pathways and biological processes, that were selected based on p-values smaller than 0.05 (D. Huang et al., 2007; Yingyao Zhou et al., 2019).

CHAPTER 4

Discussion and Future Perspectives

4.1 Investigating macrophage polarization through an integrative analysis of miRNA and transcript isoforms

We have applied bulk and single-cell RNA-seq and ATAC-seq techniques to investigate macrophage polarization towards M1 and M2 subtypes in Chapter 2. Another relevant assay that can provide insight into how macrophages polarize is microRNA sequencing. microRNAs (miRNAs) are short pieces of non-coding RNA (20-24nt). They are key post-transcriptional regulatory factors that affect the expression of their target mRNAs by destabilizing and degrading them via 5' to 3' exonuclease activity (Braun et al., 2012). The 3' region of the miRNA is usually complimentary to its target mRNA in its 3' untranslated region (UTR) which improves the efficacy of the targeting (Moore et al., 2015), although studies have indicated many non-canonical imperfect targets pairing (Seok et al., 2016). miRNA expression helps regulate cellular differentiation and specialization and aberrant miRNA expression has been shown to play important roles in many diseases (Peng & Croce, 2016; Tribolet et al., 2020).

A number of studies have compared miRNA expression between M1 and M2 polarized macrophages and found that miRNAs are important regulators of polarization (Essandoh et al. 2016). Over-expression of miRNA-155 seems to promote M1 polarization, whereas overexpression of miRNA-223 seems to promote M2 polarization (Self-Fordham et al., 2017). However, few studies use a fine temporal resolution to identify the transiently expressed miRNAs between the naïve M0 and the spectrum of polarizing M1 and M2 (Curtale et al., 2019). In order to gain further insight into the role that miRNAs play during macrophage polarization, a next step of our study would be to analyze a recently built time-course of miRNA-seq libraries of HL-60-derived M0 polarizing towards M1 or M2 over a period of 24 hours. The information obtained from analyzing the time course of miRNA-seq would feed back into refining our characterization

of the regulatory mechanisms that underlie M0 to M1 or M2 polarization. Furthermore, we can integrate TF binding sites from our Chapter 2 study to miRNA target data in order to build a very comprehensive GRN of macrophage polarization.

Short-read sequencing is widely used to measure gene expression (RNA-seq), miRNA expression (miRNA-seq), and chromatin accessibility (ATAC-seq), as aforementioned. However, RNA-seq has a limited ability to detect full-length isoform level changes in expression. Long-read RNA sequencing technologies allow for isoform-level quantification, as well *de novo* transcriptome analysis and discovery of new transcripts (Amarasinghe et al., 2020; Wyman and Balderrama-Gutierrez et al., 2020). Specific transcript isoforms can be linked to pathologies. For instance, distinct isoforms of the MAPT gene are differentially expressed during Alzheimer's disease progression, formation of tangles and neurodegeneration (Love et al., 2015).

One of the main long-read sequencing technologies available is the Pacific Biosciences (PacBio) Sequel II, which has sequencing error rate of only 1% after circular consensus correction and can yield up to 8 million reads per SMRT cell. In order to identify full length transcript isoforms present during macrophage polarization towards M1s or M2s, we could also build long-read PacBio libraries of HL-60-derived M0s and across a 24 hour time course of polarizing M1s and M2s. At each time point, we would characterize the isoforms expressed for a given gene, at which level they are expressed, and whether a specific isoform is associated with either M1 or M2 polarization. Furthermore, we can integrate the transcript isoform data with our miRNA data to provide a more complete investigation of the regulatory mechanisms that drive macrophage polarization towards M1 or M2.

A thorough analysis of gene expression requires understanding transcription at the level of individual transcript isoforms being generated or degraded, thus profiling long-read transcriptome

sequencing and microRNA-seq provides a higher resolution comprehension of transcriptional dynamics. The identification of specific transcript isoforms and microRNAs that are being made during macrophage polarization will help understand both transcription and degradation rates. Therefore, applying an integrative analysis of miRNA and long read mRNA expression dynamics during HL-60-derived macrophage polarization towards M1 or M2 is a useful tool to further our understanding of M1 and M2 genomics. Considering the variety of studies targeting M1 or M2 polarization to treat diseases, our integrative analysis of bulk and single-cell RNA-seq and ATAC-seq in Chapter 2, combined with miRNA-seq and transcript isoforms investigation can provide valuable targets to modulate macrophage polarization for disease therapeutics.

4.2 Using HL-60 to model human macrophage polarization

PMA is a protein kinase C (PKC) agonist and activate PKC irreversibly. The human leukemia HL-60 cell line activated with PMA acquire several characteristics that are distinct from undifferentiated cells including adherence to surfaces, loss of aberrant proliferative ability, expression of myelomonocytic enzymes such as lysozymes, acquisition of phagocytic capabilities, CSF1R expression, and eventually apoptosis (Seo et al., 2000; Collins, 1987). It is well stablished that HL-60 can differentiate into naïve tissue-resident macrophages (M0), including microglia-like cells (Tsutsumi et al., 2020; Wenzel et al., 2020; Ramirez et al., 2017). Although studies have used the HL-60-derived M0 model to investigate macrophage polarization (Takahashi et al., 2014), it is less clear how similar HL-60-derived M1 and M2 macrophages are to primary tissue resident M0 polarized into M1s and M2s.

A valuable next step of our project would be to activate primary human M0 macrophages towards M1 and M2, collect bulk and single-cell RNA-seq and ATAC-seq libraries and compare

the main polarization markers identified in our Chapter 2 to those of polarized primary macrophages. It would be particularly interesting to use methods where RNA-seq and ATAC-seq libraries can be built from the same single-cells. Furthermore, building the GRN of polarizing primary macrophages and comparing the results to our Chapter 2 GRN connections would provide great insights into how similar those cell types are and what their regulatory elements are. One important limitation of using primary cells for multi-omics sequencing experiments, such as bulk and single-cell RNA-seq and ATAC-seq, is the high number of cells required to build each library. Specifically, when applying a time series analysis of multi-omics sequencing, we need several million cells as input for library building. Understanding how similar HL-60-derived M1 and M2 are from *in vivo* M1 and M2 will highlight the potential of using HL-60 to model macrophage polarization. Moreover, scientists will be able to take advantage of the endless source of cells and the ability to control the experimental steps, reducing the time required to conduct important research. Considering the importance of M1 and M2 polarization for disease prognosis, using the HL-60-derived M0 model may be a valuable tool to pre-clinical research.

4.3 ID2 as a possible novel marker to module M2 polarization

In Chapter 2 our M1- and M2-specific GRNs revealed subtype-specific transcription factors, how they affected downstream targets, and created a map of TF-TF interactions for M1 or M2 activation. These TFs are potential targets for modulating polarization towards a desired subtype. Our polarization GRNs helps understand how targeting one specific TF will affect downstream TFs that may be essential for other cellular processes and could help guide pre-clinical decisions. In addition, our newly identified M2 marker ID2 could be a potential target to reduce

M2 polarization in order to treat solid cancers that show better prognosis when there's a high ratio of M1s to M2s.

We have used siRNA to knock down ID2 in M2 macrophages and will verify whether ID2 knock down affects the macrophage ability to polarize into an M2 phenotype. We have collected bulk RNA-seq and ATAC-seq libraries of M2-ID2^{KD}. Next, we can compare the gene expression and chromatin accessibility profiles of those ID2^{KD} macrophages to our M1s and M2s in order to identify if ID2 knock down can inhibit M2 polarization. If our macrophages lacking ID2 become more M1-like, this will indicate that ID2 is a possible therapeutic target to reduce M2-like TAMs which are associated with poor prognosis of diseases such as breast, esophageal, and lung cancers, as previously discussed.

4.4 Using HL-60 to model human microglia inflammation

Differentiated HL-60 have been used to model select microglial functions, such as phagocytosis (Wenzel et al., 2020; McKenzie & Klegeris, 2018). HL-60 were differentiated with dimethyl sulfoxide (DMSO) for 5 days and stimulated with LPS for 24 hours. Differentiated HL-60 were used to study microglial phagocytic activity in which the cells were incubated with beads culminating with engulfment/phagocytosis of a percentage of the beads (McKenzie & Klegeris, 2018). Another study differentiated HL-60 into monocytic-like cells by applying 1α,25-dihydroxyvitamin D3 (VitD3), which were incubated with Aβ and human brain microvascular endothelial cells (HBMVEC). The presence of Aβ resulted in increased adhesion and transendothelial migration of HL-60-derived monocytic-like cells *in vitro*. These results corroborate *in vivo* studies that show that accumulation of Aβ in AD brain leads to increased presence of microglia/monocytes (Giri et al., 2000) and suggest that differentiated HL-60 can

mimic that effect. However, it is less clear if HL-60-derived microglia display native microglia transcriptomic profiles or if they can be activated into a DAM-like phenotype.

To gain insight into the ability to use HL-60 to model microglia, a clear next step that combines our Chapters 2 and 3 would be to differentiate HL-60 into microglia-like cells using either PMA, VitD3 or DMSO for 5 days and incubate these cells with Aβ. We would then compare the transcriptome profiled by bulk RNA-seq and the chromatin accessibility profiled by ATAC-seq of both differentiated HL-60 and differentiated HL-60 primed with Aβ to those of microglia and DAM, respectively. If the differentiated HL-60 cells show open regions of chromatin around and expression of microglial genes such as CX3CR1, TMEM119, and P2RY12 (Bonham et al., 2019) it would be an indication that HL-60-derived microglia are a viable system to study microglial genomics. Furthermore, if the differentiated HL-60 cells incubated with Aβ express DAM genes, such as TREM2, which is not expressed by tissue-resident macrophages, with exception of osteoclasts (Lee et al., 2021), as well as express DAM genes TYROBP, CST7, and LPL, it would suggest that we can use the HL-60-differentiated microglia to study DAM inflammation.

4.5 Targeting C5a-C5aR1 microglial signaling to treat Alzheimer's disease

The complement fragment C5a is one of the most potent inflammatory mediators of the complement cascade, which binds to C5a receptor 1 (C5aR1) and C5a receptor-like 2 (C5aR2) (Li et al., 2013). The activation of the C5a-C5aR1 signaling pathway is thought to drive inflammation in many neurodegenerative diseases (J. D. Lee et al., 2017; Woodruff et al., 2006). Therefore, the development or discovery of selective C5aR1 inhibitors is an active area of research. PMX205 is a cyclic hexapeptide that act as a potent noncompetitive complement C5a receptor inhibitor. This

drug has shown to be well absorbed through both oral (23% availability) and subcutaneous routes, with elimination half-life of approximately 20 minutes. In addition, PMX205 has been granted "orphan drug" designation by the Food and Drug Administration (FDA), which may allow for accelerated progression to clinical trials (Ricklin & Lambris, 2016). PMX205 has demonstrated a safe profile with no drug accumulation in the brain, blood or spinal cord. PMX205 has also shown high bioavailability with CNS exposure (Kumar et al., 2020) and therefore poses to be a promising drug to treat diseases associated with neuroinflammation.

We have investigated the benefits of reducing complement-mediated inflammation in the Arctic mouse model of Alzheimer's disease in Chapter 3. We targeted glial cell inflammation by genetically knocking out C5aR1 and thus reducing the C5a-C5aR1 signaling. We found that there was improved cognition and decreased inflammation and cholesterol biosynthesis in the KO cohort compared to control (Hernandez, Jiang, et al., 2017). We are currently investigating the preclinical effects of the pharmacologic C5aR1 inhibitor PMX205 in the Tg2576 mouse model of Alzheimer's disease. We have been treating Tg2576 mice with daily oral doses of PMX205 and collecting single cells from cortices and hippocampi of control and treated mice cohorts during disease progression. We will investigate changes in gene expression in microglia and astrocyte populations, identify the main populations associated with worsening pathology, and explore the main markers of each subpopulation. Furthermore, we will evaluate changes in cognition, brain morphology, and brain plaques density in all cohorts in response to PMX205. We hope to evaluate the effects of PMX205 in AD disease pathology using the Tg2576 mouse model. If we confirm a decrease in disease progression and/or improved cognition, a future goal of this study is to help bring PMX205 to clinical trials to treat Alzheimer's disease.

REFERENCES

Aibar, S., González-Blas, C. B., Moerman, T., Huynh-Thu, V. A., Imrichova, H., Hulselmans, G., … Aerts, S. (2017). SCENIC: single-cell regulatory network inference and clustering. *Nature Methods*, *14*(11), 1083–1086. https://doi.org/10.1038/nmeth.4463

Amarasinghe, S. L., Su, S., Dong, X., Zappia, L., Ritchie, M. E., & Gouil, Q. (2020). Opportunities and challenges in long-read sequencing data analysis. *Genome Biology*, *21*(1), 30. https://doi.org/10.1186/s13059-020-1935-5

Amemiya, H. M., Kundaje, A., & Boyle, A. P. (2019). The ENCODE Blacklist: Identification of Problematic Regions of the Genome. *Scientific Reports*, *9*(1), 9354. https://doi.org/10.1038/s41598-019-45839-z

Annabi, B., Currie, J.-C., Moghrabi, A., & Béliveau, R. (2007). Inhibition of HuR and MMP-9 expression in macrophage-differentiated HL-60 myeloid leukemia cells by green tea polyphenol EGCg. *Leukemia Research*, *31*(9), 1277–1284. https://doi.org/10.1016/J.LEUKRES.2006.10.001

Antwi, E. B., Olins, A., Teif, V. B., Bieg, M., Bauer, T., Gu, Z., … Ishaque, N. (2020). *Whole-genome fingerprint of the DNA methylome during chemically induced differentiation of the human AML cell line HL-60/S4*. https://doi.org/10.1242/bio.044222

Argyle, D., & Kitamura, T. (2018). Targeting Macrophage-Recruiting Chemokines as a Novel Therapeutic Strategy to Prevent the Progression of Solid Tumors. *Frontiers in Immunology*, *9*, 2629. https://doi.org/10.3389/fimmu.2018.02629

Armoskus, C., Moreira, D., Bollinger, K., Jimenez, O., Taniguchi, S., & Tsai, H.-W. (2014). Identification of sexually dimorphic genes in the neonatal mouse cortex and hippocampus. *Brain Research*, *1562*, 23–38. https://doi.org/10.1016/J.BRAINRES.2014.03.017

Atri, C., Guerfali, F. Z., & Laouini, D. (2018). Role of Human Macrophage Polarization in Inflammation during Infectious Diseases. *International Journal of Molecular Sciences*, *19*(6). https://doi.org/10.3390/ijms19061801

Baillie, J. K., Arner, E., Daub, C., De Hoon, M., Itoh, M., Kawaji, H., … Hume, D. A. (2017). Analysis of the human monocyte-derived macrophage transcriptome and response to lipopolysaccharide provides new insights into genetic aetiology of inflammatory bowel disease. *PLoS Genetics*, *13*(3), e1006641. https://doi.org/10.1371/journal.pgen.1006641

Berg, D. E., Schmandt, M. A., & Lowe, J. B. (1983). SPECIFICITY OF TRANSPOSON Tn5 INSERTION. *Genetics*, *105*(4).

Bertram, L., & Tanzi, R. E. (2019). Alzheimer disease risk genes: 29 and counting. *Nature Reviews Neurology*, *15*(4), 191–192. https://doi.org/10.1038/s41582-019-0158-4

Biggins, P. J. C., Brennan, F. H., Taylor, S. M., Woodruff, T. M., & Ruitenberg, M. J. (2017). The Alternative Receptor for Complement Component 5a, C5aR2, Conveys Neuroprotection in Traumatic Spinal Cord Injury. *Journal of Neurotrauma*, *34*(12), 2075–2085. https://doi.org/10.1089/neu.2016.4701

Bok, E., Chung, Y. C., Kim, K.-S., Baik, H. H., Shin, W.-H., & Jin, B. K. (2018). Modulation of M1/M2 polarization by capsaicin contributes to the survival of dopaminergic neurons in the lipopolysaccharide-lesioned substantia nigra in vivo. *Experimental & Molecular Medicine*, *50*(7), 76. https://doi.org/10.1038/s12276-018-0111-4

Bonham, L. W., Sirkis, D. W., & Yokoyama, J. S. (2019). The Transcriptional Landscape of Microglial Genes in Aging and Neurodegenerative Disease. *Frontiers in Immunology*, *10*, 1170. https://doi.org/10.3389/fimmu.2019.01170

Bosurgi, L., Corna, G., Vezzoli, M., Touvier, T., Cossu, G., Manfredi, A. A., … Rovere-Querini,

P. (2012). Transplanted mesoangioblasts require macrophage IL-10 for survival in a mouse model of muscle injury. *Journal of Immunology (Baltimore, Md. : 1950)*, *188*(12), 6267–6277. https://doi.org/10.4049/jimmunol.1102680

Braun, J. E., Huntzinger, E., & Izaurralde, E. (2012). A molecular link between miRISCs and deadenylases provides new insight into the mechanism of gene silencing by microRNAs. *Cold Spring Harbor Perspectives in Biology*, *4*(12), a012328. https://doi.org/10.1101/cshperspect.a012328

Briggs, J. A., Weinreb, C., Wagner, D. E., Megason, S., Peshkin, L., Kirschner, M. W., & Klein, A. M. (2018). The dynamics of gene expression in vertebrate embryogenesis at single-cell resolution. *Science (New York, N.Y.)*, *360*(6392), eaar5780. https://doi.org/10.1126/science.aar5780

Budhu, S., Giese, R., Gupta, A., Fitzgerald, K., Zappasodi, R., Schad, S., … Merghoub, T. (2021). Targeting Phosphatidylserine Enhances the Anti-tumor Response to Tumor-Directed Radiation Therapy in a Preclinical Model of Melanoma. *Cell Reports*, *34*(2), 108620. https://doi.org/10.1016/j.celrep.2020.108620

Buenrostro, J. D., Corces, M. R., Lareau, C. A., Wu, B., Schep, A. N., Aryee, M. J., … Greenleaf, W. J. (2018). Integrated Single-Cell Analysis Maps the Continuous Regulatory Landscape of Human Hematopoietic Differentiation. *Cell*, *173*(6), 1535-1548.e16. https://doi.org/10.1016/J.CELL.2018.03.074

Buenrostro, J. D., Wu, B., Chang, H. Y., & Greenleaf, W. J. (2015). ATAC-seq: A Method for Assaying Chromatin Accessibility Genome-Wide. *Current Protocols in Molecular Biology*, *109*, 21.29.1-9. https://doi.org/10.1002/0471142727.mb2129s109

Chan, M. W. Y., & Viswanathan, S. (2019). Recent progress on developing exogenous

monocyte/macrophage-based therapies for inflammatory and degenerative diseases. *Cytotherapy*, *21*(4), 393–415. https://doi.org/10.1016/J.JCYT.2019.02.002

Chauhan, A., Sun, Y., Sukumaran, P., Sharma, J., Singh, B. B., Mishra, B. B., … Birnbaumer, L. (2018). M1 Macrophage Polarization Is Dependent on TRPC1-Mediated Calcium Entry. *ISCIENCE*, *8*, 85–102. https://doi.org/10.1016/j.isci.2018.09.014

Chávez-Galán, L., Olleros, M. L., Vesin, D., & Garcia, I. (2015). Much More than M1 and M2 Macrophages, There are also CD169(+) and TCR(+) Macrophages. *Frontiers in Immunology*, *6*, 263. https://doi.org/10.3389/fimmu.2015.00263

Chen, G., Tan, C. S., Teh, B. K., & Lu, J. (2011). Molecular mechanisms for synchronized transcription of three complement C1q subunit genes in dendritic cells and macrophages. *The Journal of Biological Chemistry*, *286*(40), 34941–34950. https://doi.org/10.1074/jbc.M111.286427

Chen, P., Cescon, M., & Bonaldo, P. (2014). Autophagy-mediated regulation of macrophages and its applications for cancer. *Autophagy*, *10*(2), 192–200. https://doi.org/10.4161/auto.26927

Cheng, I. H., Palop, J. J., Esposito, L. A., Bien-Ly, N., Yan, F., & Mucke, L. (2004). Aggressive amyloidosis in mice expressing human amyloid peptides with the Arctic mutation. *Nature Medicine*, *10*(11), 1190–1192. https://doi.org/10.1038/nm1123

Cheng, I. H., Scearce-Levie, K., Legleiter, J., Palop, J. J., Gerstein, H., Bien-Ly, N., … Mucke, L. (2007). Accelerating amyloid-beta fibrillization reduces oligomer levels and functional deficits in Alzheimer disease mouse models. *The Journal of Biological Chemistry*, *282*(33), 23818–23828. https://doi.org/10.1074/jbc.M701078200

Chistiakov, D. A., Myasoedova, V. A., Revin, V. V., Orekhov, A. N., & Bobryshev, Y. V.

(2018). The impact of interferon-regulatory factors to macrophage differentiation and polarization into M1 and M2. *Immunobiology*, *223*(1), 101–111. https://doi.org/10.1016/J.IMBIO.2017.10.005

Cho, J., Yusuf, R., Kook, S., Attar, E., Lee, D., Park, B., … Lee, B. C. (2014). Purinergic P2Y14 receptor modulates stress-induced hematopoietic stem/progenitor cell senescence. *The Journal of Clinical Investigation*, *124*(7), 3159–3171. https://doi.org/10.1172/JCI61636

Chung, J., Serezani, C. H., Huang, S. K., Stern, J. N. H., Keskin, D. B., Jagirdar, R., … Peters-Golden, M. (2008). Rap1 activation is required for Fc gamma receptor-dependent phagocytosis. *Journal of Immunology (Baltimore, Md. : 1950)*, *181*(8), 5501–5509. https://doi.org/10.4049/jimmunol.181.8.5501

Codoni, V., Blum, Y., Civelek, M., Proust, C., Franzén, O., Cardiogenics Consortium, C., … Trégouët, D.-A. (2016). Preservation Analysis of Macrophage Gene Coexpression Between Human and Mouse Identifies PARK2 as a Genetically Controlled Master Regulator of Oxidative Phosphorylation in Humans. *G3 (Bethesda, Md.)*, *6*(10), 3361–3371. https://doi.org/10.1534/g3.116.033894

Collins, S. J. (1987). The HL-60 Promyelocytic Leukemia Cell Line: Proliferation, Differentiation, and Cellular Oncogene Expression. *Blood*, *70*(5), 1233–1244. https://doi.org/10.1182/BLOOD.V70.5.1233.1233

COLLINS, S. J., GALLO, R. C., & GALLAGHER, R. E. (1977). Continuous growth and differentiation of human myeloid leukaemic cells in suspension culture. *Nature*, *270*(5635), 347–349. https://doi.org/10.1038/270347a0

Contreras, O., Rebolledo, D. L., Oyarzún, J. E., Olguín, H. C., & Brandan, E. (2016). Connective tissue cells expressing fibro/adipogenic progenitor markers increase under chronic damage:

relevance in fibroblast-myofibroblast differentiation and skeletal muscle fibrosis. *Cell and Tissue Research*, *364*(3), 647–660. https://doi.org/10.1007/s00441-015-2343-0

Cooper, C., Ketley, D., & Livingston, G. (2014). Systematic review and meta-analysis to estimate potential recruitment to dementia intervention studies. *International Journal of Geriatric Psychiatry*, *29*(5), 515–525. https://doi.org/10.1002/gps.4034

Corces, M. R., Trevino, A. E., Hamilton, E. G., Greenside, P. G., Sinnott-Armstrong, N. A., Vesuna, S., … Chang, H. Y. (2017a). An improved ATAC-seq protocol reduces background and enables interrogation of frozen tissues. *Nature Methods*, *14*(10), 959–962. https://doi.org/10.1038/nmeth.4396

Corces, M. R., Trevino, A. E., Hamilton, E. G., Greenside, P. G., Sinnott-Armstrong, N. A., Vesuna, S., … Chang, H. Y. (2017b, August 29). *Omni-ATAC-seq: Improved ATAC-seq protocol*.

Coscia, M., Quaglino, E., Iezzi, M., Curcio, C., Pantaleoni, F., Riganti, C., … Massaia, M. (2010). Zoledronic acid repolarizes tumour-associated macrophages and inhibits mammary carcinogenesis by targeting the mevalonate pathway. *Journal of Cellular and Molecular Medicine*, *14*(12), 2803–2815. https://doi.org/10.1111/j.1582-4934.2009.00926.x

Coulthard, L. G., Hawksworth, O. A., Li, R., Balachandran, A., Lee, J. D., Sepehrband, F., … Woodruff, T. M. (2017). Complement C5aR1 Signaling Promotes Polarization and Proliferation of Embryonic Neural Progenitor Cells through PKCζ. *The Journal of Neuroscience : The Official Journal of the Society for Neuroscience*, *37*(22), 5395–5407. https://doi.org/10.1523/JNEUROSCI.0525-17.2017

Cucak, H., Grunnet, L. G., & Rosendahl, A. (2014). Accumulation of M1-like macrophages in type 2 diabetic islets is followed by a systemic shift in macrophage polarization. *Journal of*

Leukocyte Biology, *95*(1), 149–160. https://doi.org/10.1189/jlb.0213075

Cummings, J., Lee, G., Ritter, A., Sabbagh, M., & Zhong, K. (2020). Alzheimer's disease drug development pipeline: 2020. *Alzheimer's & Dementia: Translational Research & Clinical Interventions*, *6*(1), e12050. https://doi.org/10.1002/trc2.12050

Curtale, G., Rubino, M., & Locati, M. (2019). MicroRNAs as Molecular Switches in Macrophage Activation. *Frontiers in Immunology*, *10*, 799. https://doi.org/10.3389/fimmu.2019.00799

Cusanovich, D. A., Daza, R., Adey, A., Pliner, H. A., Christiansen, L., Gunderson, K. L., … Shendure, J. (2015). Multiplex single cell profiling of chromatin accessibility by combinatorial cellular indexing. *Science (New York, N.Y.)*, *348*(6237), 910–914. https://doi.org/10.1126/science.aab1601

Czimmerer, Z., Nagy, Z. S., Nagy, G., Horvath, A., Silye-Cseh, T., Kriston, A., … Nagy, L. (2018). Extensive and functional overlap of the STAT6 and RXR cistromes in the active enhancer repertoire of human CD14+ monocyte derived differentiating macrophages. *Molecular and Cellular Endocrinology*, *471*, 63–74. https://doi.org/10.1016/J.MCE.2017.07.034

Czirr, E., Castello, N. A., Mosher, K. I., Castellano, J. M., Hinkson, I. V, Lucin, K. M., … Wyss-Coray, T. (2017). Microglial complement receptor 3 regulates brain Aβ levels through secreted proteolytic activity. *The Journal of Experimental Medicine*, *214*(4), 1081–1092. https://doi.org/10.1084/jem.20162011

Daems, W. T., & De Bakker, J. M. (1982). Do Resident Macrophages Proliferate? *Immunobiology*, *161*(3–4), 204–211. https://doi.org/10.1016/S0171-2985(82)80075-2

Dani, M., Wood, M., Mizoguchi, R., Fan, Z., Walker, Z., Morgan, R., … Edison, P. (2018).

Microglial activation correlates in vivo with both tau and amyloid in Alzheimer's disease. *Brain : A Journal of Neurology*, *141*(9), 2740–2754. https://doi.org/10.1093/brain/awy188

Dao, T., Salahuddin, S., Charfi, C., Sicard, A.-A., Jenabian, M.-A., & Annabi, B. (2020). Pharmacological targeting of neurotensin response by diet-derived EGCG in macrophage-differentiated HL-60 promyelocytic leukemia cells. *PharmaNutrition*, *12*, 100191. https://doi.org/10.1016/J.PHANU.2020.100191

Davies, L. C., & Taylor, P. R. (2015). Tissue-resident macrophages: then and now. *Immunology*, *144*(4), 541–548. https://doi.org/10.1111/imm.12451

Deczkowska, A., Amit, I., & Schwartz, M. (2018). Microglial immune checkpoint mechanisms. *Nature Neuroscience*, *21*(6), 779–786. https://doi.org/10.1038/s41593-018-0145-x

Deczkowska, A., Keren-Shaul, H., Weiner, A., Colonna, M., Schwartz, M., & Amit, I. (2018). Disease-Associated Microglia: A Universal Immune Sensor of Neurodegeneration. *Cell*, *173*(5), 1073–1081. https://doi.org/10.1016/J.CELL.2018.05.003

DeKoter, R. P., & Singh, H. (2000). Regulation of B lymphocyte and macrophage development by graded expression of PU.1. *Science (New York, N.Y.)*, *288*(5470), 1439–1441. https://doi.org/10.1126/SCIENCE.288.5470.1439

DeNardo, D. G., & Ruffell, B. (2019). Macrophages as regulators of tumour immunity and immunotherapy. *Nature Reviews Immunology*, *19*(6), 369–382. https://doi.org/10.1038/s41577-019-0127-6

DeTure, M. A., & Dickson, D. W. (2019). The neuropathological diagnosis of Alzheimer's disease. *Molecular Neurodegeneration*, *14*(1), 32. https://doi.org/10.1186/s13024-019-0333-5

Dieu-Nosjean, M.-C., Massacrier, C., Homey, B., Vanbervliet, B., Pin, J.-J., Vicari, A., … Caux,

C. (2000). Macrophage Inflammatory Protein 3α Is Expressed at Inflamed Epithelial Surfaces and Is the Most Potent Chemokine Known in Attracting Langerhans Cell Precursors. *The Journal of Experimental Medicine*, *192*(5), 705. https://doi.org/10.1084/JEM.192.5.705

Ding, N., Wang, Y., Dou, C., Liu, F., Guan, G., Wei, K., … Zhu, C. (2019). Physalin D regulates macrophage M1/M2 polarization via the STAT1/6 pathway. *Journal of Cellular Physiology*, *234*(6), 8788–8796. https://doi.org/10.1002/jcp.27537

Dobin, A., Davis, C. A., Schlesinger, F., Drenkow, J., Zaleski, C., Jha, S., … Gingeras, T. R. (2013). STAR: ultrafast universal RNA-seq aligner. *Bioinformatics*, *29*(1), 15–21. https://doi.org/10.1093/bioinformatics/bts635

Dong, Y., Li, X., Cheng, J., & Hou, L. (2019). Drug Development for Alzheimer's Disease: Microglia Induced Neuroinflammation as a Target? *International Journal of Molecular Sciences*, *20*(3). https://doi.org/10.3390/ijms20030558

Dort, J., Fabre, P., Molina, T., & Dumont, N. A. (2019). Macrophages Are Key Regulators of Stem Cells during Skeletal Muscle Regeneration and Diseases. *Stem Cells International*, *2019*, 4761427. https://doi.org/10.1155/2019/4761427

Dreyfus, J.-C., Schapira, G., & Schapira, F. (1958). SERUM ENZYMES IN THE PHYSIOPATHOLOGY OF MUSCLE. *Annals of the New York Academy of Sciences*, *75*(1), 235–249. https://doi.org/10.1111/j.1749-6632.1958.tb36870.x

Drissen, R., Buza-Vidas, N., Woll, P., Thongjuea, S., Gambardella, A., Giustacchini, A., … Nerlov, C. (2016). Distinct myeloid progenitor–differentiation pathways identified through single-cell RNA sequencing. *Nature Immunology*, *17*(6), 666–676. https://doi.org/10.1038/ni.3412

Duan, D., Goemans, N., Takeda, S., Mercuri, E., & Aartsma-Rus, A. (2021). Duchenne muscular dystrophy. *Nature Reviews Disease Primers*, *7*(1), 13. https://doi.org/10.1038/s41572-021-00248-3

Dube, P. R., Birnbaumer, L., & Vazquez, G. (2017). Evidence for constitutive bone morphogenetic protein-2 secretion by M1 macrophages: Constitutive auto/paracrine osteogenic signaling by BMP-2 in M1 macrophages. *Biochemical and Biophysical Research Communications*, *491*(1), 154–158. https://doi.org/10.1016/J.BBRC.2017.07.065

Dulmovits, B. M., Zhao, Y., Peters, L. L., & Blanc, L. (2015). RASA3 Is Involved in Cell Cycle Progression, Hemoglobinization and Generation of Reactive Oxygen Species during Mammalian Erythropoiesis. *Blood*, *126*(23), 3328–3328. https://doi.org/10.1182/blood.V126.23.3328.3328

Duren, Z., Chen, X., Xin, J., Wang, Y., & Wong, W. H. (2020). Time course regulatory analysis based on paired expression and chromatin accessibility data. *Genome Research*, *30*(4), 622–634. https://doi.org/10.1101/gr.257063.119

Efthymiou, A. G., & Goate, A. M. (2017). Late onset Alzheimer's disease genetics implicates microglial pathways in disease risk. *Molecular Neurodegeneration*, *12*(1), 43. https://doi.org/10.1186/s13024-017-0184-x

Ennis, D., Yeung, R. S., & Pagnoux, C. (2020). Long-term use and remission of granulomatosis with polyangiitis with the oral C5a receptor inhibitor avacopan. *BMJ Case Reports*, *13*(10), e236236. https://doi.org/10.1136/bcr-2020-236236

Essandoh, K., Li, Y., Huo, J., & Fan, G.-C. (2016). MiRNA-Mediated Macrophage Polarization and its Potential Role in the Regulation of Inflammatory Response. *Shock (Augusta, Ga.)*, *46*(2), 122–131. https://doi.org/10.1097/SHK.0000000000000604

Fonseca, M. I., Ager, R. R., Chu, S.-H., Yazan, O., Sanderson, S. D., LaFerla, F. M., … Tenner, A. J. (2009). Treatment with a C5aR antagonist decreases pathology and enhances behavioral performance in murine models of Alzheimer's disease. *Journal of Immunology (Baltimore, Md. : 1950)*, *183*(2), 1375–1383. https://doi.org/10.4049/jimmunol.0901005

Forner, S., Kawauchi, S., Balderrama-Gutierrez, G., Kramár, E. A., Matheos, D. P., Phan, J., … Green, K. N. (2021). Systematic Phenotyping and Characterization of the 5xFAD mouse model of Alzheimer's Disease. *BioRxiv*, 2021.02.17.431716. https://doi.org/10.1101/2021.02.17.431716

Fraser, D. A., Pisalyaput, K., & Tenner, A. J. (2010). C1q enhances microglial clearance of apoptotic neurons and neuronal blebs, and modulates subsequent inflammatory cytokine production. *Journal of Neurochemistry*, *112*(3), 733–743. https://doi.org/10.1111/j.1471-4159.2009.06494.x

Friedman, B. A., Srinivasan, K., Ayalon, G., Meilandt, W. J., Lin, H., Huntley, M. A., … Hansen, D. V. (2018). Diverse Brain Myeloid Expression Profiles Reveal Distinct Microglial Activation States and Aspects of Alzheimer's Disease Not Evident in Mouse Models. *Cell Reports*, *22*(3), 832–847. https://doi.org/10.1016/J.CELREP.2017.12.066

Fujimura, T., Kambayashi, Y., Fujisawa, Y., Hidaka, T., & Aiba, S. (2018). Tumor-Associated Macrophages: Therapeutic Targets for Skin Cancer. *Frontiers in Oncology*, *8*, 3. https://doi.org/10.3389/fonc.2018.00003

Fujisaka, S., Usui, I., Bukhari, A., Ikutani, M., Oya, T., Kanatani, Y., … Tobe, K. (2009). Regulatory mechanisms for adipose tissue M1 and M2 macrophages in diet-induced obese mice. *Diabetes*, *58*(11), 2574–2582. https://doi.org/10.2337/db08-1475

Funes, S. C., Rios, M., Escobar-Vera, J., & Kalergis, A. M. (2018). Implications of macrophage

polarization in autoimmunity. *Immunology*, *154*(2), 186–195. https://doi.org/10.1111/imm.12910

Gaudino, S. J., & Kumar, P. (2019). Cross-Talk Between Antigen Presenting Cells and T Cells Impacts Intestinal Homeostasis, Bacterial Infections, and Tumorigenesis. *Frontiers in Immunology*, *10*, 360. https://doi.org/10.3389/fimmu.2019.00360

Germano, G., Frapolli, R., Belgiovine, C., Anselmo, A., Pesce, S., Liguori, M., … Allavena, P. (2013). Role of macrophage targeting in the antitumor activity of trabectedin. *Cancer Cell*, *23*(2), 249–262. https://doi.org/10.1016/j.ccr.2013.01.008

Ginhoux, F., & Guilliams, M. (2016). Review Tissue-Resident Macrophage Ontogeny and Homeostasis. *Immunity*, *44*, 439–449. https://doi.org/10.1016/j.immuni.2016.02.024

Giri, R., Shen, Y., Stins, M., Yan, S. DU, Marie Schmidt, A., Stern, D., … Kim, K.-S. (2000). *Amyloid-induced migration of monocytes across human brain endothelial cells involves RAGE and PECAM-1*. Retrieved from http://www.ajpcell.org

Gnanakkumaar, P., Murugesan, R., & Ahmed, S. S. S. J. (2019). Gene Regulatory Networks in Peripheral Mononuclear Cells Reveals Critical Regulatory Modules and Regulators of Multiple Sclerosis. *Scientific Reports*, *9*(1), 12732. https://doi.org/10.1038/s41598-019-49124-x

Gordon, S., & Martinez, F. O. (2010). Alternative activation of macrophages: mechanism and functions. *Immunity*, *32*(5), 593–604. https://doi.org/10.1016/j.immuni.2010.05.007

Gordon, S., & Plüddemann, A. (2018). Macrophage Clearance of Apoptotic Cells: A Critical Assessment. *Frontiers in Immunology*, *9*. https://doi.org/10.3389/FIMMU.2018.00127

Gordon, S. R., Maute, R. L., Dulken, B. W., Hutter, G., George, B. M., McCracken, M. N., … Weissman, I. L. (2017). PD-1 expression by tumour-associated macrophages inhibits

phagocytosis and tumour immunity. *Nature*, *545*(7655), 495–499. https://doi.org/10.1038/nature22396

Gosselin, D., Link, V. M., Romanoski, C. E., Fonseca, G. J., Eichenfield, D. Z., Spann, N. J., … Glass, C. K. (2014). Environment Drives Selection and Function of Enhancers Controlling Tissue-Specific Macrophage Identities. *Cell*, *159*(6), 1327–1340. https://doi.org/10.1016/j.cell.2014.11.023

Gottschalk, W. K., Mihovilovic, M., Roses, A. D., & Chiba-Falek, O. (2016). The Role of Upregulated APOE in Alzheimer's Disease Etiology. *Journal of Alzheimer's Disease & Parkinsonism*, *6*(1). https://doi.org/10.4172/2161-0460.1000209

Griciuc, A., & Tanzi, R. E. (2021). The role of innate immune genes in Alzheimer's disease. *Current Opinion in Neurology*, *34*(2), 228–236. https://doi.org/10.1097/WCO.0000000000000911

Griffin, W. S., Stanley, L. C., Ling, C., White, L., MacLeod, V., Perrot, L. J., … Araoz, C. (1989). Brain interleukin 1 and S-100 immunoreactivity are elevated in Down syndrome and Alzheimer disease. *Proceedings of the National Academy of Sciences of the United States of America*, *86*(19), 7611–7615. https://doi.org/10.1073/pnas.86.19.7611

Guerriero, J. L. (2018). Macrophages: The Road Less Traveled, Changing Anticancer Therapy. *Trends in Molecular Medicine*, *24*(5), 472–489. https://doi.org/10.1016/J.MOLMED.2018.03.006

Gurvich, O. L., Puttonen, K. A., Bailey, A., Kailaanmäki, A., Skirdenko, V., Sivonen, M., … Kekarainen, T. (2020). *transcriptomics uncovers substantial variability associated with alterations in manufacturing processes of macrophage cell therapy products*. *10*, 14049. https://doi.org/10.1038/s41598-020-70967-2

Guzman-Martinez, L., Maccioni, R. B., Andrade, V., Navarrete, L. P., Pastor, M. G., & Ramos-Escobar, N. (2019). Neuroinflammation as a Common Feature of Neurodegenerative Disorders. *Frontiers in Pharmacology*, *10*, 1008. https://doi.org/10.3389/fphar.2019.01008

Habib, N., McCabe, C., Medina, S., Varshavsky, M., Kitsberg, D., Dvir-Szternfeld, R., … Schwartz, M. (2020). Disease-associated astrocytes in Alzheimer's disease and aging. *Nature Neuroscience*, *23*(6), 701–706. https://doi.org/10.1038/s41593-020-0624-8

Hacker, C., Kirsch, R. D., Ju, X.-S., Hieronymus, T., Gust, T. C., Kuhl, C., … Zenke, M. (2003). Transcriptional profiling identifies Id2 function in dendritic cell development. *Nature Immunology*, *4*(4), 380–386. https://doi.org/10.1038/ni903

Harney, A. S., Karagiannis, G. S., Pignatelli, J., Smith, B. D., Kadioglu, E., Wise, S. C., … Condeelis, J. S. (2017). The Selective Tie2 Inhibitor Rebastinib Blocks Recruitment and Function of Tie2Hi Macrophages in Breast Cancer and Pancreatic Neuroendocrine Tumors. *Molecular Cancer Therapeutics*, *16*(11), 2486–2501. https://doi.org/10.1158/1535-7163.MCT-17-0241

Harry, G. J. (2013). Microglia during development and aging. *Pharmacology & Therapeutics*, *139*(3), 313–326. https://doi.org/10.1016/J.PHARMTHERA.2013.04.013

Heinz, S., Benner, C., Spann, N., Bertolino, E., Lin, Y. C., Laslo, P., … Glass, C. K. (2010). Simple Combinations of Lineage-Determining Transcription Factors Prime cis-Regulatory Elements Required for Macrophage and B Cell Identities. *Molecular Cell*, *38*(4), 576–589. https://doi.org/10.1016/J.MOLCEL.2010.05.004

Hernandez, M. X., Jiang, S., Cole, T. A., Chu, S.-H., Fonseca, M. I., Fang, M. J., … Tenner, A. J. (2017). Prevention of C5aR1 signaling delays microglial inflammatory polarization, favors clearance pathways and suppresses cognitive loss. *Molecular Neurodegeneration*,

12(1), 66. https://doi.org/10.1186/s13024-017-0210-z

Hernandez, M. X., Namiranian, P., Nguyen, E., Fonseca, M. I., & Tenner, A. J. (2017a). C5a Increases the Injury to Primary Neurons Elicited by Fibrillar Amyloid Beta. *ASN Neuro*, *9*(1), 1759091416687871. https://doi.org/10.1177/1759091416687871

Hernandez, M. X., Namiranian, P., Nguyen, E., Fonseca, M. I., & Tenner, A. J. (2017b). C5a Increases the Injury to Primary Neurons Elicited by Fibrillar Amyloid Beta. *ASN Neuro*, *9*(1), 175909141668787. https://doi.org/10.1177/1759091416687871

Hickman, S., Izzy, S., Sen, P., Morsett, L., & El Khoury, J. (2018). Microglia in neurodegeneration. *Nature Neuroscience*, *21*(10), 1359–1369. https://doi.org/10.1038/s41593-018-0242-x

Hirayama, D., Iida, T., & Nakase, H. (2018). The Phagocytic Function of Macrophage-Enforcing Innate Immunity and Tissue Homeostasis. *International Journal of Molecular Sciences*, *19*(1). https://doi.org/10.3390/IJMS19010092

Hoeffel, G., & Ginhoux, F. (2018). Fetal monocytes and the origins of tissue-resident macrophages. *Cellular Immunology*. https://doi.org/10.1016/J.CELLIMM.2018.01.001

Hollmann, T. J., Mueller-Ortiz, S. L., Braun, M. C., & Wetsel, R. A. (2008). Disruption of the C5a receptor gene increases resistance to acute Gram-negative bacteremia and endotoxic shock: Opposing roles of C3a and C5a. *Molecular Immunology*, *45*(7), 1907–1915. https://doi.org/10.1016/j.molimm.2007.10.037

Holness, C., & Simmons, D. (1993). Molecular cloning of CD68, a human macrophage marker related to lysosomal glycoproteins. *Blood*, *81*(6). Retrieved from http://www.bloodjournal.org/content/81/6/1607.short?sso-checked=true

Hortobagyi, G. N., Van Poznak, C., Harker, W. G., Gradishar, W. J., Chew, H., Dakhil, S. R., …

Lipton, A. (2017). Continued Treatment Effect of Zoledronic Acid Dosing Every 12 vs 4 Weeks in Women With Breast Cancer Metastatic to Bone: The OPTIMIZE-2 Randomized Clinical Trial. *JAMA Oncology*, *3*(7), 906–912. https://doi.org/10.1001/jamaoncol.2016.6316

Hu, J. M., Liu, K., Liu, J. H., Jiang, X. L., Wang, X. L., Chen, Y. Z., … Li, F. (2017). CD163 as a marker of M2 macrophage, contribute to predicte aggressiveness and prognosis of Kazakh esophageal squamous cell carcinoma. *Oncotarget*, *8*(13), 21526–21538. https://doi.org/10.18632/oncotarget.15630

Huang, D., Sherman, B. T., Tan, Q., Collins, J. R., Alvord, W. G., Roayaei, J., … Lempicki, R. A. (2007). The DAVID Gene Functional Classification Tool: a novel biological module-centric algorithm to functionally analyze large gene lists. *Genome Biology*, *8*(9), R183. https://doi.org/10.1186/gb-2007-8-9-r183

Huang, X., Li, Y., Fu, M., & Xin, H.-B. (2018). *Polarizing Macrophages In Vitro*. https://doi.org/10.1007/978-1-4939-7837-3_12

Hur, J.-Y., Frost, G. R., Wu, X., Crump, C., Pan, S. J., Wong, E., … Li, Y.-M. (2020). The innate immunity protein IFITM3 modulates γ-secretase in Alzheimer's disease. *Nature*, *586*(7831), 735–740. https://doi.org/10.1038/s41586-020-2681-2

Iwata, H., Goettsch, C., Sharma, A., Ricchiuto, P., Goh, W. W. Bin, Halu, A., … Aikawa, M. (2016). PARP9 and PARP14 cross-regulate macrophage activation via STAT1 ADP-ribosylation. *Nature Communications*, *7*(1), 12849. https://doi.org/10.1038/ncomms12849

Jansen, C., Ramirez, R. N., El-Ali, N. C., Gomez-Cabrero, D., Tegner, J., Merkenschlager, M., … Mortazavi, A. (2019). Building gene regulatory networks from scATAC-seq and scRNA-seq using Linked Self Organizing Maps. *PLoS Computational Biology*, *15*(11),

e1006555. https://doi.org/10.1371/journal.pcbi.1006555

Jayasingam, S. D., Citartan, M., Thang, T. H., Mat Zin, A. A., Ang, K. C., & Ch'ng, E. S. (2019). Evaluating the Polarization of Tumor-Associated Macrophages Into M1 and M2 Phenotypes in Human Cancer Tissue: Technicalities and Challenges in Routine Clinical Practice. *Frontiers in Oncology*, *9*, 1512. https://doi.org/10.3389/fonc.2019.01512

Jenkins, S. J., Ruckerl, D., Cook, P. C., Jones, L. H., Finkelman, F. D., Rooijen, N. van, … Allen, J. E. (2011). Local macrophage proliferation, rather than recruitment from the blood, is a signature of Th2 inflammation. *Science (New York, N.Y.)*, *332*(6035), 1284. https://doi.org/10.1126/SCIENCE.1204351

Jetten, N., Verbruggen, S., Gijbels, M. J., Post, M. J., De Winther, M. P. J., & Donners, M. M. P. C. (2014). Anti-inflammatory M2, but not pro-inflammatory M1 macrophages promote angiogenesis in vivo. *Angiogenesis*, *17*(1), 109–118. https://doi.org/10.1007/s10456-013-9381-6

Jha, M. K., Jo, M., Kim, J.-H., & Suk, K. (2019). Microglia-Astrocyte Crosstalk: An Intimate Molecular Conversation. *The Neuroscientist : A Review Journal Bringing Neurobiology, Neurology and Psychiatry*, *25*(3), 227–240. https://doi.org/10.1177/1073858418783959

Juban, G., Saclier, M., Yacoub-Youssef, H., Kernou, A., Arnold, L., Boisson, C., … Chazaud, B. (2018). AMPK Activation Regulates LTBP4-Dependent TGF-β1 Secretion by Pro-inflammatory Macrophages and Controls Fibrosis in Duchenne Muscular Dystrophy. *Cell Reports*, *25*(8), 2163-2176.e6. https://doi.org/10.1016/J.CELREP.2018.10.077

Kamphuis, W., Kooijman, L., Schetters, S., Orre, M., & Hol, E. M. (2016). Transcriptional profiling of CD11c-positive microglia accumulating around amyloid plaques in a mouse model for Alzheimer's disease. *Biochimica et Biophysica Acta (BBA) - Molecular Basis of*

Disease, *1862*(10), 1847–1860. https://doi.org/10.1016/J.BBADIS.2016.07.007

Kang, K., Park, S. H., Chen, J., Qiao, Y., Giannopoulou, E., Berg, K., … Ivashkiv, L. B. (2017). Interferon-γ Represses M2 Gene Expression in Human Macrophages by Disassembling Enhancers Bound by the Transcription Factor MAF. *Immunity*, *47*(2), 235-250.e4. https://doi.org/10.1016/j.immuni.2017.07.017

Karpurapu, M., Wang, X., Deng, J., Park, H., Xiao, L., Sadikot, R. T., … Christman, J. W. (2011). Functional PU.1 in macrophages has a pivotal role in NF-κB activation and neutrophilic lung inflammation during endotoxemia. *Blood*, *118*(19), 5255–5266. https://doi.org/10.1182/blood-2011-03-341123

Keren-Shaul, H., Spinrad, A., Weiner, A., Matcovitch-Natan, O., Dvir-Szternfeld, R., Ulland, T. K., … Amit, I. (2017). A Unique Microglia Type Associated with Restricting Development of Alzheimer's Disease. *Cell*, *169*(7), 1276-1290.e17. https://doi.org/10.1016/J.CELL.2017.05.018

Kinney, J. W., Bemiller, S. M., Murtishaw, A. S., Leisgang, A. M., Salazar, A. M., & Lamb, B. T. (2018). Inflammation as a central mechanism in Alzheimer's disease. *Alzheimer's & Dementia: Translational Research & Clinical Interventions*, *4*, 575–590. https://doi.org/10.1016/J.TRCI.2018.06.014

Klemm, S. L., Shipony, Z., & Greenleaf, W. J. (2019). Chromatin accessibility and the regulatory epigenome. *Nature Reviews Genetics*, *20*(4), 207–220. https://doi.org/10.1038/s41576-018-0089-8

Klos, A., Wende, E., Wareham, K. J., & Monk, P. N. (2013). *International Union of Basic and Clinical Pharmacology. LXXXVII. Complement Peptide C5a, C4a, and C3a Receptors*. https://doi.org/10.1124/pr.111.005223

Kovaleva, O. V., Samoilova, D. V., Shitova, M. S., & Gratchev, A. (2016). Tumor Associated Macrophages in Kidney Cancer. *Analytical Cellular Pathology*, *2016*, 1–6. https://doi.org/10.1155/2016/9307549

Kulakovskiy, I. V., Medvedeva, Y. A., Schaefer, U., Kasianov, A. S., Vorontsov, I. E., Bajic, V. B., & Makeev, V. J. (2013). HOCOMOCO: a comprehensive collection of human transcription factor binding sites models. *Nucleic Acids Research*, *41*(D1), D195–D202. https://doi.org/10.1093/nar/gks1089

Kumar, V., Lee, J. D., Clark, R. J., Noakes, P. G., Taylor, S. M., & Woodruff, T. M. (2020). Preclinical Pharmacokinetics of Complement C5a Receptor Antagonists PMX53 and PMX205 in Mice. *ACS Omega*, *5*(5), 2345–2354. https://doi.org/10.1021/acsomega.9b03735

La Manno, G., Soldatov, R., Zeisel, A., Braun, E., Hochgerner, H., Petukhov, V., … Kharchenko, P. V. (2018). RNA velocity of single cells. *Nature*, *560*(7719), 494–498. https://doi.org/10.1038/s41586-018-0414-6

Labonte, A. C., Kegerreis, B., Geraci, N. S., Bachali, P., Madamanchi, S., Robl, R., … Grammer, A. C. (2018). Identification of alterations in macrophage activation associated with disease activity in systemic lupus erythematosus. *PLOS ONE*, *13*(12), e0208132. https://doi.org/10.1371/journal.pone.0208132

Lachmann, A., Xu, H., Krishnan, J., Berger, S. I., Mazloom, A. R., & Ma'ayan, A. (2010). ChEA: transcription factor regulation inferred from integrating genome-wide ChIP-X experiments. *Bioinformatics*, *26*(19), 2438. https://doi.org/10.1093/BIOINFORMATICS/BTQ466

Langlais, D., Barreiro, L. B., & Gros, P. (2016). The macrophage IRF8/IRF1 regulome is

required for protection against infections and is associated with chronic inflammation. *The Journal of Experimental Medicine*, *213*(4), 585–603. https://doi.org/10.1084/jem.20151764

Langmead, B., & Salzberg, S. L. (2012). Fast gapped-read alignment with Bowtie 2. *Nature Methods*, *9*(4), 357–359. https://doi.org/10.1038/nmeth.1923

Lara, P. C., Burgos, J., & Macias, D. (2020). Low dose lung radiotherapy for COVID-19 pneumonia. The rationale for a cost-effective anti-inflammatory treatment. *Clinical and Translational Radiation Oncology*, *23*, 27–29. https://doi.org/10.1016/J.CTRO.2020.04.006

Lareau, C. A., Duarte, F. M., Chew, J. G., Kartha, V. K., Burkett, Z. D., Kohlway, A. S., … Buenrostro, J. D. (2019). Droplet-based combinatorial indexing for massive-scale single-cell chromatin accessibility. *Nature Biotechnology*, *37*(8), 916–924. https://doi.org/10.1038/s41587-019-0147-6

Laslo, P., Spooner, C. J., Warmflash, A., Lancki, D. W., Lee, H.-J., Sciammas, R., … Singh, H. (2006). Multilineage transcriptional priming and determination of alternate hematopoietic cell fates. *Cell*, *126*(4), 755–766. https://doi.org/10.1016/j.cell.2006.06.052

Lattin, J. E., Greenwood, K. P., Daly, N. L., Kelly, G., Zidar, D. A., Clark, R. J., … Sweet, M. J. (2009). Beta-arrestin 2 is required for complement C1q expression in macrophages and constrains factor-independent survival. *Molecular Immunology*, *47*(2–3), 340–347. https://doi.org/10.1016/J.MOLIMM.2009.09.012

Lee, B., Wu, C.-Y., Lin, Y.-W., Park, S. W., & Wei, L.-N. (2016). Synergistic activation of *Arg1* gene by retinoic acid and IL-4 involves chromatin remodeling for transcription initiation and elongation coupling. *Nucleic Acids Research*, *44*(16), 7568–7579. https://doi.org/10.1093/nar/gkw392

Lee, H., Fessler, M. B., Qu, P., Heymann, J., & Kopp, J. B. (2020). Macrophage polarization in

innate immune responses contributing to pathogenesis of chronic kidney disease. *BMC Nephrology*, *21*(1), 270. https://doi.org/10.1186/s12882-020-01921-7

Lee, J.-W., Lee, I.-H., Iimura, T., & Kong, S. W. (2021). Two macrophages, osteoclasts and microglia: from development to pleiotropy. *Bone Research*, *9*(1), 11. https://doi.org/10.1038/s41413-020-00134-w

Lee, J. D., Kumar, V., Fung, J. N. T., Ruitenberg, M. J., Noakes, P. G., & Woodruff, T. M. (2017). Pharmacological inhibition of complement C5a-C5a $_1$ receptor signalling ameliorates disease pathology in the hSOD1 ^{G93A} mouse model of amyotrophic lateral sclerosis. *British Journal of Pharmacology*, *174*(8), 689–699. https://doi.org/10.1111/bph.13730

Lee, S. H., Chaves, M. M., Kamenyeva, O., Gazzinelli-Guimaraes, P. H., Kang, B., Pessenda, G., … Sacks, D. L. (2020). M2-like, dermal macrophages are maintained via IL-4/CCL24-mediated cooperative interaction with eosinophils in cutaneous leishmaniasis. *Science Immunology*, *5*(46). https://doi.org/10.1126/sciimmunol.aaz4415

Leonard, F., Curtis, L. T., Hamed, A. R., Zhang, C., Chau, E., Sieving, D., & Godin, B. (2020). *Nonlinear response to cancer nanotherapy due to macrophage interactions revealed by mathematical modeling and evaluated in a murine model via CRISPR-modulated macrophage polarization*. *69*, 731–744. https://doi.org/10.1007/s00262-020-02504-z

Li, B., & Dewey, C. N. (2011). RSEM: accurate transcript quantification from RNA-Seq data with or without a reference genome. *BMC Bioinformatics*, *12*(1), 323. https://doi.org/10.1186/1471-2105-12-323

Li, C., Xu, X., Wei, S., Jiang, P., Xue, L., Wang, J., & Senior Correspondence. (2021). Tumor-associated macrophages: potential therapeutic strategies and future prospects in cancer.

Journal for Immunotherapy of Cancer, *9*(1), e001341. https://doi.org/10.1136/jitc-2020-001341

Li, H., & Durbin, R. (2009). Fast and accurate short read alignment with Burrows-Wheeler transform. *Bioinformatics*, *25*(14), 1754–1760. https://doi.org/10.1093/bioinformatics/btp324

Li, Heng, Jiang, T., Li, M.-Q., Zheng, X.-L., & Zhao, G.-J. (2018). Transcriptional Regulation of Macrophages Polarization by MicroRNAs. *Frontiers in Immunology*, *9*, 1175. https://doi.org/10.3389/fimmu.2018.01175

Li, Q., Brown, J. B., Huang, H., & Bickel, P. J. (2011). Measuring reproducibility of high-throughput experiments. *The Annals of Applied Statistics*, *5*(3), 1752–1779. https://doi.org/10.1214/11-AOAS466

Li, R., Coulthard, L. G., Wu, M. C. L., Taylor, S. M., & Woodruff, T. M. (2013). C5L2: a controversial receptor of complement anaphylatoxin, C5a. *The FASEB Journal*, *27*(3), 855–864. https://doi.org/10.1096/fj.12-220509

Li, X. X., Clark, R. J., & Woodruff, T. M. (2020). C5aR2 Activation Broadly Modulates the Signaling and Function of Primary Human Macrophages. *Journal of Immunology (Baltimore, Md. : 1950)*, *205*(4), 1102–1112. https://doi.org/10.4049/jimmunol.2000407

Li, X. X., Lee, J. D., Kemper, C., & Woodruff, T. M. (2019). The Complement Receptor C5aR2: A Powerful Modulator of Innate and Adaptive Immunity. *Journal of Immunology (Baltimore, Md. : 1950)*, *202*(12), 3339–3348. https://doi.org/10.4049/jimmunol.1900371

Li, Yanfang, Sun, H., Chen, Z., Xu, H., Bu, G., & Zheng, H. (2016). Implications of GABAergic Neurotransmission in Alzheimer's Disease. *Frontiers in Aging Neuroscience*, *8*, 31. https://doi.org/10.3389/FNAGI.2016.00031

Li, Yiming, Zhai, P., Zheng, Y., Zhang, J., Kellum, J. A., & Peng, Z. (2020). Csf2 Attenuated Sepsis-Induced Acute Kidney Injury by Promoting Alternative Macrophage Transition. *Frontiers in Immunology*, *11*, 1415. https://doi.org/10.3389/fimmu.2020.01415

Li, Yiyang, Kong, N., Li, Z., Tian, R., Liu, X., Liu, G., … Yang, P. (2019). Bone marrow macrophage M2 polarization and adipose-derived stem cells osteogenic differentiation synergistically promote rehabilitation of bone damage. *Journal of Cellular Biochemistry*, *120*(12), 19891–19901. https://doi.org/10.1002/jcb.29297

Li, Z., Schulz, M. H., Look, T., Begemann, M., Zenke, M., & Costa, I. G. (2019). Identification of transcription factor binding sites using ATAC-seq. *Genome Biology*, *20*(1), 45. https://doi.org/10.1186/s13059-019-1642-2

Liang, C.-P., Han, S., Senokuchi, T., & Tall, A. R. (2007). The macrophage at the crossroads of insulin resistance and atherosclerosis. *Circulation Research*, *100*(11), 1546–1555. https://doi.org/10.1161/CIRCRESAHA.107.152165

Liddelow, S. A., Guttenplan, K. A., Clarke, L. E., Bennett, F. C., Bohlen, C. J., Schirmer, L., … Barres, B. A. (2017a). Neurotoxic reactive astrocytes are induced by activated microglia. *Nature*, *541*(7638), 481–487. https://doi.org/10.1038/nature21029

Liddelow, S. A., Guttenplan, K. A., Clarke, L. E., Bennett, F. C., Bohlen, C. J., Schirmer, L., … Barres, B. A. (2017b). Neurotoxic reactive astrocytes are induced by activated microglia. *Nature*, *541*(7638), 481–487. https://doi.org/10.1038/nature21029

Lie-A-Ling, M., Marinopoulou, E., Li, Y., Patel, R., Stefanska, M., Bonifer, C., … Lacaud, G. (2014). RUNX1 positively regulates a cell adhesion and migration program in murine hemogenic endothelium prior to blood emergence. *Blood*, *124*(11), e11–e20. https://doi.org/10.1182/blood-2014-04-572958

Lin, Y., Xu, J., & Lan, H. (2019). Tumor-associated macrophages in tumor metastasis: biological roles and clinical therapeutic applications. *Journal of Hematology & Oncology*, *12*(1), 76. https://doi.org/10.1186/s13045-019-0760-3

Liu, K., Zhao, E., Ilyas, G., Lalazar, G., Lin, Y., Haseeb, M., … Czaja, M. J. (2015). Impaired macrophage autophagy increases the immune response in obese mice by promoting proinflammatory macrophage polarization. *Autophagy*, *11*(2), 271–284. https://doi.org/10.1080/15548627.2015.1009787

Love, J. E., Hayden, E. J., & Rohn, T. T. (2015). Alternative Splicing in Alzheimer's Disease. *Journal of Parkinson's Disease and Alzheimer's Disease*, *2*(2). https://doi.org/10.13188/2376-922X.1000010

Lu, C.-H., Lai, C.-Y., Yeh, D.-W., Liu, Y.-L., Su, Y.-W., Hsu, L.-C., … Chuang, T.-H. (2018). Involvement of M1 Macrophage Polarization in Endosomal Toll-Like Receptors Activated Psoriatic Inflammation. *Mediators of Inflammation*, *2018*, 1–14. https://doi.org/10.1155/2018/3523642

Lumeng, C. N., Bodzin, J. L., & Saltiel, A. R. (2007). Obesity induces a phenotypic switch in adipose tissue macrophage polarization. *The Journal of Clinical Investigation*, *117*(1), 175–184. https://doi.org/10.1172/JCI29881

Macciò, A., Gramignano, G., Cherchi, M. C., Tanca, L., Melis, L., & Madeddu, C. (2020). Role of M1-polarized tumor-associated macrophages in the prognosis of advanced ovarian cancer patients. *Scientific Reports*, *10*(1), 6096. https://doi.org/10.1038/s41598-020-63276-1

Macosko, E. Z., Basu, A., Satija, R., Nemesh, J., Shekhar, K., Goldman, M., … McCarroll, S. A. (2015). Highly Parallel Genome-wide Expression Profiling of Individual Cells Using Nanoliter Droplets. *Cell*, *161*(5), 1202–1214. https://doi.org/10.1016/J.CELL.2015.05.002

Makita, N., Hizukuri, Y., Yamashiro, K., Murakawa, M., & Hayashi, Y. (2015). IL-10 enhances the phenotype of M2 macrophages induced by IL-4 and confers the ability to increase eosinophil migration. *International Immunology*, *27*(3), 131–141. https://doi.org/10.1093/intimm/dxu090

Malfitano, A. M., Pisanti, S., Napolitano, F., Di Somma, S., Martinelli, R., & Portella, G. (2020). Tumor-Associated Macrophage Status in Cancer Treatment. *Cancers*, *12*(7). https://doi.org/10.3390/cancers12071987

Mantovani, A., Martinez, F. O., Gordon, S., & Locati, M. (2006). *Gene Expression Polarization: New Molecules and Patterns of and Monocyte-to-Macrophage Differentiation Transcriptional Profiling of the Human*. https://doi.org/10.4049/jimmunol.177.10.7303

Mantovani, A., Sica, A., Sozzani, S., Allavena, P., Vecchi, A., & Locati, M. (2004). The chemokine system in diverse forms of macrophage activation and polarization. *Trends in Immunology*, *25*(12), 677–686. https://doi.org/10.1016/J.IT.2004.09.015

Mathys, H., Adaikkan, C., Gao, F., Young, J. Z., Manet, E., Hemberg, M., … Tsai, L.-H. (2017). Temporal Tracking of Microglia Activation in Neurodegeneration at Single-Cell Resolution. *Cell Reports*, *21*(2), 366–380. https://doi.org/10.1016/J.CELREP.2017.09.039

McKenzie, J. A., & Klegeris, A. (2018). Modulation of microglial functions by methyl jasmonate. *Neural Regeneration Research*, *13*(7), 1290–1293. https://doi.org/10.4103/1673-5374.235078

McWhorter, F. Y., Wang, T., Nguyen, P., Chung, T., & Liu, W. F. (2013). Modulation of macrophage phenotype by cell shape. *Proceedings of the National Academy of Sciences of the United States of America*, *110*(43), 17253–17258. https://doi.org/10.1073/pnas.1308887110

Michalska, A., Blaszczyk, K., Wesoly, J., & Bluyssen, H. A. R. (2018). A Positive Feedback Amplifier Circuit That Regulates Interferon (IFN)-Stimulated Gene Expression and Controls Type I and Type II IFN Responses. *Frontiers in Immunology*, *9*, 1135. https://doi.org/10.3389/fimmu.2018.01135

Miller, M. M., Barik, S., Cattin-Roy, A. N., Ukah, T. K., Hoeman, C. M., & Zaghouani, H. (2019). A New IRF-1–Driven Apoptotic Pathway Triggered by IL-4/IL-13 Kills Neonatal Th1 Cells and Weakens Protection against Viral Infection. *The Journal of Immunology*, *202*(11), 3173–3186. https://doi.org/10.4049/JIMMUNOL.1800943

Mills, C. D., Kincaid, K., Alt, J. M., Heilman, M. J., & Hill, A. M. (2000a). M-1/M-2 macrophages and the Th1/Th2 paradigm. *Journal of Immunology (Baltimore, Md. : 1950)*, *164*(12), 6166–6173. Retrieved from http://www.ncbi.nlm.nih.gov/pubmed/10843666

Mills, C. D., Kincaid, K., Alt, J. M., Heilman, M. J., & Hill, A. M. (2000b). M-1/M-2 macrophages and the Th1/Th2 paradigm. *Journal of Immunology (Baltimore, Md. : 1950)*, *164*(12), 6166–6173. Retrieved from http://www.ncbi.nlm.nih.gov/pubmed/10843666

Minar, P., Haberman, Y., Jurickova, I., Wen, T., Rothenberg, M. E., Kim, M.-O., … Denson, L. A. (2014). Utility of Neutrophil Fcγ Receptor I (CD64) Index as a Biomarker for Mucosal Inflammation in Pediatric Crohn's Disease. *Inflammatory Bowel Diseases*, *20*(6), 1. https://doi.org/10.1097/MIB.0000000000000049

Mojumdar, K., Liang, F., Giordano, C., Lemaire, C., Danialou, G., Okazaki, T., … Petrof, B. J. (2014). Inflammatory monocytes promote progression of Duchenne muscular dystrophy and can be therapeutically targeted via CCR2. *EMBO Molecular Medicine*, *6*(11), 1476–1492. https://doi.org/10.15252/emmm.201403967

Moore, M. J., Scheel, T. K. H., Luna, J. M., Park, C. Y., Fak, J. J., Nishiuchi, E., … Darnell, R.

B. (2015). miRNA-target chimeras reveal miRNA 3'-end pairing as a major determinant of Argonaute target specificity. *Nature Communications*, *6*, 8864. https://doi.org/10.1038/ncomms9864

Mortazavi, A., Williams, B. A., McCue, K., Schaeffer, L., & Wold, B. (2008). Mapping and quantifying mammalian transcriptomes by RNA-Seq. *Nature Methods*, *5*(7), 621–628. https://doi.org/10.1038/nmeth.1226

Mosser, D. M., Hamidzadeh, K., & Goncalves, R. (2021). Macrophages and the maintenance of homeostasis. *Cellular & Molecular Immunology*, *18*(3), 579–587. https://doi.org/10.1038/s41423-020-00541-3

Mukaka, M. M. (2012). Statistics corner: A guide to appropriate use of correlation coefficient in medical research. *Malawi Medical Journal : The Journal of Medical Association of Malawi*, *24*(3), 69–71. Retrieved from http://www.ncbi.nlm.nih.gov/pubmed/23638278

Muñoz-Rojas, A. R., Kelsey, I., Pappalardo, J. L., Chen, M., & Miller-Jensen, K. (2021). Co-stimulation with opposing macrophage polarization cues leads to orthogonal secretion programs in individual cells. *Nature Communications*, *12*(1), 301. https://doi.org/10.1038/s41467-020-20540-2

Murao, S.-I., Gemmell, M. A., Callaham, M. F., Anderson, N. L., & Huberman2, E. (1983). Control of Macrophage Cell Differentiation in Human Promyelocytic HL-60 Leukemia Cells by 1,25-Dihydroxyvitamin D3 and Phorbol-12-myristate- 13-acetate1. *CANCER RESEARCH*, *43*, 4989–4996. Retrieved from http://cancerres.aacrjournals.org/content/canres/43/10/4989.full.pdf

Nayak, D., Roth, T. L., & McGavern, D. B. (2014). Microglia development and function. *Annual Review of Immunology*, *32*, 367–402. https://doi.org/10.1146/annurev-immunol-032713-

120240

Neamatallah, T. (2019). Mitogen-Activated Protein Kinase Pathway: A Critical Regulator in Tumor-associated Macrophage Polarization. *Journal of Microscopy and Ultrastructure*, *7*(2), 53. https://doi.org/10.4103/JMAU.JMAU_68_18

Nerlov, C., & Graf, T. (1998). PU.1 induces myeloid lineage commitment in multipotent hematopoietic progenitors. *Genes & Development*, *12*(15), 2403–2412. https://doi.org/10.1101/gad.12.15.2403

Ning, S., Huye, L. E., & Pagano, J. S. (2005). Regulation of the Transcriptional Activity of the IRF7 Promoter by a Pathway Independent of Interferon Signaling. *Journal of Biological Chemistry*, *280*(13), 12262–12270. https://doi.org/10.1074/JBC.M404260200

Nueda, M. J., Tarazona, S., & Conesa, A. (2014a). Next maSigPro: updating maSigPro bioconductor package for RNA-seq time series. *Bioinformatics*, *30*(18), 2598–2602. https://doi.org/10.1093/bioinformatics/btu333

Nueda, M. J., Tarazona, S., & Conesa, A. (2014b). Next maSigPro: updating maSigPro bioconductor package for RNA-seq time series. *Bioinformatics*, *30*(18), 2598–2602. https://doi.org/10.1093/bioinformatics/btu333

Ohsawa, K., Imai, Y., Sasaki, Y., & Kohsaka, S. (2004). Microglia/macrophage-specific protein Iba1 binds to fimbrin and enhances its actin-bundling activity. *Journal of Neurochemistry*, *88*(4), 844–856. https://doi.org/10.1046/j.1471-4159.2003.02213.x

Olsson, A., Venkatasubramanian, M., Chaudhri, V. K., Aronow, B. J., Salomonis, N., Singh, H., & Grimes, H. L. (2016). Single-cell analysis of mixed-lineage states leading to a binary cell fate choice. *Nature*, *537*(7622), 698–702. https://doi.org/10.1038/nature19348

Orecchioni, M., Ghosheh, Y., Pramod, A. B., & Ley, K. (2019a). Macrophage Polarization:

Different Gene Signatures in M1(LPS+) vs. Classically and M2(LPS–) vs. Alternatively Activated Macrophages. *Frontiers in Immunology*, *10*, 1084. https://doi.org/10.3389/fimmu.2019.01084

Orecchioni, M., Ghosheh, Y., Pramod, A. B., & Ley, K. (2019b). Macrophage Polarization: Different Gene Signatures in M1(LPS+) vs. Classically and M2(LPS–) vs. Alternatively Activated Macrophages. *Frontiers in Immunology*, *10*, 1084. https://doi.org/10.3389/fimmu.2019.01084

Oxford, A. E., Stewart, E. S., & Rohn, T. T. (2020). Clinical Trials in Alzheimer's Disease: A Hurdle in the Path of Remedy. *International Journal of Alzheimer's Disease*, *2020*, 5380346. https://doi.org/10.1155/2020/5380346

Pachter, J. S., de Vries, H. E., & Fabry, Z. (2003). The blood-brain barrier and its role in immune privilege in the central nervous system. *Journal of Neuropathology and Experimental Neurology*, *62*(6), 593–604. https://doi.org/10.1093/jnen/62.6.593

Palma, A., Jarrah, A. S., Tieri, P., Cesareni, G., & Castiglione, F. (2018). Gene Regulatory Network Modeling of Macrophage Differentiation Corroborates the Continuum Hypothesis of Polarization States. *Frontiers in Physiology*, *9*. https://doi.org/10.3389/FPHYS.2018.01659

Panchal, M., Loeper, J., Cossec, J.-C., Perruchini, C., Lazar, A., Pompon, D., & Duyckaerts, C. (2010). Enrichment of cholesterol in microdissected Alzheimer's disease senile plaques as assessed by mass spectrometry. *Journal of Lipid Research*, *51*(3), 598–605. https://doi.org/10.1194/jlr.M001859

Papadopoulos, K. P., Gluck, L., Martin, L. P., Olszanski, A. J., Tolcher, A. W., Ngarmchamnanrith, G., … Stephenson, J. (2017). First-in-Human Study of AMG 820, a

Monoclonal Anti-Colony-Stimulating Factor 1 Receptor Antibody, in Patients with Advanced Solid Tumors. *Clinical Cancer Research*, *23*(19), 5703–5710. https://doi.org/10.1158/1078-0432.CCR-16-3261

Parisi, L., Gini, E., Baci, D., Tremolati, M., Fanuli, M., Bassani, B., … Mortara, L. (2018). Macrophage Polarization in Chronic Inflammatory Diseases: Killers or Builders? *Journal of Immunology Research*, *2018*, 1–25. https://doi.org/10.1155/2018/8917804

Pavlovski, D., Thundyil, J., Monk, P. N., Wetsel, R. A., Taylor, S. M., & Woodruff, T. M. (2012). Generation of complement component C5a by ischemic neurons promotes neuronal apoptosis. *The FASEB Journal*, *26*(9), 3680–3690. https://doi.org/10.1096/fj.11-202382

Pei, Y., Yin, X., & Liu, X. (2018). TOP2A induces malignant character of pancreatic cancer through activating β-catenin signaling pathway. *Biochimica et Biophysica Acta (BBA) - Molecular Basis of Disease*, *1864*(1), 197–207. https://doi.org/10.1016/J.BBADIS.2017.10.019

Peña, C. G., Nakada, Y., Saatcioglu, H. D., Aloisio, G. M., Cuevas, I., Zhang, S., … Castrillon, D. H. (2015). LKB1 loss promotes endometrial cancer progression via CCL2-dependent macrophage recruitment. *The Journal of Clinical Investigation*, *125*(11), 4063–4076. https://doi.org/10.1172/JCI82152

Peng, Y., & Croce, C. M. (2016). The role of MicroRNAs in human cancer. *Signal Transduction and Targeted Therapy*, *1*(1), 15004. https://doi.org/10.1038/sigtrans.2015.4

Peter, I. S., & Davidson, E. H. (2011). Evolution of gene regulatory networks controlling body plan development. *Cell*, *144*(6), 970–985. https://doi.org/10.1016/j.cell.2011.02.017

Peter, I. S., & Davidson, E. H. (2015). *Genomic Control Process*. https://doi.org/10.1016/C2012-0-02817-7

Picelli, S., Faridani, O. R., Björklund, Å. K., Winberg, G., Sagasser, S., & Sandberg, R. (2014). Full-length RNA-seq from single cells using Smart-seq2. *Nature Protocols*, *9*(1), 171–181. https://doi.org/10.1038/nprot.2014.006

Piper, J., Elze, M. C., Cauchy, P., Cockerill, P. N., Bonifer, C., & Ott, S. (2013). Wellington: a novel method for the accurate identification of digital genomic footprints from DNase-seq data. *Nucleic Acids Research*, *41*(21), e201. https://doi.org/10.1093/nar/gkt850

Platanitis, E., & Decker, T. (2018). Regulatory Networks Involving STATs, IRFs, and NFκB in Inflammation. *Frontiers in Immunology*, *9*, 2542. https://doi.org/10.3389/fimmu.2018.02542

Poplutz, M. K., Wessels, I., Rink, L., & Uciechowski, P. (2014). Regulation of the Interleukin-6 gene expression during monocytic differentiation of HL-60 cells by chromatin remodeling and methylation. *Immunobiology*, *219*(8), 619–626. https://doi.org/10.1016/J.IMBIO.2014.03.016

Puranik, A. S., Leaf, I. A., Jensen, M. A., Hedayat, A. F., Saad, A., Kim, K.-W., … Lerman, L. O. (2018). Kidney-resident macrophages promote a proangiogenic environment in the normal and chronically ischemic mouse kidney. *Scientific Reports*, *8*(1), 13948. https://doi.org/10.1038/s41598-018-31887-4

Qiu, S.-Q., Waaijer, S. J. H., Zwager, M. C., de Vries, E. G. E., van der Vegt, B., & Schröder, C. P. (2018). Tumor-associated macrophages in breast cancer: Innocent bystander or important player? *Cancer Treatment Reviews*, *70*, 178–189. https://doi.org/10.1016/J.CTRV.2018.08.010

Qiu, X., Mao, Q., Tang, Y., Wang, L., Chawla, R., Pliner, H. A., & Trapnell, C. (2017). *Reversed graph embedding resolves complex single-cell trajectories*.

https://doi.org/10.1038/nmeth.4402

Räihä, M. R., & Puolakkainen, P. A. (2018). Tumor-associated macrophages (TAMs) as biomarkers for gastric cancer: A review. *Chronic Diseases and Translational Medicine*, *4*(3), 156–163. https://doi.org/10.1016/J.CDTM.2018.07.001

Ramachandran, B., Yu, G., Li, S., Zhu, B., & Gulick, T. (2008). Myocyte Enhancer Factor 2A Is Transcriptionally Autoregulated. *Journal of Biological Chemistry*, *283*(16), 10318–10329. https://doi.org/10.1074/JBC.M707623200

Ramirez, R. N., El-Ali, N. C., Mager, M. A., Wyman, D., Conesa, A., & Mortazavi, A. (2017). Dynamic Gene Regulatory Networks of Human Myeloid Differentiation. *Cell Systems*, *4*(4), 416-429.e3. https://doi.org/10.1016/J.CELS.2017.03.005

Ransohoff, R. M. (2016). A polarizing question: do M1 and M2 microglia exist? *Nature Neuroscience*, *19*(8), 987–991. https://doi.org/10.1038/nn.4338

Rautela, J., Dagley, L. F., Kratina, T., Anthony, A., Goh, W., Surgenor, E., … Huntington, N. D. (2019). Generation of novel Id2 and E2-2, E2A and HEB antibodies reveals novel Id2 binding partners and species-specific expression of E-proteins in NK cells. *Molecular Immunology*, *115*, 56–63. https://doi.org/10.1016/J.MOLIMM.2018.08.017

Reece, J. J., Siracusa, M. C., & Scott, A. L. (2006). Innate immune responses to lung-stage helminth infection induce alternatively activated alveolar macrophages. *Infection and Immunity*, *74*(9), 4970–4981. https://doi.org/10.1128/IAI.00687-06

Reiman, R., Torres, A. C., Martin, B. K., Ting, J. P., Campbell, I. L., & Barnum, S. R. (2005). Expression of C5a in the brain does not exacerbate experimental autoimmune encephalomyelitis. *Neuroscience Letters*, *390*(3), 134–138. https://doi.org/10.1016/J.NEULET.2005.08.022

Reis, E. S., Mastellos, D. C., Hajishengallis, G., & Lambris, J. D. (2019). New insights into the immune functions of complement. *Nature Reviews Immunology*, *19*(8), 503–516. https://doi.org/10.1038/s41577-019-0168-x

Ricklin, D., & Lambris, J. D. (2016). New milestones ahead in complement-targeted therapy. *Seminars in Immunology*, *28*(3), 208–222. https://doi.org/10.1016/j.smim.2016.06.001

Robinson, M. D., McCarthy, D. J., & Smyth, G. K. (2010). edgeR: a Bioconductor package for differential expression analysis of digital gene expression data. *Bioinformatics*, *26*(1), 139–140. https://doi.org/10.1093/bioinformatics/btp616

Robinson, Mark D, & Oshlack, A. (2010). A scaling normalization method for differential expression analysis of RNA-seq data. *Genome Biology*, *11*(3), R25. https://doi.org/10.1186/gb-2010-11-3-r25

Romagnoli, D., Boccalini, G., Bonechi, M., Biagioni, C., Fassan, P., Bertorelli, R., … Benelli, M. (2018). ddSeeker: a tool for processing Bio-Rad ddSEQ single cell RNA-seq data. *BMC Genomics*, *19*(1), 960. https://doi.org/10.1186/s12864-018-5249-x

Rong, L., Zhang, Y., Li, W.-S., Su, Z., Fadhil, J. I., & Zhang, C. (2019). Iron chelated melanin-like nanoparticles for tumor-associated macrophage repolarization and cancer therapy. *Biomaterials*, *225*, 119515. https://doi.org/10.1016/J.BIOMATERIALS.2019.119515

Rosa, L. F. B. P. C., Safi, D. A., Cury, Y., & Curi, R. (1996). The effect of insulin on macrophage metabolism and function. *Cell Biochemistry and Function*, *14*(1), 33–42. https://doi.org/10.1002/cbf.637

Rőszer, T. (2015a). Understanding the Mysterious M2 Macrophage through Activation Markers and Effector Mechanisms. *Mediators of Inflammation*, *2015*, 816460. https://doi.org/10.1155/2015/816460

Rőszer, T. (2015b). Understanding the Mysterious M2 Macrophage through Activation Markers and Effector Mechanisms. *Mediators of Inflammation*, *2015*, 816460. https://doi.org/10.1155/2015/816460

Rőszer, T. (2015c). Understanding the Mysterious M2 Macrophage through Activation Markers and Effector Mechanisms. *Mediators of Inflammation*, *2015*, 816460. https://doi.org/10.1155/2015/816460

Saradna, A., Do, D. C., Kumar, S., Fu, Q.-L., & Gao, P. (2018). Macrophage polarization and allergic asthma. *Translational Research : The Journal of Laboratory and Clinical Medicine*, *191*, 1–14. https://doi.org/10.1016/j.trsl.2017.09.002

Sarlus, H., & Heneka, M. T. (2017). Microglia in Alzheimer's disease. *The Journal of Clinical Investigation*, *127*(9), 3240–3249. https://doi.org/10.1172/JCI90606

Satija, R., Farrell, J. A., Gennert, D., Schier, A. F., & Regev, A. (2015). Spatial reconstruction of single-cell gene expression data. *Nature Biotechnology*, *33*(5), 495–502. https://doi.org/10.1038/nbt.3192

Scharer, C. D., Barwick, B. G., Guo, M., Bally, A. P. R., & Boss, J. M. (2018). Plasma cell differentiation is controlled by multiple cell division-coupled epigenetic programs. *Nature Communications*, *9*(1), 1698. https://doi.org/10.1038/s41467-018-04125-8

Schartz, N. D., & Tenner, A. J. (2020). The good, the bad, and the opportunities of the complement system in neurodegenerative disease. *Journal of Neuroinflammation*, *17*(1), 354. https://doi.org/10.1186/s12974-020-02024-8

Self-Fordham, J. B., Naqvi, A. R., Uttamani, J. R., Kulkarni, V., & Nares, S. (2017). MicroRNA: Dynamic Regulators of Macrophage Polarization and Plasticity. *Frontiers in Immunology*, *8*, 1062. https://doi.org/10.3389/fimmu.2017.01062

Seo, J., Kim, M., & Kim, J. (2000). Identification of novel genes differentially expressed in PMA-induced HL-60 cells using cDNA microarrays. *Molecules and Cells*, *10*(6), 733–739. https://doi.org/10.1007/s10059-000-0733-x

Seok, H., Ham, J., Jang, E.-S., & Chi, and S. W. (2016). MicroRNA Target Recognition: Insights from Transcriptome-Wide Non-Canonical Interactions. *Molecules and Cells*, *39*(5), 375–381. https://doi.org/10.14348/molcells.2016.0013

Sevenich, L. (2018). Brain-Resident Microglia and Blood-Borne Macrophages Orchestrate Central Nervous System Inflammation in Neurodegenerative Disorders and Brain Cancer. *Frontiers in Immunology*, *9*, 697. https://doi.org/10.3389/fimmu.2018.00697

Shaked, Y. (2019). The pro-tumorigenic host response to cancer therapies. *Nature Reviews Cancer*, *19*(12), 667–685. https://doi.org/10.1038/s41568-019-0209-6

Sharma, A., Seow, J. J. W., Dutertre, C.-A., Pai, R., Blériot, C., Mishra, A., … DasGupta, R. (2020). Onco-fetal Reprogramming of Endothelial Cells Drives Immunosuppressive Macrophages in Hepatocellular Carcinoma. *Cell*, *183*(2), 377-394.e21. https://doi.org/10.1016/J.CELL.2020.08.040

Shouval, D. S., Biswas, A., Goettel, J. A., McCann, K., Conaway, E., Redhu, N. S., … Snapper, S. B. (2014). Interleukin-10 Receptor Signaling in Innate Immune Cells Regulates Mucosal Immune Tolerance and Anti-Inflammatory Macrophage Function. *Immunity*, *40*(5), 706. https://doi.org/10.1016/J.IMMUNI.2014.03.011

Shu, Y., Qin, M., Song, Y., Tang, Q., Huang, Y., Shen, P., & Lu, Y. (2020). M2 polarization of tumor-associated macrophages is dependent on integrin β 3 via peroxisome proliferator-activated receptor- γ up-regulation in breast cancer. *Immunology*, *160*(4), 345–356. https://doi.org/10.1111/imm.13196

Sica, A., & Mantovani, A. (2012). Macrophage plasticity and polarization: in vivo veritas. *Journal of Clinical Investigation*, *122*(3), 787–795. https://doi.org/10.1172/JCI59643

Sierksma, A., Lu, A., Mancuso, R., Fattorelli, N., Thrupp, N., Salta, E., … Fiers, M. (2020). Novel Alzheimer risk genes determine the microglia response to amyloid-β but not to TAU pathology. *EMBO Molecular Medicine*, *12*(3), e10606. https://doi.org/10.15252/emmm.201910606

Smith, L., Hohaus, S., Gonzalez, D., Dziennis, S., & Tenen, D. (1996). PU.1 (Spi-1) and C/EBP alpha regulate the granulocyte colony- stimulating factor receptor promoter in myeloid cells. *Blood*, *88*(4), 1234–1247. https://doi.org/10.1182/blood.V88.4.1234.bloodjournal8841234

Srivastava, P. K., Hull, R. P., Behmoaras, J., Petretto, E., & Aitman, T. J. (2013). JunD/AP1 regulatory network analysis during macrophage activation in a rat model of crescentic glomerulonephritis. *BMC Systems Biology*, *7*, 93. https://doi.org/10.1186/1752-0509-7-93

Stepien, D. M., Hwang, C., Marini, S., Pagani, C. A., Sorkin, M., Visser, N. D., … Levi, B. (2020). Tuning Macrophage Phenotype to Mitigate Skeletal Muscle Fibrosis. *Journal of Immunology (Baltimore, Md. : 1950)*, *204*(8), 2203–2215. https://doi.org/10.4049/jimmunol.1900814

Strittmatter, W. J., Saunders, A. M., Schmechel, D., Pericak-Vance, M., Enghild, J., Salvesen, G. S., & Roses, A. D. (2009). Apolipoprotein E: high-avidity binding to beta-amyloid and increased frequency of type 4 allele in late-onset familial Alzheimer disease. *Proceedings of the National Academy of Sciences of the United States of America*, *90*(5), 1977–1981. https://doi.org/10.1073/pnas.90.5.1977

Sung, M.-H., Baek, S., & Hager, G. L. (2016). Genome-wide footprinting: ready for prime time?

Nature Methods, *13*(3), 222. https://doi.org/10.1038/NMETH.3766

Takahashi, H., Hatta, Y., Iriyama, N., Hasegawa, Y., Uchida, H., Nakagawa, M., … Takei, M. (2014). Induced Differentiation of Human Myeloid Leukemia Cells into M2 Macrophages by Combined Treatment with Retinoic Acid and 1α,25-Dihydroxyvitamin D3. *PLoS ONE*, *9*(11), e113722. https://doi.org/10.1371/journal.pone.0113722

Talker, S. C., Tuba Barut, G., Rufener, R., Von Münchow, L., & Summerfield, A. (n.d.). *Transcriptomic signature and metabolic programming of bovine classical and nonclassical monocytes indicate distinct functional specializations*. https://doi.org/10.1101/2020.10.30.362731

Tang, Y., Govers, C., Wichers, H. J., & Mes, J. J. (2017). Macrophages treated with non-digestible polysaccharides reveal a transcriptionally unique phenotype. *Journal of Functional Foods*, *36*, 280–289. https://doi.org/10.1016/J.JFF.2017.07.003

Tanzi, R. E. (2012). The genetics of Alzheimer disease. *Cold Spring Harbor Perspectives in Medicine*, *2*(10). https://doi.org/10.1101/cshperspect.a006296

Tenner, A. J. (2020). Complement-Mediated Events in Alzheimer's Disease: Mechanisms and Potential Therapeutic Targets. *Journal of Immunology (Baltimore, Md. : 1950)*, *204*(2), 306–315. https://doi.org/10.4049/jimmunol.1901068

Tesar, V., & Hruskova, Z. (2018). Avacopan in the treatment of ANCA-associated vasculitis. *Expert Opinion on Investigational Drugs*, *27*(5), 491–496. https://doi.org/10.1080/13543784.2018.1472234

Thepen, T., Huhn, M., Melmer, G., Tur, M. K., & Barth, S. (2009). Fcgamma receptor 1 (CD64), a target beyond cancer. *Current Pharmaceutical Design*, *15*(23), 2712–2718. Retrieved from http://www.ncbi.nlm.nih.gov/pubmed/19689341

Tiainen, S., Tumelius, R., Rilla, K., Hämäläinen, K., Tammi, M., Tammi, R., … Auvinen, P. (2015). High numbers of macrophages, especially M2-like (CD163-positive), correlate with hyaluronan accumulation and poor outcome in breast cancer. *Histopathology*, *66*(6), 873–883. https://doi.org/10.1111/his.12607

Traag, V. A., Waltman, L., & van Eck, N. J. (2019). From Louvain to Leiden: guaranteeing well-connected communities. *Scientific Reports*, *9*(1), 5233. https://doi.org/10.1038/s41598-019-41695-z

Tribolet, L., Kerr, E., Cowled, C., Bean, A. G. D., Stewart, C. R., Dearnley, M., & Farr, R. J. (2020). MicroRNA Biomarkers for Infectious Diseases: From Basic Research to Biosensing. *Frontiers in Microbiology*, *11*, 1197. https://doi.org/10.3389/fmicb.2020.01197

Tsutsumi, S., Tokunaga, Y., Shimizu, S., Kinoshita, H., Ono, M., Kurogi, K., … Yasuda, S. (2020). Investigation of the effects of indoxyl sulfate, a uremic toxin, on the intracellular oxidation level and phagocytic activity using an HL-60-differentiated human macrophage cell model. *Bioscience, Biotechnology, and Biochemistry*, *84*(5), 1023–1029. https://doi.org/10.1080/09168451.2020.1715782

Ulger, C., Toruner, G. A., Alkan, M., Mohammed, M., Damani, S., Kang, J., … Dermody, J. J. (2003). Comprehensive genome-wide comparison of DNA and RNA level scan using microarray technology for identification of candidate cancer-related genes in the HL-60 cell line. *Cancer Genetics and Cytogenetics*, *147*(1), 28–35. https://doi.org/10.1016/s0165-4608(03)00155-9

Vergunst, C. E., Gerlag, D. M., Dinant, H., Schulz, L., Vinkenoog, M., Smeets, T. J. M., … Tak, P. P. (2007). Blocking the receptor for C5a in patients with rheumatoid arthritis does not reduce synovial inflammation. *Rheumatology*, *46*(12), 1773–1778.

https://doi.org/10.1093/rheumatology/kem222

Verheijen, J., & Sleegers, K. (2018). Understanding Alzheimer Disease at the Interface between Genetics and Transcriptomics. *Trends in Genetics*, *34*, 434–447. https://doi.org/10.1016/j.tig.2018.02.007

Vogel-Ciernia, A., & Wood, M. A. (2014). Examining object location and object recognition memory in mice. *Current Protocols in Neuroscience*, *69*, 8.31.1-17. https://doi.org/10.1002/0471142301.ns0831s69

Walentynowicz, K. A., Ochocka, N., Pasierbinska, M., Wojnicki, K., Stepniak, K., Mieczkowski, J., … Kaminska, B. (2018). In Search for Reliable Markers of Glioma-Induced Polarization of Microglia. *Frontiers in Immunology*, *9*, 1329. https://doi.org/10.3389/fimmu.2018.01329

Walker, D. G., & Lue, L.-F. (2015). Immune phenotypes of microglia in human neurodegenerative disease: challenges to detecting microglial polarization in human brains. *Alzheimer's Research & Therapy*, *7*(1), 56. https://doi.org/10.1186/s13195-015-0139-9

Wang, H.-W., & Joyce, J. A. (2010). Alternative activation of tumor-associated macrophages by IL-4: Priming for protumoral functions. *Cell Cycle*, *9*(24), 4824. https://doi.org/10.4161/CC.9.24.14322

Wang, H. A., Lee, J. D., Lee, K. M., Woodruff, T. M., & Noakes, P. G. (2017). Complement C5a-C5aR1 signalling drives skeletal muscle macrophage recruitment in the hSOD1G93A mouse model of amyotrophic lateral sclerosis. *Skeletal Muscle*, *7*(1), 10. https://doi.org/10.1186/s13395-017-0128-8

Wang, Y., Wang, Y. P., Zheng, G., Lee, V. W. S., Ouyang, L., Chang, D. H. H., … Harris, D. C. H. (2007). Ex vivo programmed macrophages ameliorate experimental chronic inflammatory renal disease. *Kidney International*, *72*(3), 290–299.

https://doi.org/10.1038/SJ.KI.5002275

Wang, Yang, Han, C., Cui, D., Li, Y., Ma, Y., & Wei, W. (2017). Is macrophage polarization important in rheumatoid arthritis? *International Immunopharmacology*, *50*, 345–352. https://doi.org/10.1016/J.INTIMP.2017.07.019

Webb, M. W., Sun, J., Sheard, M. A., Liu, W., Wu, H., Jackson, J. R., … Seeger, R. C. (2018). C olony stimulating factor 1 receptor blockade improves the efficacy of chemotherapy against human neuroblastoma in the absence of T lymphocytes. *International Journal of Cancer*, *143*(6), 1483–1493. https://doi.org/10.1002/ijc.31532

Webster, S., Lue, L.-F., Brachova, L., Tenner, A. ., McGeer, P. ., Terai, K., … Rogers, J. (1997). Molecular and Cellular Characterization of the Membrane Attack Complex, C5b-9, in Alzheimer's Disease. *Neurobiology of Aging*, *18*(4), 415–421. https://doi.org/10.1016/S0197-4580(97)00042-0

Wenzel, T. J., Gates, E. J., Ranger, A. L., & Klegeris, A. (2020). Short-chain fatty acids (SCFAs) alone or in combination regulate select immune functions of microglia-like cells. *Molecular and Cellular Neuroscience*, *105*, 103493. https://doi.org/10.1016/J.MCN.2020.103493

Woodruff, T. M., Costantini, K. J., Crane, J. W., Atkin, J. D., Monk, P. N., Taylor, S. M., & Noakes, P. G. (2008). The complement factor C5a contributes to pathology in a rat model of amyotrophic lateral sclerosis. *Journal of Immunology (Baltimore, Md. : 1950)*, *181*(12), 8727–8734. https://doi.org/10.4049/jimmunol.181.12.8727

Woodruff, T. M., Crane, J. W., Proctor, L. M., Buller, K. M., Shek, A. B., De Vos, K., … Taylor, A. S. M. (2006). Therapeutic activity of C5a receptor antagonists in a rat model of neurodegeneration. *The FASEB Journal*, *20*(9), 1407–1417. https://doi.org/10.1096/fj.05-5814com

Wu, P., Wu, D., Zhao, L., Huang, L., Chen, G., Shen, G., … Chai, Y. (2016). Inverse role of distinct subsets and distribution of macrophage in lung cancer prognosis: a meta-analysis. *Oncotarget*, *7*(26), 40451–40460. https://doi.org/10.18632/oncotarget.9625

Wyman, D., Balderrama-Gutierrez, G., Reese, F., Jiang, S., Rahmanian, S., Forner, S., … Mortazavi, A. (2020). A technology-agnostic long-read analysis pipeline for transcriptome discovery and quantification. *BioRxiv*, 672931. https://doi.org/10.1101/672931

Wynn, T. (2008). Cellular and molecular mechanisms of fibrosis. *The Journal of Pathology*, *214*(2), 199–210. https://doi.org/10.1002/path.2277

Xiao, Hong, Guo, Y., Li, B., Li, X., Wang, Y., Han, S., … Shuai, X. (2020). M2-Like Tumor-Associated Macrophage-Targeted Codelivery of STAT6 Inhibitor and IKKβ siRNA Induces M2-to-M1 Repolarization for Cancer Immunotherapy with Low Immune Side Effects. *ACS Central Science*, *6*(7), 1208–1222. https://doi.org/10.1021/acscentsci.9b01235

Xiao, Hui, Wu, Y., Yang, C., Yi, Z., Zeng, N., Xu, Y., … Wu, M. (2020). Knockout of E2F1 enhances the polarization of M2 phenotype macrophages to accelerate the wound healing process. *The Kaohsiung Journal of Medical Sciences*, *36*(9), 692–698. https://doi.org/10.1002/kjm2.12222

XIE, C., LIU, C., WU, B., LIN, Y., MA, T., XIONG, H., … TU, Z. (2016). Effects of IRF1 and IFN-β interaction on the M1 polarization of macrophages and its antitumor function. *International Journal of Molecular Medicine*, *38*(1), 148–160. https://doi.org/10.3892/ijmm.2016.2583

Yang, J., Wise, L., & Fukuchi, K. (2020). TLR4 Cross-Talk With NLRP3 Inflammasome and Complement Signaling Pathways in Alzheimer's Disease. *Frontiers in Immunology*, *11*, 724. https://doi.org/10.3389/fimmu.2020.00724

Yang, X., Schadt, E. E., Wang, S., Wang, H., Arnold, A. P., Ingram-Drake, L., … Lusis, A. J. (2006). Tissue-specific expression and regulation of sexually dimorphic genes in mice. *Genome Research*, *16*(8), 995–1004. https://doi.org/10.1101/gr.5217506

Yin, C., Vrieze, A. M., Rosoga, M., Akingbasote, J., Pawlak, E. N., Jacob, R. A., … Heit, B. (2020). Efferocytic Defects in Early Atherosclerosis Are Driven by GATA2 Overexpression in Macrophages. *Frontiers in Immunology*, *11*, 2746. https://doi.org/10.3389/fimmu.2020.594136

Yu, H., Pardoll, D., & Jove, R. (2009). STATs in cancer inflammation and immunity: a leading role for STAT3. *Nature Reviews Cancer*, *9*(11), 798–809. https://doi.org/10.1038/nrc2734

Yu, T., Gan, S., Zhu, Q., Dai, D., Li, N., Wang, H., … Xiao, Y. (2019). Modulation of M2 macrophage polarization by the crosstalk between Stat6 and Trim24. *Nature Communications*, *10*(1), 4353. https://doi.org/10.1038/s41467-019-12384-2

Yuan, A., Hsiao, Y.-J., Chen, H.-Y., Chen, H.-W., Ho, C.-C., Chen, Y.-Y., … Yang, P.-C. (2015). Opposite Effects of M1 and M2 Macrophage Subtypes on Lung Cancer Progression. *Scientific Reports*, *5*(1), 14273. https://doi.org/10.1038/srep14273

Zenke, K., Muroi, M., & Tanamoto, K. (2018). IRF1 supports DNA binding of STAT1 by promoting its phosphorylation. *Immunology and Cell Biology*, *96*(10), 1095–1103. https://doi.org/10.1111/imcb.12185

Zhang, F., Parayath, N. N., Ene, C. I., Stephan, S. B., Koehne, A. L., Coon, M. E., … Stephan, M. T. (2019). Genetic programming of macrophages to perform anti-tumor functions using targeted mRNA nanocarriers. *Nature Communications*, *10*(1), 3974. https://doi.org/10.1038/s41467-019-11911-5

Zhang, X., Tian, W., Cai, X., Wang, X., Dang, W., Tang, H., … Chen, T. (2013).

Hydrazinocurcumin Encapsuled nanoparticles "re-educate" tumor-associated macrophages and exhibit anti-tumor effects on breast cancer following STAT3 suppression. *PloS One*, *8*(6), e65896. https://doi.org/10.1371/journal.pone.0065896

Zhang, Yong, Liu, T., Meyer, C. A., Eeckhoute, J., Johnson, D. S., Bernstein, B. E., … Liu, X. S. (2008). Model-based Analysis of ChIP-Seq (MACS). *Genome Biology*, *9*(9), R137. https://doi.org/10.1186/gb-2008-9-9-r137

Zhang, Yuqing, Parmigiani, G., & Johnson, W. E. (2020). ComBat-seq: batch effect adjustment for RNA-seq count data. *NAR Genomics and Bioinformatics*, *2*(3). https://doi.org/10.1093/nargab/lqaa078

Zheng, X., Turkowski, K., Mora, J., Brüne, B., Seeger, W., Weigert, A., & Savai, R. (2017a). Redirecting tumor-associated macrophages to become tumoricidal effectors as a novel strategy for cancer therapy. *Oncotarget*, *8*(29), 48436–48452. https://doi.org/10.18632/oncotarget.17061

Zheng, X., Turkowski, K., Mora, J., Brüne, B., Seeger, W., Weigert, A., & Savai, R. (2017b). Redirecting tumor-associated macrophages to become tumoricidal effectors as a novel strategy for cancer therapy. *Oncotarget*, *8*(29), 48436–48452. https://doi.org/10.18632/oncotarget.17061

Zheng, Y., Wang, Y., Zhang, X., Tan, Y., Peng, S., Chen, L., & He, Y. (2017). C19, a C-terminal peptide of CKLF1, decreases inflammation and proliferation of dermal capillaries in psoriasis. *Scientific Reports*, *7*(1), 13890. https://doi.org/10.1038/s41598-017-13799-x

Zhou, D., Yang, K., Chen, L., Zhang, W., Xu, Z., Zuo, J., … Luan, J. (2017). Promising landscape for regulating macrophage polarization: epigenetic viewpoint. *Oncotarget*, *8*(34), 57693–57706. https://doi.org/10.18632/oncotarget.17027

Zhou, J., Fonseca, M. I., Pisalyaput, K., & Tenner, A. J. (2008). Complement C3 and C4 expression in C1q sufficient and deficient mouse models of Alzheimer's disease. *Journal of Neurochemistry*, *106*(5), 2080–2092. https://doi.org/10.1111/j.1471-4159.2008.05558.x

Zhou, Yingyao, Zhou, B., Pache, L., Chang, M., Khodabakhshi, A. H., Tanaseichuk, O., … Chanda, S. K. (2019). Metascape provides a biologist-oriented resource for the analysis of systems-level datasets. *Nature Communications*, *10*(1), 1523. https://doi.org/10.1038/s41467-019-09234-6

Zhou, Yingyue, Song, W. M., Andhey, P. S., Swain, A., Levy, T., Miller, K. R., … Colonna, M. (2020). Human and mouse single-nucleus transcriptomics reveal TREM2-dependent and TREM2-independent cellular responses in Alzheimer's disease. *Nature Medicine*, *26*(1), 131–142. https://doi.org/10.1038/s41591-019-0695-9

Ziegenhain, C., Vieth, B., Parekh, S., Reinius, B., Guillaumet-Adkins, A., Smets, M., … Enard, W. (2017). Comparative Analysis of Single-Cell RNA Sequencing Methods. *Molecular Cell*, *65*(4), 631-643.e4. https://doi.org/10.1016/J.MOLCEL.2017.01.023

Zotova, E., Bharambe, V., Cheaveau, M., Morgan, W., Holmes, C., Harris, S., … Boche, D. (2013). Inflammatory components in human Alzheimer's disease and after active amyloid-β42 immunization. *Brain*, *136*(9), 2677–2696. https://doi.org/10.1093/brain/awt210